THESIS FOR THE DEGREE OF LICENTIATE OF ENGINEERING

Wood-derived lignin-based fibers as supercapacitor electrodes

AZEGA RAJENDRA BABU KALAI ARASI

Department of Microtechnology and Nanoscience

CHALMERS UNIVERSITY OF TECHNOLOGY

Gothenburg, Sweden 2010

Wood-derived lignin-based fibers as supercapacitor electrodes

AZEGA RAJENDRA BABU KALAI ARASI

Technical Report MC2- 458
ISSN 1652-0769

Chalmers University of Technology
Department of Microtechnology and Nanoscience – MC2
Electronics Materials and Systems Laboratory
Micro- and Nanosystems Group
SE-412 96 Gothenburg
Sweden
Telephone + 46 (0)31-772 1000

Printed by Chalmers Reproservice
Gothenburg, Sweden 2022

Dedicated to my family

Wood-derived lignin-based fibers as supercapacitor electrodes

AZEGA RAJENDRA BABU KALAI ARASI

Department of Microtechnology and Nanoscience

Chalmers University of Technology

Abstract

Today, in order to replace fossil energy sources with renewable energy sources such as solar and wind, reliable energy storage systems that can provide power regardless of the intermittent nature of the energy sources must be created. Especially with the future's rising energy demands the development of such energy storage systems from green-collar materials with the least negative environmental impact is pressing. Transforming the major cheap and replenishable forest resource, wood, to carbon materials with desirable morphologies can potentially be used as supercapacitors (SC) electrodes with long cycle life and higher power density than batteries today.

Forest materials are abundant, but their extraction to manufacturing hold practicality issues due to yet not established procedures. Active research has focused on advancing lignin-based electrospun carbon fibers (ELCFs) and activated carbons with simple, high-yielding mass production units. The ECLF is self-standing and flexible, making them a prospective candidate for flexible and wearable electronics. As of today, the materials face shortcomings such as low electrical conductivity and poor mechanical stability post thermal carbonization especially if the spinning discards fossil based secondary polymers. Research on optimized fractionated high molecular weight lignin solutions from black liquor - an industrial paper and pulp industry byproduct - have improved their spinnability. Turning these lignin-based materials to commercial utilization requires more investigation and understanding of the materials.

This thesis discusses the electrochemical performance of lignin fibers as highly reliable supercapacitor electrode material. Grafting the right amount of beneficial functional groups on the ELCF surface by low-power oxygen plasma treatment, the properties of the electrode-electrolyte interface significantly improved the wettability, increased active sites favorable for pseudocapacitance, reduced diffusion limitation, thus enhancing its electrochemical storage ability. Quite often, the surface functional groups have a detrimental impact on a device's electrochemical performance such as increased resistance, low power performance, low stability, and high self-discharge rate. However, the non-invasive nature of the conducted plasma treatment made a remarkable improvement in the capacitive performance in KOH aqueous medium without compromising power and energy performance metrics. Preliminary quantification performed to understand the charge storage behavior in other aqueous electrolytes H_2SO_4 and Li_2SO_4 are also revealed. Furthermore, the observation of enhanced electrochemical performance via applying a voltage of 1.2 V and 10 000 charge-discharge cycles is discussed.

With the competition of supercapacitors energy storage ability with batteries, efforts have been taken to make thick electrodes to boost energy density. Electrodes with high areal mass loading in supercapacitor maximize the packing density of the electroactive electrode materials while lowering the manufacturing cost by reducing the number of inactive material layers. Herein, the fabrication and electrochemical performance of 180-280 μm thick activated carbon (AC) electrodes with 2 wt% of hair-like carbonized lignin carbon fibers (LCF) as conductive agent alongside carbon black in the electrode matrix was assessed. In the resulting electrodes, the LCF inclusions into the AC matrix increased flexibility and contributed to improved capacitances due to better conductivity in the electrodes. The reduced resistances suggest that LCFs act as an intermediate layer among AC particles and serve as conductive pathways, facilitating electronic conductivity of more AC particles in deeper layers. Considering the biologically hazardous nature of other commonly used binders like polytetrafluoroethylene, and polyvinylidene fluoride, environmentally friendly binder microfibrillated cellulose (MFC) binder was successfully used to fabricate freestanding electrodes.

Keywords: energy storage, supercapacitor, lignin, green electrode materials

Acknowledgments

This book contains my licentiate thesis, a product of my halfway through this Ph.D. journey that started in early 2020. I feel greatly pleased to have met a lot of people who have greatly inspired and supported me since then.

I would want to start by immensely thanking my supervisor, Professor Per Lundgren for his constant support and inspiration. I enjoy the illuminating discussions with him during our weekly meeting when he turns up with ingenious, unexpected approaches to solving our research problems. I am truly so appreciative of his constant understanding, and encouragement all this time, without which I would not have reached this far.

Special thanks to Professor Peter Enoksson, who made my Ph.D. research at Chalmers possible to start with. He always provided me with help and support since I started out as a new student in Sweden until now. I am greatly obliged to still be able to receive your expert advice every now and then during your visits to Chalmers.

I would like to express my sincere thanks to my co-supervisor Professor Hans Theliander for his guidance and for the motivation he has infused me with enthusiasm for researching lignin materials. Look forward to continuing to learn more from you while we have the hardwood lignin fiber project going on.

I would like to express my thanks to Mazharul Haque, Qi Li (SmolTek Hydrogen AB), Jenny Bengtsson (RISE), Kerstin Jedvert (RISE), and Jinhua Sun (IMS, Chalmers) for providing insightful knowledge in their fields of expertise and helping me to explore and understand new materials for my research.

My gratitude is greatly acknowledged to my project funders, the Wallenberg Wood Science Center (WWSC) financed by the Knut and Alice Wallenberg Foundation for its financial support, and the Chalmers University of Technology for giving me the opportunity with wonderful research space and knowledgeable people to undergo my research. I also feel obliged to thank the GreEnergy Project for their funding support to our group.

My thanks also go to all my close friends and Chalmers colleagues, especially Dhiya, Rishi, Simin, Shameena, Vidya, Divya, Sadia, Agin, Adarsh, Carl, Vivek, Pascal, Amit, Shirin, and many more other friends for their support during this Ph.D. journey of mine. Immense thanks to my work colleagues for making the working atmosphere most pleasant for me both in the corridor and while hosting interesting conversations during our daily lunches and fikas. They made the COVID era survivable for me.

Finally, this acknowledgment would not be complete without thanking my dear parents, little sister, grandparents, and relatives from back home, who have supported and loved me all along. Thank you!

Göteborg, June 2022

Azega

Appended publications related to the thesis

[Paper I] "Effect of plasma treatment on the electrochemical performance of lignin carbon fibers for supercapacitor application", Azega. R.K, Mazharul Haque, Qi Li, Omid Hosseinaei, Hans Theliander, Peter Enoksson, and Per Lundgren. Submitted.

[Paper II] "Durable activated carbon electrodes with a green binder", R.K. Azega, M. Haque, A. Vyas, P.L. Tam, A.D. Smith, P. Lundgren, P. Enoksson, Physica Status Solid B, Volume 259, Issue 2, January 2022, DOI: https://doi.org/10.1002/pssb.202100311

Other publications related to the author that is not included in the thesis

[1] "Spin-Coated Heterogenous Stacked Electrodes for Performance Enhancement in CMOS-Compatible On-Chip Microsupercapacitors", Agin Vyas, Simin Zare Hajibagher, Ulises Méndez-Romero, Shameel Thurakkal, Qi Li, Mazharul Haque, R.K. Azega, Ergang Wang, Xiaoyan Zhang, Per Lundgren, Peter Enoksson, Anderson Smith, ACS Applied Energy Materials, March 2022, DOI: https://doi.org/10.1021/acsaem.1c03745

[2] "Alkyl-Amino Functionalized Reduced-Graphene-Oxide–heptadecan-9-amine-Based Spin-Coated Microsupercapacitors for On-Chip Low Power Electronics", Agin Vyas, Simin Zare Hajibagher, Ulises Mendez Romero, R.K. Azega, Ergang Wang, Per Lundgren, Peter Enoksson, Anderson D. Smith, Physica Status Solid B, Volume259, Issue 2, February 2022, DOI: https://doi.org/10.1002/pssb.202100304

[3] "Exploiting low-grade waste heat to produce electricity through supercapacitor containing carbon electrodes and ionic liquid electrolytes", Mazharul Haque, Iqbaal Abdurrokhman, Alexander Idström, Qi Li, R.K. Azega, Anna Martinelli, Lars Evenäs, Per Lundgren, Peter Enoksson, Electrochimica Acta, Volume 403, 139640, January 2022, DOI: https://doi.org/10.1016/j.electacta.2021.139640

[4] "Identification of self-discharge mechanisms of ionic liquid electrolyte based supercapacitor under high-temperature operation", Mazharul Haque, Qi Li, Cristina Rigato, R.K. Azega, Anderson D. Smith, Per Lundgren, Peter Enoksson, Journal of Power Sources, Volume 485, 229328, February 2021, DOI: https://doi.org/10.1016/j.jpowsour.2020.229328

Conference and workshop contributions

[1] "Investigations on the capacitance increase during repetitive charging/discharging of lignin carbon nanofiber-based supercapacitors", R.K. Azega, Qi Li, Mazharul Haque, Per Lundgren, and Peter Enoksson, 2021 Virtual MRS Spring Meeting & Exhibit, April 2021.

[2] "Durable activated carbon electrodes with a green binder", R.K. Azega, M. Haque, A. Vyas, A.D. Smith, P. Lundgren, P. Enoksson, Compound Semiconductor Week, May 2021.

Table of contents

1. Introduction

1.1. Energy storage devices

In the mid-Devonian age, about 390 million years ago, the plants began evolving into woody plants. True wood was a requisite creation that enabled conduction of ample water and mineral from root to leaf whilst it supported plants to grow taller for accessing light. This purpose to thrive by competition transmogrified the wood to the more intricate and complex structure as we know it today. Approximately 1 million years ago, our fellow species, Homo erectus exploited the firewood for thermal energy from the discovery of fire. Even today, burning wood is the primary source of energy for about 6% of the global population [1]. But not until the mid-20th century did humans invest in the idea of transforming wood into components in energy storage devices.

Table 1: Supercapacitor performance metrics compared to standard lithium batteries.

	Supercapacitor	**Lithium battery [a] [5], [6]**
Charge storage	Double-layer capacitance (electrostatic)	Intercalation
Electrodes	Carbon materials	$LiCoO_2$ cathode and graphite anode
Electrolyte	Organic	Lithium salt in an organic solvent
Operating voltage	Up to 3 V	3.0 – 4.4 V
Energy density	3~5 Wh/kg	120-190 Wh/kg
Power density	9000 W/kg	1000-3000 W/kg
Thermal runaway risk	No danger	Yes
Operating temperature	-40 °C to +65 °C	0-45 °C
Self-discharge	High (weeks)	Less (years)
Operation lifetime at RT	10-20 years	2-3 years
High temperature operation [b]	2,000 hours	Deteriorates device life
High voltage operation [b]	1,500 hours	Becomes unstable
Cycle life	1,000,000 cycles	>500 cycles
Shelf life	10-18 years	7-15 years
Availability	Commercially available	Commercially available
Cost/kWh	$100-500	$100-170
Current applications	Memory backup	UPS, portable electronics, and so on.
Toxic level	Low	High

[a] The $LiCoO_2$ cathode-based LIBs, which are typically used to power portable consumer gadgets, serve as a representative of the lithium-ion battery family in this context.

A simple discovery of rubbing amber with fur revealed the possibility to store electrical energy on the surfaces of materials due to buildup of electrostatic charge. In 1957, H. I. Becker proposed a device model called electrolytic capacitor showing a similar phenomenon by using porous carbon electrodes [2]. This observation contributing to capacitance from an electrostatic double-layer occurring at an electrode/electrolyte interface was understood by Hermann von Helmholtz as early as 1879. But not until the early 1990s was the research in the field vitalized. When NEC in Japan created their energy storage technology in the 1990s, they coined the term "*supercapacitor*" [3]. Technically, it is known as an EDLC, or Electrochemical Double Layer Capacitor, which is presumably why the term "supercapacitor" stuck. The

Maxwell Technology later dubbed their EDLC device also as an ultracapacitor. On better material and device understanding the technology further broadened over the discovery of high-capacity metal oxide electrode materials like RuO_2. Trasatti and Buzzanca first recognized this type of capacitor-like electrochemical reaction of hydrous RuO_2 thin films in 1971 [4]. Ever since, a plethora of so-called pseudocapacitive materials has been identified.

Supercapacitors (SC) grew to be efficient energy storage devices in high power density applications by delivering sufficient energy instantaneously. The absence of surface degrading Faradaic reactions in EDLC electrodes extends the device's cycle life to almost infinite. However, SC has lower energy storage capacity compared to the technologically more developed and advanced electrochemical energy storage device called *battery*. It was in the early 1990s that lithium-ion secondary batteries gained prominence due to their high specific or volumetric power, energy density, low self-discharge, wide temperature range of operation, and high cycle lifetime, all of which distinguish them from other rechargeable batteries such as lead-acid or nickel-metal hydride. Many of these performance metrics are compared for battery with supercapacitors in Table 1. Lithium not being an infinite resource, along with environmental issues of battery materials (like cobalt, lead, cadmium etc.) and an ever-increasing global energy demand, necessitates the search for alternate sustainable energy materials in an effective energy storage system [7]. The present efforts in enhancing energy density in cutting-edge lithium-ion batteries (LIBs) is too sluggish to meet the practical demands of portable electronic gadgets and electric cars [8], [9].

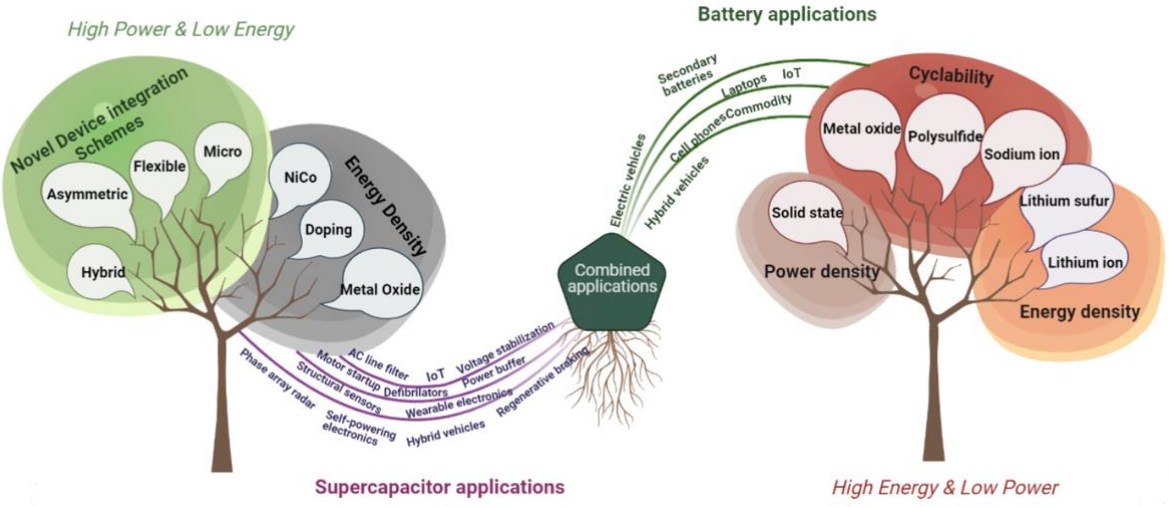

Figure 1. Supercapacitor and battery technology migration to close the energy gap is largely driven by a number of important emphasis areas (corresponding technology's most notable research-focused branches in the last 12 years). Each technique has often only been used in specialized applications. New possible applications emerge when the technologies change and converge.

Technological advancement, improvement of traditional cell designs, and the use of alternate electrode chemistries have been the most studied ways for boosting energy and power density. In fact, in specialized applications SCs have been exploited to co-benefit from or even replace batteries. For instance, in electric automobiles, the otherwise lost kinetic energy from regenerative braking is collected by power supercapacitors to enhance the efficiency and range [10]. Likewise, SC/battery hybrid energy storage systems (HESS) are also considered interesting to power microgrid systems from renewable power generating sources such as solar and wind for a similar reason to avoid variable current demands taking a toll on the battery's life [11]. However, now, a SC as a standalone device only meets small-scale energy-power demands. Nonetheless, in some applications, it has been recognized as a viable energy storage that is more than a battery supplementary in situations where the loss of energy is acceptable in exchange for higher power. Sunwin, a Chinese startup company, runs a SC as a complete standalone power source to

power short-range electric buses that require charging at each bus stop [12]. Because of its small range, along with a high self-discharge rate over time, their specialty is not convenient for personal or other heavy long-range vehicles. Other barriers to commercialization for SC include the device's greater material cost and poor performance when compared to currently prevalent energy options. This, combined with the present hurdles with material, device, and manufacturing efficiencies, means that SC technology needs more development to be able to power our electrical appliances as a standalone device in the future. Nevertheless, the possibility of SC to serve innumerable applications with diverse demands makes exploration of the plethora of its materials in various manifestations for standalone or combined energy storage applications with battery (Figure 1) worthwhile.

1.2. Why supercapacitors when there are already batteries?

Concern about the environment is one factor driving interest in alternative energy sources and devices. It includes the increasing cost of fossil fuel and every other product that depends on it. The increasing energy demand worldwide fulfilled so far from the fuel-based resources contributes to greenhouse emissions. Moreover, the prolonged dependence on their resources will someday lead to depletion of their limited reserves. As a result, climate change, pollution, and the high cost of fossil fuels there is already a very strong demand on sustainable (environmental-, economic- and social- friendly) energy alternatives. As one of the climate change mitigation efforts, the world is switching to battery-powered electric vehicles. Although batteries are today the most popular and commonly utilized electrical energy storage device, efforts to enhance them by considering critical performance and environmental factors including cost, cyclability, environmental sustainability, recyclability/disposability, and combustibility are already ongoing. But battery materials by themselves are condemned to being linked to higher environmental toxicity threats [13]. Added on, their mineral sources are lean to serve all our growing global energy consumption. So, the want for energy devices from abundant resources with an ecologically sound footprint is compelling. This has been motivating for the research and development of green electrodes for supercapacitors energy storage devices.

SCs are well-known to deliver high power with sufficiently high energies stored. On representing the relation of power density and energy density of different energy storage devices in a Ragone plot (Figure 2): the fuel cells are high-energy systems while supercapacitors are high-power systems. Batteries come up with intermediary power and energy capabilities.

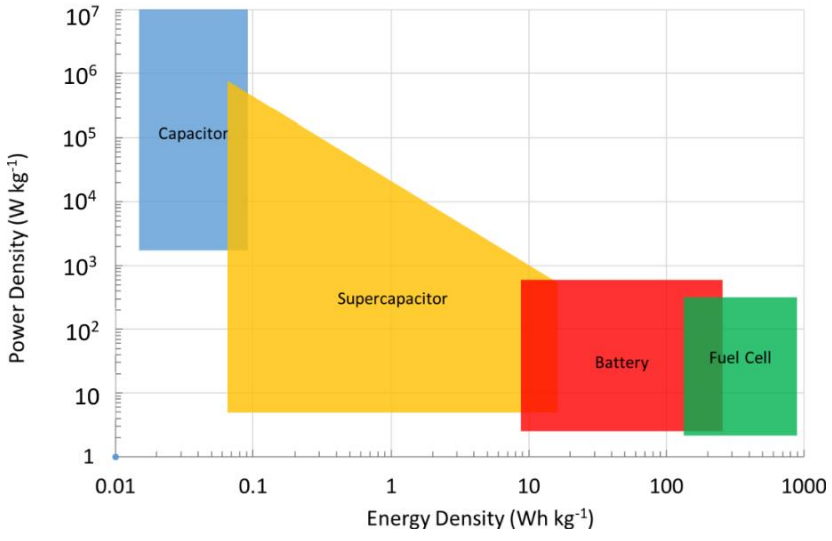

Figure 2. Ragone plot of different electrochemical energy conversion devices

The supercapacitors also display excellent cycle life, and rapid charge and discharge compared to conventional batteries making them a highly open candidate for upcoming electrical energy reservoir and harvesting requisites. Moreover, they are almost maintenance-free, clean, and the safest means of electrochemical energy storage. Scaling SC alongside batteries could potentially be a huge scope for energy in rural areas where power grids are unavailable due to lack of access to urban infrastructure [14]. However, the SC fall behind in their energy densities compared to conventional batteries. To overcome this, in SC many efforts have been focused on improving the energy output by advanced tuning of the electrode, electrolyte material's properties or creating innovative combinations of device configurations such as asymmetrics and hybrids.

Equally critical, obtaining a fitting application for specific supercapacitor electrode materials has been challenging for researchers; especially regarding the optimization challenges with the diversity of functional materials (generally carbon, pseudocapacitive and hybrid electrode materials; aqueous, ionic, organic electrolytes) and in attaining synergistic benefits in their hybridization with or without batteries.

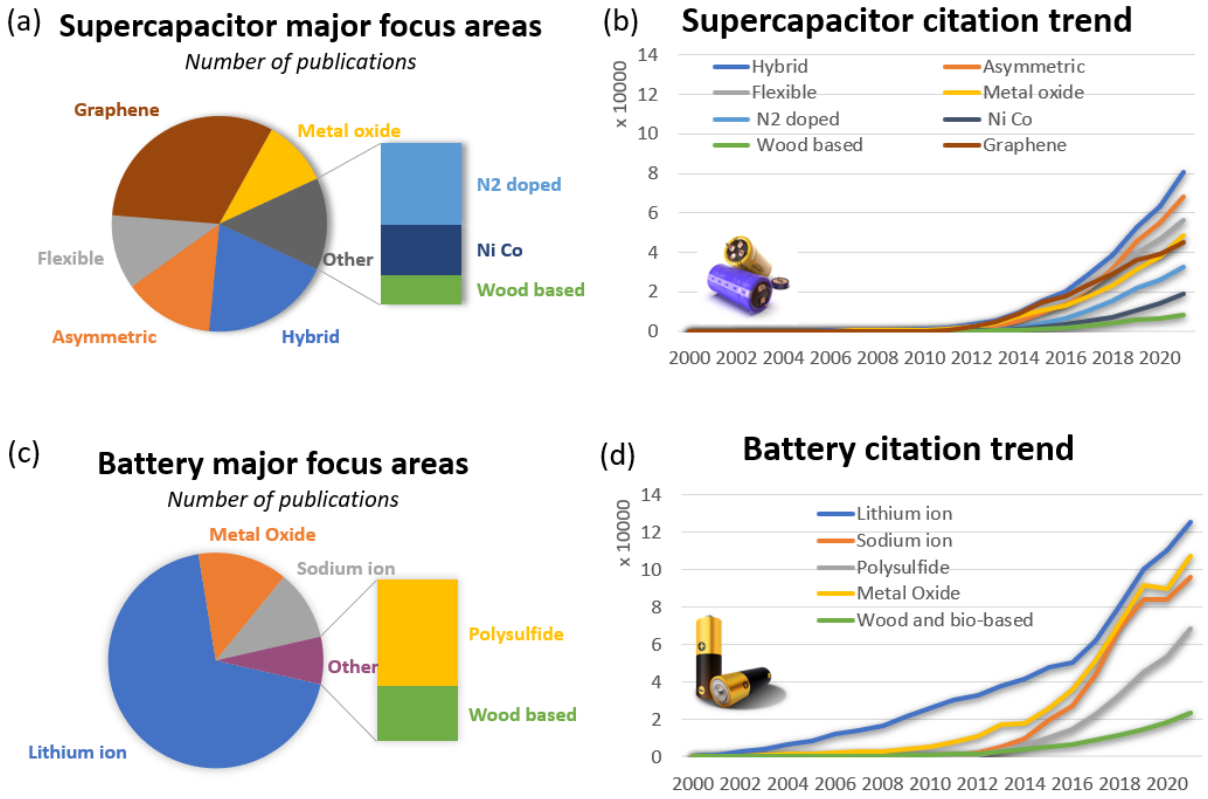

Figure 3 a) Total supercapacitor field publications during the preceding 12 years, broken down by categories. b) Citation trends for the major subfields of supercapacitor research in the last 20 years. c) The dissemination of publications for the main battery-related research areas. d) The total number of citations for the battery sub-fields during the past 20 years.

According to web of science analytics, the key areas of attention in the battery sector during the previous two decades have been lithium-ion, lithium-sulfur, sodium-ion, solid-state electrolytes, metal oxides, polysulfide-based, and wood-based batteries as shown in Figure 3 c and d. Their research is increasingly focused on improving cyclability and power density toward the capabilities of supercapacitors. Similarly, most of the supercapacitor research is centered on boosting energy density. Some of their specific research focus areas (Figure 3 a and b) were asymmetric, hybrid, flexible designs, metal oxide electrodes, nitrogen-doped electrodes, wood-based electrodes, and the use of nickel cobalt electrodes. Citations in the

supercapacitor field show that more than 80% of the work is aimed at enhancing energy density, with unique asymmetric and hybrid supercapacitor device designs accounting for more than 60% of those efforts. The remainder of the studies have been focused on supercapacitor integration designs, such as flexible/wearable technology and micro-supercapacitors, that are known to be useful to meet the needs of diverse digital electronics and data storage system applications. Batteries are the topic of more diverse research, with a focus on the device's environmental friendliness, an interest in hazardous chemicals and replacement components in existing lithium-based batteries, and harmful replaceable sodium ion-based batteries [15]. The top citations for metal-oxide-based capacitive materials for batteries, in addition to Na-ion batteries (Figure 3 d), indicate that efforts to produce batteries more like supercapacitors are also viewed as promising research directions. To address expanding material sustainability issues, eco-friendly efforts to manufacture wood-based carbon electrodes have evolved dramatically in recent years. As a result, in the last decade, sustainable efforts to produce wood-based carbon as electrode components for both supercapacitors and batteries have begun to advance significantly [16]–[19].

1.3. Safety, price, and environmental benignity of the devices

a. Environment/Sustainability

The introduction of electric and hybrid cars has helped to promote energy independence and perhaps lower greenhouse gas (GHG) emissions from the transportation industry. To take sustainability, reusability, and ethical considerations into account when choosing materials for energy storage systems is crucial. The main issues with existing batteries are the negative effects of the materials used on the environment, the high energy demand during manufacturing, and the depletion of natural sources of the elements needed to make batteries. Unfortunately, lithium has a very low abundance compared to aluminum and copper, both of which are utilized as current collectors. Additionally, several of the chemical components utilized in electrodes today, particularly cobalt, are recognized carcinogens [20]. Considering the various limitations of battery materials, carbon-based electrodes from renewable bioresources or even replenishable biowastes such as agriculture wastes, or wood is a much sustainable choice. However, the environmental impact of modern electrode materials containing metal oxide species and synthetic production processes is still unfavorable for similar reasons to replace battery or its materials. Therefore, opting environmentally friendly starting materials and processing with limited chemicals from extraction to final product production is desired. For example, SC electrode binders and electrolytes are produced of non-renewable, poisonous, and dangerous elements that are harmful for the environment. Biopolymers and ionic liquids as alternative for replacing more harmful options [21], [22]. On the same motivation note, the initiative to produce electrodes from wood-based derivatives is undertaken. Lignin is one of the main components of wood and a major by-product from the paper and pulp industry. Every year, approximately 130 million tons of lignin are precipitated from black liquor, which is otherwise mostly incinerated to generate heat [13]. With proper processing steps it can be utilized to make energy storage electrodes.

From the device point of view, ideally, SC have an infinite cycle life; unlike batteries, they do not wear out or age from their basic mode of operation. SC, in contrast to batteries, are not consumables; instead, they last for the entirety of a product's life cycle. When their device energy is less than 0.3 Wh, they are free from dangerous goods requirements and can be delivered and disposed of without check [23]. These characteristics of SC make it possible to regard them as sustainable as a device to be implanted in day-to-day commodities.

Life-Cycle Assessment (LCA) is a well-established but continually growing approach for accounting for and analyzing the possible environmental consequences of goods, processes, or activities [24]. Early integrated LCA estimates provide a bleak picture, revealing that more than 400 kWh are required to manufacture a 1 kWh Li-ion battery, resulting in the release of around 75 kg of CO_2. Batteries must be utilized beyond hundreds of cycles to have a good influence on the environment. Hybridizing it with supercapacitors exploit the benefits of both by combining them at the cell level to create a hybrid capacitor. A lithium-ion capacitor (LIC), also known as a hybrid capacitor, is composed of an environmentally

sustainable activated carbon electrode and a graphitic carbon material pre-doped with lithium ions as the anode. In addition to charging faster than batteries with the same amount of electricity (high power) and having higher storage capacities (energy densities), LICs have the advantages of supercapacitors, allowing them to function at temperatures ranging from -20 to 70 °C while retaining long cycle lifetimes [25]. Mining, ore transport, ore treatment, and associated operations are the major contributors to CO_2 emissions and energy costs for rare earth battery and supercapacitor materials manufacture [25], [26]. The viable solutions to these problems are: 1) recycling of electrode materials to recover rare materials [27], 2) designing of electroactive materials with comparable performances but requiring less energy and emitting less CO_2 during production than existing ones, 3) replacement of toxic elements used in electrode materials, and 4) generation of clean, greenhouse gas-free electricity. The present research focus is on biomass and wood-based energy storage systems. Furthermore, as potential applications for SC and LIC systems, the sectors of wind power generation, uninterruptible power sources, solar power generation, energy recovery systems, and automotives already encourages delivery of clean and green electricity.

b. Cost

Reducing the cost of supercapacitors is one of the key market impetuses besides the yet to be scaled market. In commercial supercapacitors, the activated carbon (AC) material has a relatively low price which is one of the reasons behind the supercapacitors becoming popular. Other electrode materials such as carbons with manganese oxides have a higher energy density but metal is the most critical material from the cost perspective and thus the current trend is to only use activated carbon electrodes to reduce the cost. Reducing the cost of raw material sources already is a huge advantage to provoke development. For instance, by producing carbon fibers with lignin, the price will be substantially lowered compared to the commercial carbon fibers produced today. Besides the raw materials, the manufacturing process affects the final price of the supercapacitors to a large extent. With the development and maturation of the fabrication technology, the manufacturing cost is assumed to be reduced in the future.

c. Lifetime/Cyclability

The lifespan of a battery is highly dependable on the charging and discharging cycles, which makes this one of the top issues in battery research. In the case of lithium and lead-acid batteries, the charging and discharging are limited from 300 to 500 cycles, sometimes it can be a maximum of 1000 times. The lifespan without charging and discharging can be up to 7 years [28]. Elevating temperatures and exceeding operation regimes beyond the electrochemical stable window (over voltage, effective current) tend to accelerate the process of aging [29]. Although second-life usage of batteries has been receiving attention lately they suffer significant underperformance. On the contrary, a supercapacitor capable of almost infinite charge cycles can be charged and discharged for between 100,000 to 1,000,000 times or even further depending on operation environment [30]. Considering shelf lifespan, a supercapacitor can last for 10-18 years, while a lead-acid battery can last around 3-5 years only.

d. Safety

Safety has always been a big problem for lithium-ion batteries and following the problems of Samsung's Galaxy Note 7 and HP laptops, more attention have been given to assure their safety. Lithium-ion batteries include lithiated elements as well as a volatile flammable electrolyte that combusts when exposed to oxygen and humidity in the environment [31]. When mishandled, batteries burst due to overheating caused from short-circuit; supercapacitors, on the other hand, do not heat up as much because of their low internal resistance. Comparatively, therefore, SC are much safer energy storage devices than batteries. SCs can operate in a wide temperature range from -25 to 85 ºC. In addition, unlike batteries, there is no risk of combustion when voltage limits and working temperature ranges are exceeded. SC with water-in-salt and ionic electrolytes are tested safe to store and operate in various conditions. Organic electrolytes are used in conventional commercial supercapacitors nowadays. Apart from their mobility and convenience of use,

solid-state electrolytes minimize the safety concern offered by conventional liquid electrolytes, which are also flammable and heavy.

1.4. Motivation

As afore motivated, annually, the paper and pulp industry produce about 260 million tons of black liquor as a by-product [32]. It is an organic-inorganic mixture of lignin, hemicellulose, and processing chemical residues from the pulpwood digestion unit. This non-fossil fuel has been used to power the pulp mills with electricity and generate heat energy for boiler plants. The full potential of this material is yet to be exploited and should be put to better use than as a mere boiler fuel. Furthermore, modern kraft pulp mills are very energy efficient and as a consequence all lignin is not necessary to use as fuel in these pulp mills. Extracting the excess lignin from the black has the potential to provide a functional resource to make various value-adding products. Lignin as a carbon rich bio-component is attributed to be a suitable candidate to manifest various carbon materials. With that interest, research, and development on lignin derived carbon fiber mats as electrodes in energy storage devices, particularly SC, has been investigated in our work. With a better understanding of the charge storage mechanisms and the development of their morphologies, the supercapacitors are likely to suit applications either as a standalone power source or a battery-supported system. Beyond their scope as supercapacitor electrodes, they can also be attempted to replace the graphite electrodes in lithium-ion batteries. This is one of the visions of the Finland-based company Stora Enso joining hands with NorthVolt [33].

1.5. Scope of this thesis

Efforts of developing SC materials has been to increase energy output while still maintaining their credited power density. Typically, increasing surface area and improving accessibility to these active sites is vital for any material's reliable performance in devices. In order to be able to do that, increasing the mass loading of electrodes with optimum electrode-electrolyte interface interactions will be a wise way to efficiently utilize active material.

This thesis study focuses on discussing device performance factors, including the importance to improve the electrode-electrolyte interface (Paper I) and regulate electrolytes accessibility to inactive electrode layers with increasing mass loading (Paper II) to maximize supercapacitor performance. In addition to these, the thesis evaluates different strategies and approaches for improvements addressing electrolyte wettability and accessibility issues for SC. The materials in focus as electrodes are forest components, cellulose, and lignin, introduced in Chapter 2. Chapter 3 presents several types of SCs based on these materials, followed by standard electrochemical testing techniques for testing their performance in two-electrode cell devices. Additionally, the standard methodologies developed for deconvoluting different charge storage behaviors in supercapacitors has been discussed. In Chapter 4, the effect of employing basic surface treatments and incorporating lignin materials on device's performance is discussed based on different material and electrochemical characterization of the electrodes. The key steps followed in the journey of lignin from precursor to electrodes through the sequence of high temperature treatments to attain efficient electrode characteristics has also been described step after step. The need for high mass-loaded electrodes and the self-discharge effects have been briefly discussed. Finally, the thesis's primary findings are summarized, along with future g oals.

2. Major wood raw materials

2.1. Lignin

The global market of lignin is estimated to grow at an annual rate of 2% from 2020 to 2027 reaching over USD 1 billion in 2027. Their market growth is due to the demand for animal food and natural products. According to 2019 data, systematic lignin regulation procedures in Europe contributes to 40% of the global commercial lignin production for further utilization [34]. The Norwegian company Borregaard is one of the key players on this market. They separate lignin by a specialized Swedish patented separation process LignoBoost that was developed by researchers from Chalmers and RISE in the 2000s [35]. In this process the 35 - 45% of lignin in black liquor is efficiently extracted.

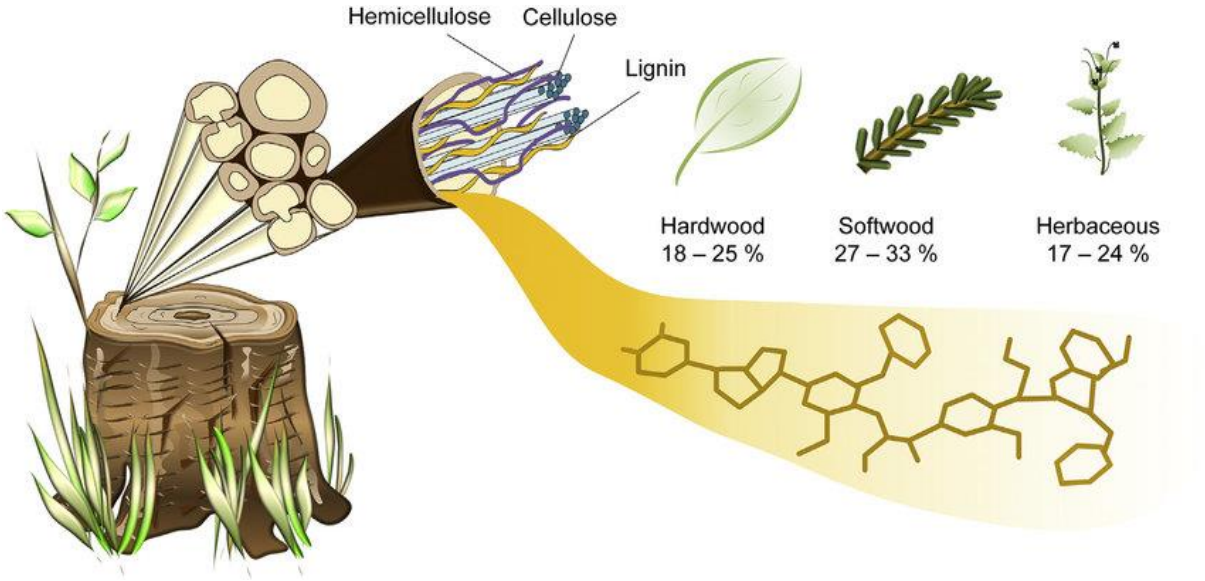

Figure 4. Wood is composed of lignin, cellulose, and hemicellulose. The amount of lignin varies depending on the source of wood [36]

Lignin is a bioresource of high aromatic carbon content compared to other major wood components. When part of the tree in the wood's cell wall, it offers compressive mechanical strength that facilitates long distance water transport and protection from pathogens – a key component that keeps the tree alive and growing. This complex and highly functional biopolymer, a material of such great importance to the trees today obtained as byproduct from the paper industry could be an engineering material of the future. From research in the last decade, it has been identified as a possible ideal precursor to develop various derivatives of carbon materials. There is already plenty of interest and on-going research by various groups and industries especially in Europe and China [37]. The motivation to it is to develop sustainable environmentally friendly materials. Already, lignin-derived chemicals and materials such as hydrogels, carbon fibers, nanomaterials, composites, and bio-asphalt are being considered as viable replacements for oil-based goods in the production of carbon-based compounds for use in a wide range of sectors such as automotive, construction, coatings, plastics, and medicines. Therefore, there is more to explore; to modify and functionalize possible lignin-based carbon materials overcoming their chemical and physical heterogeneity challenges to make them fit in more future applications. The complexity relates to lignin's complex structure and heterogeneous molecular weight that is highly dependent on the wood source (Figure 4) and isolation methodology. Despite these challenges and difficulties, being a carbon-rich replenishable bioresource, the interest for it has been worth the exploration. The possibilities of lignin derivatization and

mass manufacture are large [38]. Some of the sustainable lignin-based value-added carbon materials are discussed in the following chapter.

2.1.1. Extraction of lignin from black liquor

Kraft pulping is the most common type of chemical pulping, accounting for 80% of the entire industry. Kraft pulping is the process of digesting debarked wood chips at 150-180 °C for 2 to 4 hours under high pressure with a high aqueous solution of sodium sulfide and sodium hydroxide known as white liquor. Various chemical bonds, mostly ether bonds, are broken and the high pH ionizing the phenolic hydroxyl groups in lignin, chemically dissolves the lignin that binds the cellulose fibers together in the wood [39]. After the digestion operation, the liberated cellulose fibers are removed from the cooking liquor and washed. As a product of this separation, the obtained cooking liquor rich in solubilized lignin is known as black liquor (BL). The BL is concentrated in and evaporator train and is then used in the boilers to generate heat.

The composition of BL varies depending on several factors such as source of wood raw material, processing white liquor composition and even post storage conditions. The BL prior to evaporation normally consists of an aqueous mixture solution with lignin residues, hemicellulose, and the inorganic chemical employed in the process, and 15% w/w solids, 10% w/w of which are inorganic and 5% w/w of which are organic, where the organic contents include 30%-45% w/w aliphatic carboxylic acids, 35%-45% w/w lignin, and 5%-15% w/w other organic compounds [40], [41]. Inorganics include processing compounds as well as certain ionic species.

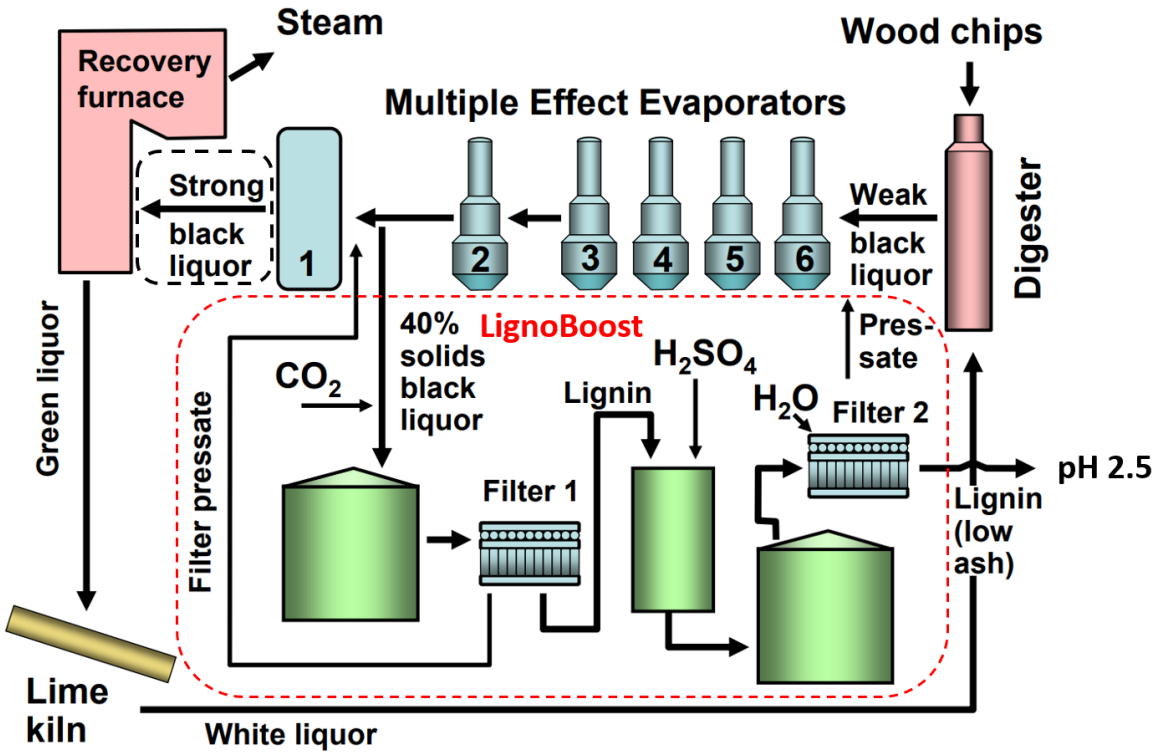

Figure 5. The sequence of steps conducted during lignin extraction from black liquor by LignoBoost method [42].

To recover lignin from the BL, the pH reaching around 9-11 leads to lignin's precipitation. The obtained filtrate after fine filtering is free of most inorganic species. The precipitated lignin is further washed by

undergoing acid precipitation in sulfuric acid of pH 2 (Figure 5). To increase the yield quantity of dried lignin solids, repeated washing is avoided.

2.2. Cellulose

Cellulose is a carbohydrate polymer composed of glucose units (> 10,000) connected by β-(1-4)-glycosidic linkages. As chains arranged in microfibril bundles, they are the most prevalent naturally occurring polysaccharide, which serves as the principal cell wall for trees, plants (Figure 6), and even algae and fungi. Wood-based cellulose, plant-based cellulose, bacteria-based cellulose (BC), algae-based cellulose, and tunicate-based cellulose are the main different types. Wood (40-50%) and plant (30-75%) became the most well-known sources of cellulose due to their high availability and low cost.

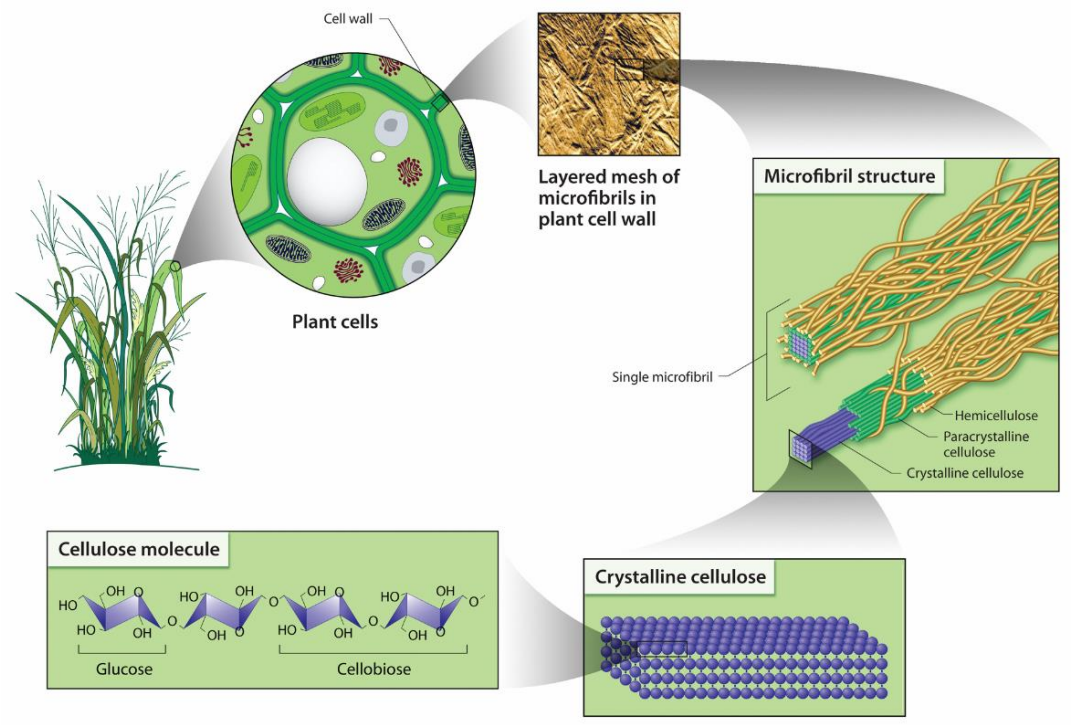

Figure 6. Chains of cellulose molecules combine with other polymers within the plant cell wall to produce linear structures with great tensile strength known as microfibrils. The cell wall is made up of layers upon layers of microfibrils. Each microfibril has a diameter of 10 to 20 nm and can include up to 40 cellulose chains [43].

The textile, construction, paper-pulp, and food industries are by far the largest users of cellulose derived from either cotton or wood pulp. Diverse cellulose derivatives have been produced to be used in various other subsidiary applications by undergoing chemical treatment or functionalization. Harsh chemical treatments such as acid hydrolysis, solvent dissolution, and bacterial fermentation are used to reduce cellulose pulp into nanofibers. The characteristics of cellulose derivatives are governed not only by the type and degree of substitution, but also by the pattern of functionalization throughout the polymer chain. The inability of cellulose to dissolve in organic solvents and the substantial steric hindrance caused by the stiff and bulky cellulose main chain hinders modification. More often, the hydroxyl group is the most targeted reactive group for derivatization by esterification or etherification. They are characterized to improve chemical structure, moisture sorption, water interaction, surface activity, and solubility [44]. Cotton, linen, and rayon for garments, nitrocellulose for explosives, and cellulose acetate for films are all examples of cellulose's industrial use. Their strong biocompatibility and superior physical and chemical qualities boost

possibilities for a wide range of bio-medical applications, including tissue engineering, wound dressing, and drug delivery systems [44].

3. Supercapacitors

The supercapacitors are classified broadly based on energy storage mechanism and their device configurations. The existing types of supercapacitors in terms of energy storage mechanisms are as shown in Figure 7. Even though activated carbon is a well-established electrode material in commercial supercapacitors today, there is an interest in finding alternative carbon electrode solutions.

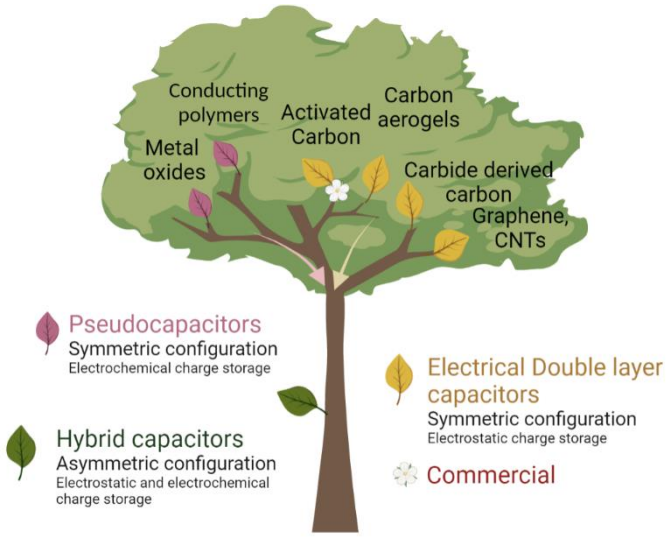

Figure 7. Broad classification of predominant types of supercapacitors that are being explored today and their corresponding charge storage mechanisms.

A supercapacitor's capacitance (C) is defined by the formula

$$C = \frac{Q}{V} \qquad \text{(Equation 1)}$$

where Q is the amount of charge stored on the electrode, and V is the working voltage window.

3.1. Classification of supercapacitors based on storage mechanism

Based on the performance metrics, SC are known to outperform common conventional energy storage systems like batteries and fuel cells in terms of long lifespan, good reversibility, high power density, shelf life, efficiency, operating temperatures, environmental friendliness, safety, and cost effectiveness.

Electrical energy storage in supercapacitors is based on two different principles: (1) non-Faradaic process where anions and cations are accumulated at the electrode/electrolyte interface electrostatically; and (2) Faradaic process where redox reactions occur by charge-transfer between the electrode and the electrolyte. They are divided based on their electrode (given in Table 2) or cell design into: (1) electrical double layer capacitors (EDLC), with carbon or carbon-derived electrodes, (2) pseudocapacitors, with metal oxide or conducting polymer electrodes, and (3) hybrid supercapacitors, with asymmetric electrodes contributing from both double-layer capacitance and pseudocapacitance storage mechanisms. Nowadays, hybrid capacitors are primely used to describe the cell designs which have a combination of battery and supercapacitor materials (e.g.: lithium-ion capacitors (LIC)). Moreover, the electrochemical performance and stability in different environments or working conditions of a supercapacitor significantly depends on the choice of its electrolyte and device design besides the choice of electrode. The higher capacitances of carbon electrodes are dependent on the high active surface areas, pore-size distribution, good intra-, inter-particle conductivity, and electrolyte accessibility in porous materials [12]. In the 1990s the pseudocapacitive material ruthenium oxide was exploited for its capacitance contribution from its reversible

surface redox reactions. Electroactive electrode materials undergo the mechanism of intercalation and electrosorption of ions alongside reduction-oxidation reactions, contributing to the overall larger capacitances.

Table 2: Classification of electrodes based on type of material

Type of electrode	***EDLcapacitive (EDLC)***	***Pseudocapacitive (PC)***	***Composites (EDLC/PC)***
Standard materials	Carbon	Metal oxides (MO)	Carbon/MO
Charge storage	Electrostatic	Electrochemical	Electrostatic and electrochemical
Electronic conductivity	High	Low	Intermediate
Rate capability	High	Low	Intermediate
Specific surface area	High	Low	Depends on carbon collector
Pore size	Tailorable	Definite	Depends on carbon collector
Chemical/thermal stability	High	Low	Intermediate
Availability	Abundant	Limited (depends on MO)	Intermediate
Cost of raw material and production	Cheap	High	Intermediate
Toxicity	Low (greener)	High	Intermediate

A. Electrochemical double-layer capacitors (EDLC)

The electrochemical double layer capacitors (EDLC) store the energy electrostatically by the adsorption of electrolyte ions onto the electrode's surface. Figure 8 shows schematic diagrams of an EDLC depicting its charge adsorption and desorption processes. On applying voltage, the charges accumulate on the surface of the electrode. The accumulation of charge in the electrical double layer is a non-Faradaic reaction that occurs by the depletion of oppositely charged species at the electrode-electrolyte interface. That is, the positive working electrode electrostatically absorbs solvated anions while the negative counter electrode attracts solvated cations, resulting in electrical double layers linked in series. Because there are no chemical processes involved in the storing mechanism, the approach is highly reversible for over 50,000 to million cycles, resulting in a longer life for EDLC. An EDLC's specific capacitance is calculated as

$$C = \frac{A \cdot \varepsilon}{d} \qquad \text{(Equation 2)}$$

where A is the electrode's electrochemically active surface area, d is the effective electrical double layer's thickness, and ε is the permittivity of the dielectric. Their specific capacitance depends mainly on the available active specific surface area in the electrode material.

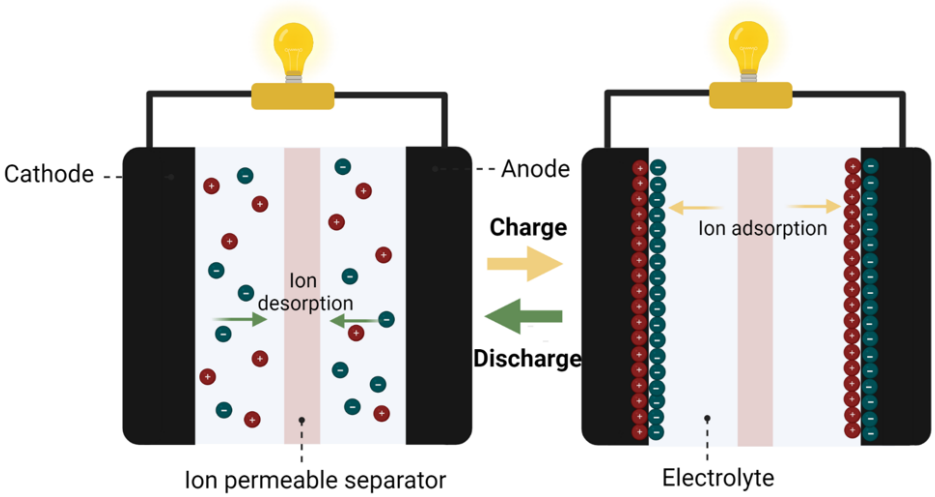

Figure 8. Schematic representation of the electrostatic charge storage mechanism during charging-discharging cycles in an EDLC device.

Carbon-based derived materials holding high surface area is the ideal choice of source material for EDLCs. Most standard materials are available in the form of activated carbon, carbon nanotubes and fibers from various renewable sources such as sawdust, biowastes, seaweeds, coconut shell [45] etc. They are suitable as electrodes owing to their high meso-porosity, high specific surface area, and high charge conductivity [46]. However, charge storage in SC is limited only to the accessible surface causing lower capacities than that of batteries. Their accessibility to the intra-porous surface areas is influenced by the tailoring of the dimensions [12] (1-D, 2-D and 3-D) of the material and interconnected pore structures with nano-micro pores enhancing capacitances and meso-macropores facilitating ion diffusion [47], [48]. Therefore, a desirable pore size distribution of the electrode with complementing electrolyte of matching radius size is an important factor to optimize in order to effectively utilize the carbon's surface area[49]. Otherwise, electrolyte ions will have difficulty to access the carbon's smaller porous walls.

B. Pseudocapacitors

Pseudocapacitors store charge by redox reactions of surface attached ions on the electroactive electrode material. In contrast to EDLCs which store the energy electrostatically, the pseudocapacitors store the charges by the occurrence of surface Faradaic reactions via successive transfer of electron charges at the electrode's reactive sites. Metal oxides (such as, MnO_2, RuO_2, Fe_3O_4, V_2O_5, NiO, etc) and conducting polymers (polypyrrole, polythiophene, polyaniline, etc.) are the commonly explored electrode materials showing pseudocapacitive behavior. For storing charge, their surface functional groups, defects and grain boundaries serve as effective reaction sites. Any metal oxide's theoretical pseudo-capacitance may be calculated as

$$C = \frac{n \cdot F}{M \cdot V} \qquad \text{(Equation 3)}$$

where n is the mean number of electrons transferred in a one-way redox reaction, F is the Faradaic constant (96,485 C/mol), M is the metal oxide's molar mass, and V is the working potential window. Metal oxides having a wide range of possible oxidation states and therefore a higher mean number of electrons for redox charge transfer are ideal as supercapacitor electrodes. RuO_2 has a maximum theoretical capacitance of 1400 F/g involving charge storage from protonation of multiple oxides (Ru^{2+}, Ru^{3+}, and Ru^{4+} couples) for conversion of OH^- to O^{2-} sites on the bulk in acidic medium. While considering practicality, agglomeration of these metal oxides considerably reduces their on-device specific capacitances. Similarly, the

capacitances of metal oxides such as MnO_2 (1370 F/g) are generated only by surface processes, without contributions from the crystal bulk. These only bulk-accessible reactions depend highly on the surface of the metal oxide and it is important to realize that it is difficult to tailor their surface areas. The Faradaic processes that occur on the electrodes are different depending on the type of electrolyte and may even influence the device's working potential window *V*. However, these reactions develop charge transfer resistances which affect the materials rate capabilities at higher scan rates or current densities. Thus, their long-term cycle stability is not as good as for EDLC electrodes.

C. EDLC/pseudocapacitor composites

As discussed before, the capacitances of pseudocapacitive metal ions are limited to contribution from the bulk's surface, which motivates their incorporation with high specific surface area EDLC materials. Carbon material's high electronic conductivity and surface area improves rate capability, and the redox reactions of metal oxides contribute with high capacitances. The advantages are brought together by decorating metal oxides on a carbon current collector in the form of composites. The transport channels depending on the carbon support promotes ion charge transfer. The ion transport time constant is calculated as

$$\tau = \frac{L^2}{D} \qquad \text{(Equation 4)}$$

where L denotes the ion transport length and D is the ion diffusion constant [50]. As a result, the carbon's appropriate pore size and electrolyte's short ion diffusion length to access the metal ions lower the ion transport barrier. Overall, the charge transport properties are enhanced in composites alongside cycle stability in comparison with their individual counterparts.

3.2. Classification of supercapacitors based on device configuration

The predominant classification based on SC configurations is symmetric, asymmetric and hybrid supercapacitors.

A. Symmetric and asymmetric supercapacitor

The symmetric configuration consists of a pair of capacitive or pseudocapacitive electrodes with identical chemical composition and mass. The asymmetric configuration is typically composed of a pair of different capacitive and pseudocapacitive electrodes (Figure 9).

Asymmetric SCs are an efficient strategy to extend the cell voltage. The main approach to extend voltage in symmetric devices is using electrolytes with high stable potential window such as organic electrolytes; aqueous electrolytes are usually limited by the water decomposition. However, choosing different metal oxides with higher over-potentials for hydrogen and oxygen evolution is yet another possible strategy to extend the potential window. Slight mass and composition imbalances between the two electrodes can cause inequalization of capacitance values due to the difference in electrolyte ions adsorbed at the positive and negative electrodes. This is again employed deliberately in supercapacitors of all configurations to widen and utilize the complete operating potential windows possible for the system.

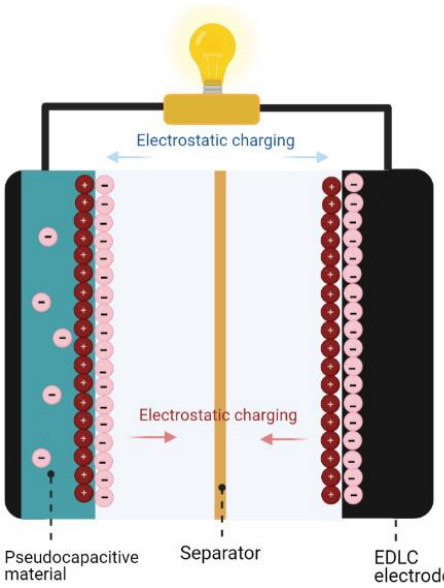

Figure 9. Schematic representation of an asymmetric configuration with different electrode materials as the anode and cathode.

The strategy for increasing the working voltage V by utilizing imbalanced electrode masses in an EDLC system is shown in equation

$$Q_+ = Q_- \qquad \text{(Equation 5)}$$

$$\frac{V_+}{V_-} = \frac{m_- C_-}{m_+ C_+} \qquad \text{(Equation 6)}$$

where Q_+ and Q_- are the charges, V_+ and V_- are the potential windows, C_+ and C_- are the specific capacitances, and m_+ and m_- are the masses of the positive and negative electrodes, respectively [51]. As from the equations, the electric charges of the both the electrodes are equal as they are connected in series. The specific capacitance and mass of the two electrodes define the potential windows for the electrodes. In a symmetric supercapacitor, one electrode reaches the potential limit before the opposite electrode without utilizing its full potential range. This is resolved by considering mass-balancing.

B. Hybrid supercapacitor

Combining both worlds together, the "hybrid supercapacitor" is a particularly promising battery-supercapacitor combination in the hunt for alternative electrochemical energy storage devices for use in e-mobility and for storing energy from renewable, abundant and cheap sources [52], [53]. Combining the pros of both systems, they can store nearly as much energy as traditional batteries and charge-discharge as rapidly as a SC [52].

A hybrid supercapacitor is considered a type of asymmetric supercapacitor. The configuration comprises a battery-like electrode (to enable high energy density) and a capacitor-like electrode (to provide high power) in the same cell. This integration benefits from the complementary capabilities of both systems as part of the efforts to close the energy-power gap. The hybrid systems' capacity is related to the porous carbon electrodes' EDL structure and the MO's Faradaic pseudocapacitance. In a LIC (Figure 10 b), the anode, which is typically the battery type electrode, has larger capacity to store energy (i.e., high energy density) by intercalation and de-intercalation of Li^+ ions within its crystalline structure limiting of the charge/discharge rate (i.e. low power density). On the other hand, the cathode is typically an EDLC material

with a well-interconnected porous structure. The fast and nondisruptive electrostatic phenomena enable high power and longer cycle life.

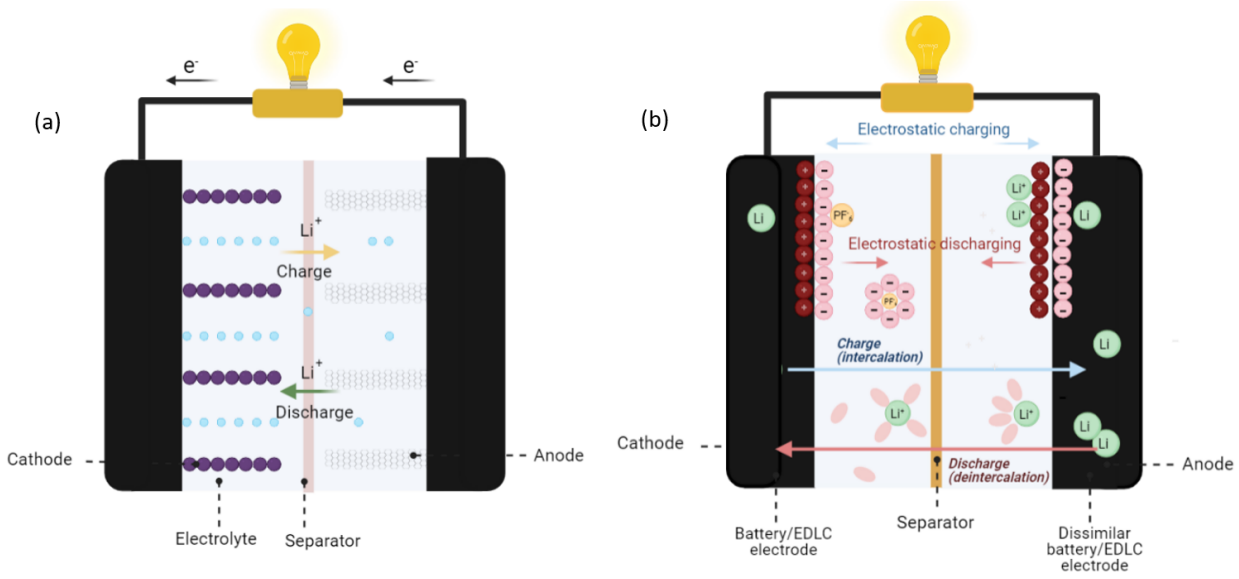

Figure 10. Schematic representation of (a) conventional lithium-ion battery and (b) hybrid configuration of lithium-ion capacitor.

The LICs compatibility with ionic liquids and organic electrolytes allows them to operate with much higher voltages [54]. In addition to modifying the electrode materials, redox electrolytes are as well employed as a technique to enhance battery-capacitor hybrids [52].

3.3. Deconvolution of different capacitive behaviors

The difference in charge storage mechanisms between supercapacitors and batteries varies largely because of their differences in thermodynamics and kinetics. As a result, for the convenience of evaluation numerous electrochemical techniques for deconvoluting the contributions from basic charge storage mechanisms such as the electrical double layer and diffusion-limited processes have been devised.

The general dependence of measured peak current (i_p) from a cyclic voltammogram measurement at different scan rates (v) is given as

$$i_p = a \cdot v^b \qquad \text{(Equation 7)}$$

Pseudocapacitors conventionally undergoing fast surface or bulk redox reactions are not diffusion-controlled and thus their peak current is known to vary linearly with scan rates as per Conway et al [55]. That is when in equation x, b is equal to or less than 1. While the storage process is diffusion-controlled, b is equal to $1/2$.

For systems exhibiting both forms of storage behavior i.e., hybrid energy storage, Dunn et al proposed deconvolution by observing the correlation of voltage dependent current with scan rates [56].

$$i_p = k_1 v + k_2 v^{1/2} \qquad \text{(Equation 8)}$$

k_1 (capacitive) and k_2 (diffusion controlled) are proportionality constants determined from the slope and Y-intercept of the plot of $i_p/v^{1/2}$ versus $v^{1/2}$ in Figure 11.

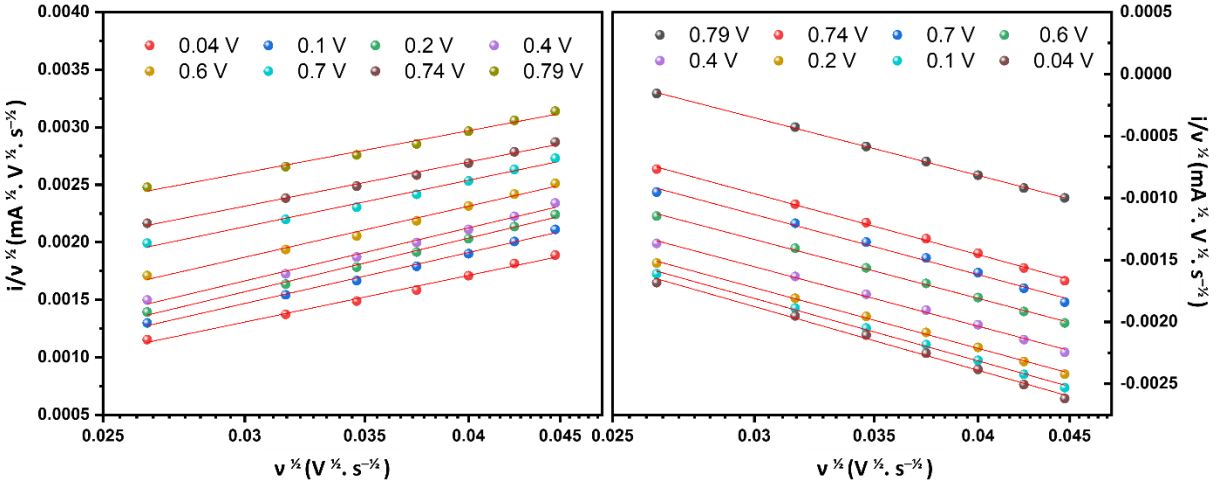

Figure 11. Linear fitting of the anodic and cathodic CV scan rates at different voltage points.

Similarly, Trasatti et.al, proposed deconvolution on observing the relationship of CV charge with varying scan rates [57]. A similar idea pertains to the diffusion-limited process at the bulk of even purely capacitive electrode materials, since raising the scan rate makes the inner surface, such as pores, less accessible for electrolyte ion diffusion. For these systems facing such kind of diffusive pattern to actively utilize the available surface area, the dependence of surface (Q_s) and bulk (Q_b) charge contributions was measured as total charge Q_t,

$$Q_t = Q_s + Q_b \qquad \text{(Equation 9)}$$

Considering that the voltametric charge Q at the surface of the material is independent of scan rate, charge is given as (when $v \to \infty$***):***

$$Q(v) = Q_s + C_1\, v^{-1/2} \qquad \text{(Equation 10)}$$

However, at lower scan rates, the charge at the surface and the bulk of the material is given as (when $v \to 0$):

$$\frac{1}{Q(v)} = \frac{1}{Q_t} + C_2\, v^{1/2} \qquad \text{(Equation 11)}$$

On an occasion when the system exhibits both forms of storage behavior it is considered as hybrid, and this is convenient to distinguish. The method modelled is suitable only for a limited range of smaller scan rates.

Donne et al. proposed a very different method, based on the current response from each potential step as a function of time [58]. The theory is based on the difference in equilibration time depending on the type of material. Materials showing EDL behavior equilibrates quickly while the diffusion limited behavior equilibrates slowly. Using the method is a good strategy to understand diffusion induced processes, especially to study efficiency of diffusion in electrodes with higher mass loadings. The SPECS (Step Potential Electrochemical Spectroscopy) model includes a current that represents the generation of an EDL at the geometric (i_{DL1}) and porous surface (i_{DL2}), as well as a current associated with the diffusion-limited (i_D) and residual processes (i_R) . The total current i_T of SPECS data may be calculated as follows:

$$i_T = i_{DL1} + i_{DL2} + i_D + i_R \quad \text{(Equation 12)}$$

Simon et al. proposed MUltiple Step ChronoAmperometry (MUSCA) [59], which was intended to decrease the ohmic drop contribution from SPECS to accurately investigate the electrochemical kinetic evaluation of a pseudocapacitive electrode. At various potential scan rates, ohmic drop corrected cyclic voltammograms of a pseudocapacitive electrode were computed using the MUSCA technique. The surface and bulk process current contributions were then recovered effectively using Dunn's methods by showing current-voltage curves with a decreased ohmic drop at various scan speeds.

3.4. Components of a supercapacitor

Electrode – Electrodes for supercapacitors are typically thin coatings that are electrically coupled to a conductive current collector. A material with good conductivity, high temperature stability, long-term chemical stability and corrosion resistance, and high surface areas per unit volume or mass is a good prospect for commercial electrode applications. Other advantageous properties include low-cost material extraction and production as well as environmental friendliness.

Figure 12. Schematic representation of a coin cell and its different components with some of their different electrode forms.

Carbon electrodes with high surface area micropores contribute more charge storage capability by forming EDLC than a planar carbon surface. Even better EDL formation is obtained in interconnected carbon fiber (Figure 12) or aerogel network [60] with higher migration rates of electrolyte ions into deeper layers. Electrodes with high mass loadings with more material are supposed to deliver high capacitances due to more available material for charge transfer. That is however not directly the case as much of the material is inaccessible to electrolyte ions. Also, a high mass loading creates increased electrical resistances between the electrode and current collector which may considerably affect the rate capability and specific power performance.

Separator - A conventional supercapacitor cell is built by connecting a pair of electrodes in series by separating them with an insulating separator. Although their primary goal is to keep the two electrodes apart to prevent electrical short circuits, the transfer of ionic charge carriers that are required to close the circuit during the passage of current in an electrochemical cell is its functional role. Different polymer membranes and cellulose based separators are used for SCs today [61], [62]. Cellulose filter paper membranes were employed as separators in Papers [I] and [II]. Their low cost, high flexibility, outstanding thermal, mechanical, and chemical stability, surface hydroxyl groups, and strong wettability make them suitable materials for use as separators and electrodes for SCs. When employed as a separator in a SC, the specific capacitance, energy density, and power density were found to be superior to those of SCs using commercially available separators [63].

Electrolyte – The predominant types of electrolytes employed in supercapacitors today are aqueous electrolyte, organic electrolyte, ionic liquids, and redox electrolytes. Aqueous electrolytes are the most utilized ones because of their low cost and excellent conductivity. Although ionic liquids and organic electrolytes are employed to broaden the potential window, they suffer from reduced conductivity and the hazardous nature of organic electrolytes [64]. Therefore, the choice of electrolyte is as influential as selecting a good electrode material to improve or control any SCs performance. To attain a maximum advantage, customizing the electrolyte based on the electrode type is critical.

Binders and additives- Typically carbon powders are brought together as an electrode by using suitable binders alongside conductive additives like carbon black (CB) to promote electrical conductivity. To fabricate robust free-standing electrodes from an environmentally friendly binder, micro fibrillated cellulose (MFC) material is tested (in Paper [II]) considering the environmental and biologically hazardous nature of other commonly used binders like PTFE, NMP, and PVDF. The electrodes composed of MFC binder are prone to cracking upon drying, especially with higher mass loadings, which leads to non-flexibility, and poor device stability. However, the LCF inclusions (shown in Figure 13) into the AC electrode with MFC binders not only increase flexibility but also contribute to better conductivity in the electrodes.

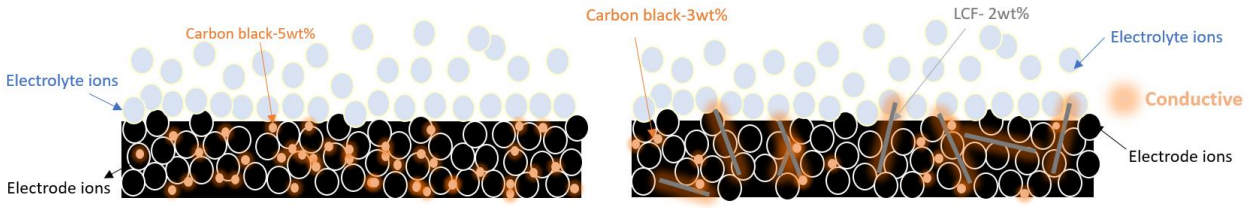

Figure 13. Comparison of electrodes with only CB additive vs LCF+CB additives (enacting as conductive pathways) (Paper II)

Lignin-based carbon fibers synthesized under optimized stabilization and carbonization conditions are well known for their higher graphitic nature suitable for better transport properties. On introducing them in the AC matrix, even randomly, allows them to serve as conductive pathways. Besides, they also serve as reinforcements to make the thicker electrodes flexible enough to handle.

3.5. Electrochemical test methods

Electrochemical testing encompasses analytical techniques to investigate cell systems by applying external electrical stimulation. It provides qualitative and quantitative responses useful for analyzing and understanding different behaviors of various surface and/or solution systems. For characterizing the electrochemical properties of a supercapacitor, cyclic voltammetry (CV), electrochemical impedance spectroscopy (EIS) and galvanostatic charge/discharge (GCD) are the commonly used analysis methods.

As a standard, electrochemical testing setups are three or two-electrode arrangements (Figure 14). A three-electrode system is used to manage and measure potentials and currents across a cell without altering the potential by huge currents passing through an electrode. The two-electrode setup delivers voltage across positive and negative electrodes immersed in electrolytes from an electrochemical workstation. In this case, the measured voltage is the whole cell voltage. In the three-electrode setup the current flows only between the working electrode (WE), and the counter electrode (CE), while the WE are referenced to a reference electrode (RE). In an idealistic situation, current flows only between WE and CE, and the WE's voltage is referenced to RE's. Common CEs include Pt, Au and REs includes saturated calomel electrodes (SCE), Ag/AgCl, and Hg/HgO electrodes with virtually constant half-reaction potentials. Three-electrode setups measure just half of the cell (or real-time WE potential) having an experimental advantage over two-

electrode setups. That is, potential changes in the working electrode are monitored independently of potential changes in the counter electrode.

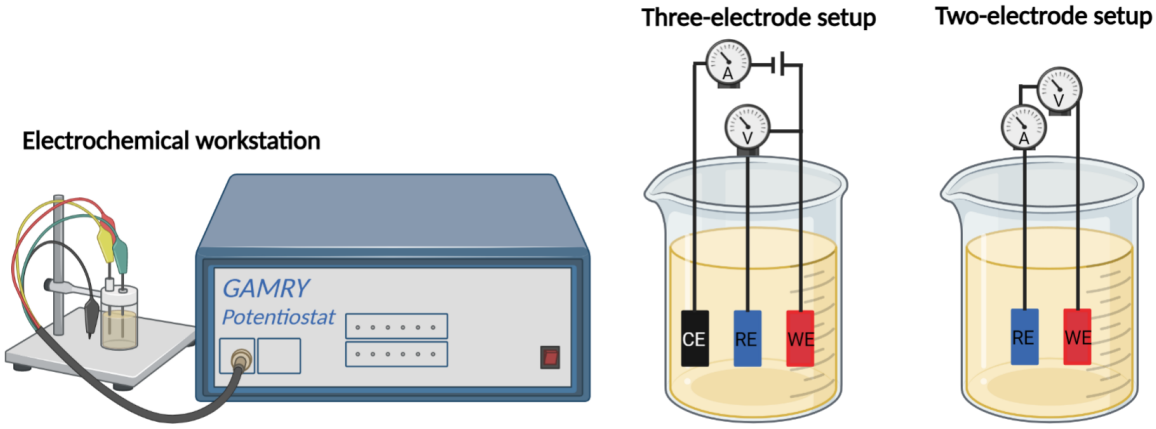

Figure 14. Schematic representation of an electrochemical workstation and the three and two-electrode setups used for electrochemical testing of supercapacitor electrode materials

All the electrochemical measurements were carried out in an electrochemical analyzer (Gamry Reference 3000AE electrochemical workstation) using a coin cell device system with electrolyte solution prepared in ambient conditions.

3.5.1. Voltammetric and galvanostatic charge-discharge methods

Cyclic Voltammetry (CV) is a potentiodynamic electrochemical technique where the potential of the analyzed electrode is ramped linearly versus time. During CV when the set potential is reached, the working electrode's potential ramp is inverted. This inversion occurs multiple times during an experiment as per the number of cycles given as input to run. The current of the working electrode is plotted versus the applied voltage to get the CV plot. A positive current peak implies oxidation, and a negative current peak implicates a reduction process at the working electrode.

In an EDLC, the specific capacitance is nearly linear over the full potential range showing a linear charge/discharge behavior in its CV curve. In fact, an EDLC capacitive behavior typically has a CV curve of rectangular shape as in Figure 15 a, whereas in pseudocapacitive materials potential-dependent redox reactions occur showing features in the characteristic curves Figure 15 b. EDLCs show constant rate of discharge whereas for pseudocapacitors the discharge rate depends on the redox reaction rate affected by potentials in Figure 15 c. Differences in CV for EDLCs from pseudocapacitors are very different when intercalation comes into the picture (Figure 15 d and e). Similarly, the slope from GCD in Figure 15 f is no more linear for both EDLC and pseudocapacitors. During galvanostatic cycling, the supercapacitor is charged and discharged at a constant applied current between two defined voltage points. The voltage recorded signifies the reactivity window of the device and the time refers the rate of charge/discharge. Also, this method in known to resemble real-world performance more closely than CV. Also, as clearly seen from Type C type of battery materials, show two pairs of distinct peak currents at which their redox reactions occur.

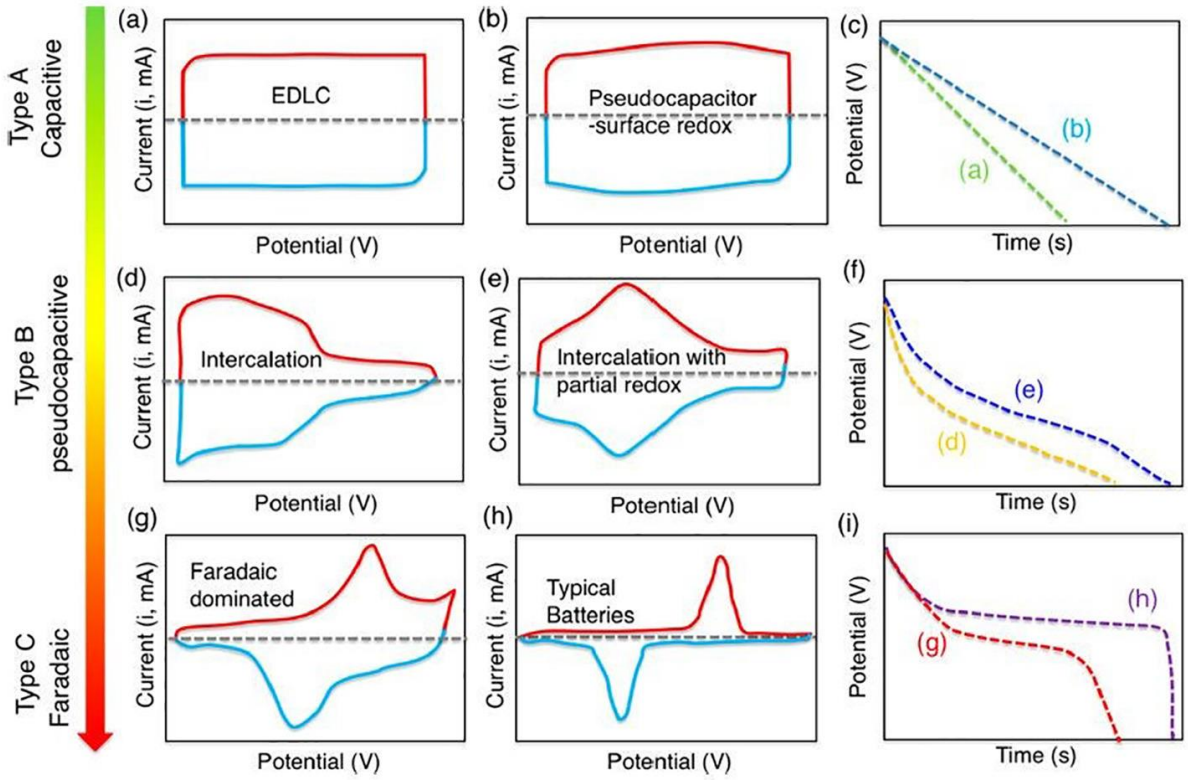

Figure 15. Schematic CV a), b), d), e) and g) with corresponding GCD c), f), and i) curves for EDLC (Type A), pseudocapacitor (Type B) and battery (Type C) materials, respectively. Capacitive trend in a pseudocapacitive materials is mostly either from (b) surface redox reactions or (d) intercalation-type. Also, there is a third special type with intercalation-type materials with broad redox peaks that are electrochemically reversible.

A. Cyclic voltammetry and galvanostatic charge discharge to measure capacitance

Capacitance is a quantitative measure of how much electrical charge a parallel plate capacitor can store when a particular voltage is applied across it. A supercapacitor's specific capacitance (C) measured in Farads (F) where Q is the amount of charge stored on the electrode, and V is the voltage across the electrode-electrolyte interface is represented as in Equation 1.

In a standard supercapacitor cell, the two electrodes separated by a separator are connected in series. Adding the 2 capacitors in series the total capacitance C_{cell} is obtained as,

$$\frac{1}{C_{cell}} = \frac{1}{C_1} + \frac{1}{C_2} \qquad \text{(Equation 13)}$$

On further accounting that both the electrodes are symmetric, i.e., C_1=C_2,

$$C_{cell} = \frac{C_e}{2} \qquad \text{(Equation 14)}$$

The capacitance under a standard electrode mass (m_e) is defined as specific capacitance (C_{sp})

$$C_{sp} = 2 \times \frac{C_{cell}}{m_e} \quad \text{(Equation 15)}$$

Accounting the mass of both electrodes (m_{tot}):

$$C_{sp} = 4 \times \frac{C_{cell}}{m_{tot}} \quad \text{(Equation 16)}$$

From CV curves when the integrated charge accumulated in the scanned potential window ΔV is Q, the specific electrode capacitance is obtained using the following equation:

$$C_{sp} = 4 \times \frac{Q}{m_{tot} \cdot \Delta V} \quad \text{(Equation 17)}$$

where $Q = \int_0^{2 \cdot \Delta V / v_s} |i| dV$

From GCD curves when the discharge time scanned between potential window ΔV is t at a particular current I_d, the specific electrode capacitance is calculated using:

$$C_{sp} = 4 \times \frac{I_d \cdot t_d}{m_{tot} \cdot \Delta V} \quad \text{(Equation 18)}$$

B. Energy density

The measure of energy that can be stored in a particular system, material, or region of space is referred to as its energy density. It can be expressed in terms of energy per volume (J/l) or energy per mass (J/kg).

$$E_{device} = \frac{C_{sp} \cdot {V_{max}}^2}{2} \quad \text{(Equation 19)}$$

Enhancing energy density in supercapacitors has been accomplished through a variety of approaches, ranging from improving electrode materials to developing asymmetric or hybrid device topologies with greater effectiveness. When energy is stated quantitatively, E indicates energy density, C represents specific capacitance, and V_{max} is a device's maximum operational voltage. It asserts that the energy in supercapacitors is proportional to capacitance (C) and the square of the maximum operating voltage (V^2_{max}). Increasing V_{max} is more economical for higher energy because of the quadratic connection. Using high-voltage electrolytes and developing novel device topologies are efficient methods for raising V_{max}. Asymmetric and hybrid device topologies with complementary working potentials from positive and negative electrodes make it easier to manufacture high voltage devices.

C. Power density

The quantity of energy delivered per unit of mass, area, volume per unit time by a particular system, material, or region of space is expressed as power density (W /kg). Furthermore, power density and efficiency are inextricably linked in power-delivery applications, and efficiency is still a driving factor in current engineering.

$$P_{device} = \frac{V^2}{4 \cdot R_s} = \frac{E_{device}}{t_d}$$ (Equation 20)

The power density (*P*) and energy density (*E*) of supercapacitors may be enhanced by lowering the equivalent series resistance (*R*) and expanding the operating potential window (*V*) as well as specific capacitance (*C*), as given by the above two equations.

D. Electrochemical impedance spectroscopy (EIS)

Electrochemical impedance spectroscopy is the method for generating Nyquist plots that depict the imaginary versus real components of the complex impedance of electrochemical cells. In any general Nyquist plot such as the one given in Figure 16, the starting point in the higher frequency domain of the Nyquist plot indicates the total ohmic resistance of the device, including ohmic resistance of the electrolyte within the separator. The radius of the semicircle in the mid-range frequency zone represents any type of electrolyte (or charge-transfer) resistance at the electrolyte/electrode interface. The inclined line connecting to the semicircle in the low frequency zone represents ion diffusion into the electrode**.**

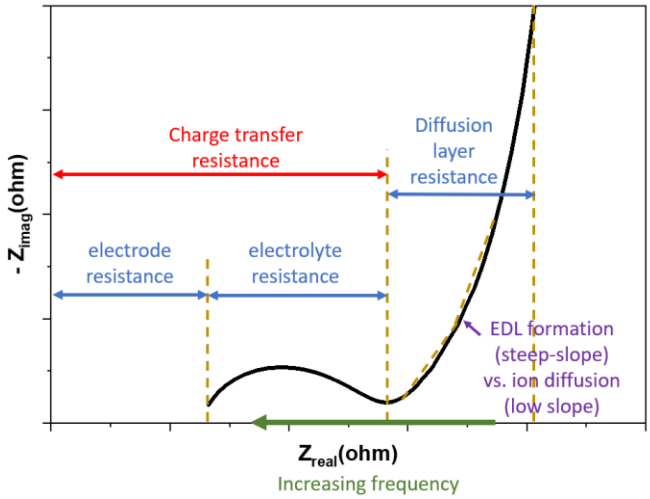

Figure 16. Nyquist plots of the impedance of a Randles circuit with Warburg impedance when the scale is orthonormal, and the low-frequency angle is 45°.

4. Compatibility of forest materials for supercapacitor applications

4.1. Lignin based materials as supercapacitor electrodes

This chapter describes the compatibility and performance of lignin derived materials for a supercapacitor application. Carbon fibers (CF) made from lignin precursors have a large specific surface area, decent mechanical flexibility, moderate electrical conductivity, and beneficial surface functions compared to particulate (such as AC) morphology counterparts. Electrospun lignin carbon fibers (ELCFs) are freestanding and useful as both a current collector and an active material, minimizing device contact resistance. In addition to electrostatic charge storage, which contributes to EDL capacitance, they exhibit contributions from the Faradaic reaction of their surface functional groups, which provides pseudocapacitance. The functional groups that contribute to capacitance are typically lost during high-temperature carbonization, also affecting the device's electrode-electrolyte interactions. In order to improve the electrochemical performance of the supercapacitor, the active material's surface is plasma treated to synergistically add controlled functional groups to the carbon matrix. The dependance of electrochemical profiles on the choice of electrolyte for lignin-based electrodes were specifically characterized in [Paper I].

Carbon fibers

There are great prospects for fibers with high carbon grade made from lignin since this is an abundant natural resource in contrast to viscose or petroleum pitch used to produce traditional carbon fibers. Lignin containing more carbon while holding a lower cost is yet more advantageous over the other sources to spin CF. However, the type of pretreatment and the manufacturing methods significantly influence their final properties and thus its suitability in various applications. The successful development of lignin technology will allow its use as a structurally lighter material in sectors such as automotive or aerospace, replacing existing commercial CFs derived from fossil-based derivatives. As desirable as it is, the development of this technology is equally challenging. The carbon fibers synthesized so far are not as stiff or strong as polyacrylonitrile (PAN) carbon fibers. However, this has not discouraged the interest to use them as carbon fiber precursor considering their function to add stiffness and strength in otherwise malleable tree cell wall. Therefore, with such motivations there is more to figure out on how to actively utilize this potentially prospective carbon rich, renewable, abundance and non-toxic natural resource.

With the existing research on developing lignin carbon fiber technologies, growing the manufacturing plant scales and production capacity will make it a cheap precursor. But still the LCFs are far from PAN-CFs achieved desirable properties. Therefore, though the available technology is scalable the competition for a CF with improved properties is still on.

4.2. From lignin to surface enhanced lignin carbon fibers

Spinnability of lignin is determined by the chemistry of separated lignin from its biomass. A variety of fibers with different structures and sizes are produced by performing different spinning techniques (such as melt-/wet-/dry-/electro-/spinning). These as-spun lignin fibers consisting mostly of organic matter has low mechanical strength and almost no conductivity. Their ability to conduct is therefore developed by following a sequence of thermal treatments in the order thermostabilization, carbonization, activation and graphitization processes. Further on, additional treatments are used to modify the surface morphology or chemistry to tailor on specific properties such as adhesion, wettability, etc. (requirements varying as per application specifics).

Lignin fractionation

The lignin has a lower molecular weight than polymers such as PAN, which makes electrospinning of the former challenging without co-polymerization with other major fossil-based polymers. Therefore, the lignin is either modified or separated based on molecular weight. Lignin fractionation is the process of dividing heterogeneous lignin into fractions with lower polydispersity, and these fractions distinct molecular weight distributions. The fraction with a greater molecular weight is preferable for spinning into

carbon fibers. The fractionation procedure described by Baker.et al. was practiced for electrospinning ELCF in [Paper I] [65]. The quantified molecular weight of lignin following the procedure is 8600 g/mol with a polydispersity index of 2.8. This high molecular weight lignin blended with polymers demonstrated significantly stronger interface connection bonds, boosting the spinnability of lignin-based polymers that furthermore improved the mechanical elastic modulus, tensile strength, and elongation characteristics of the fiber [66].

Electrospinning

Lignin, as well known, is made up of randomly dispersed aromatic units separated by aliphatic chains. Dissolving lignin in non-polymeric solvents for electrospinning does not allow for adequate chain entanglements, resulting in particle electrospraying. For lignin to be electro-spinnable, it is either blended with a secondary polymer, or solvent fractionated to eliminate low molecular weight fractions. Although the primary approach improves fiber properties, it raises the product cost. Hence the latter method involving fractionated parts of high molecular weight lignin in mixed with an organic solvent as described in Paper [I]. In order to obtain defined morphology of carbon fibers, the optimization of processing parameters such as the voltage, ambient humidity, needle size, needles distance from the collector, and spinning solution feed rate are critical [67].

Thermo-stabilization

Thermo-stabilization (TS) is an essential pre-step with the purpose to eliminate the precursor fibers' thermoplastic nature. Instead, the fibers develop thermosetting characteristics that prevent the fibers from fusing during high-temperature carbonization treatment. The most common method is an oxidative process, which entails a gradual increase in temperature in an open environment. The amount of oxidant, temperature, and heating rate all affect fiber oxidative stability. A stabilization process undergoes a variety of reeactions that decrease/eliminate the volatile compounds (such as oxidation, dehydrogenation, cyclization, elimination, condensation, and cross-linking). During TS in lignin, the reaction starts with hemolytic dissociation of the weakest β-O-4 linkage bond. It is followed by auto-oxidation that occurs in the temperature range of 200-250 °C producing carbonyl and carboxyl groups on its structure. On further increasing temperatures, these functional groups lose oxygen leading to cross-linking of the lignin structure forming, strong aromatic carbon bonds, anhydrides and esters [68].

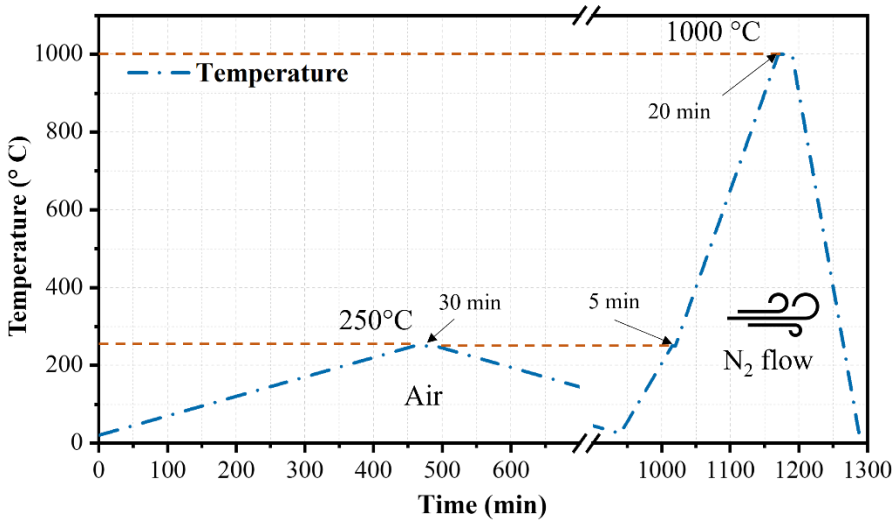

Figure 17. ELCFs carbonization profile; stabilization using Nabertherm box furnace and carbonization using Thermolyne - Open Tube/1600 °C furnace).

Typically softwood lignin having higher cross-linking than hardwood lignin which implies lower spinnability but achieves TS in shorter duration [69]. Regardless, lignin having higher carbon content makes TS of lignin fibers less energy and time-intensive process than TS of PAN fibers (16 hours to less than 2 hours at 250 °C) [70].

Carbonization

Carbonization is a popular method for transforming any form of organic raw materials via pyrolysis in temperatures typically between the range of 500 °C and 1200 °C that produces char (i.e. a bunch of cross-linked carbon atoms) enriched with high carbon content. This usually takes place in the absence of air in inert atmospheres. The porosity of the carbon material is controlled by influencing the heating rates, dwelling time and the reaction atmosphere in the heat treatment chambers. Prior to establishing a thermal treatment profile, thermogravimetric analysis (TGA) is performed by heating the organic raw material at a constant rate to determine its thermal stability and measure the loss of volatile components by its changing weight profile (Figure 18 a).

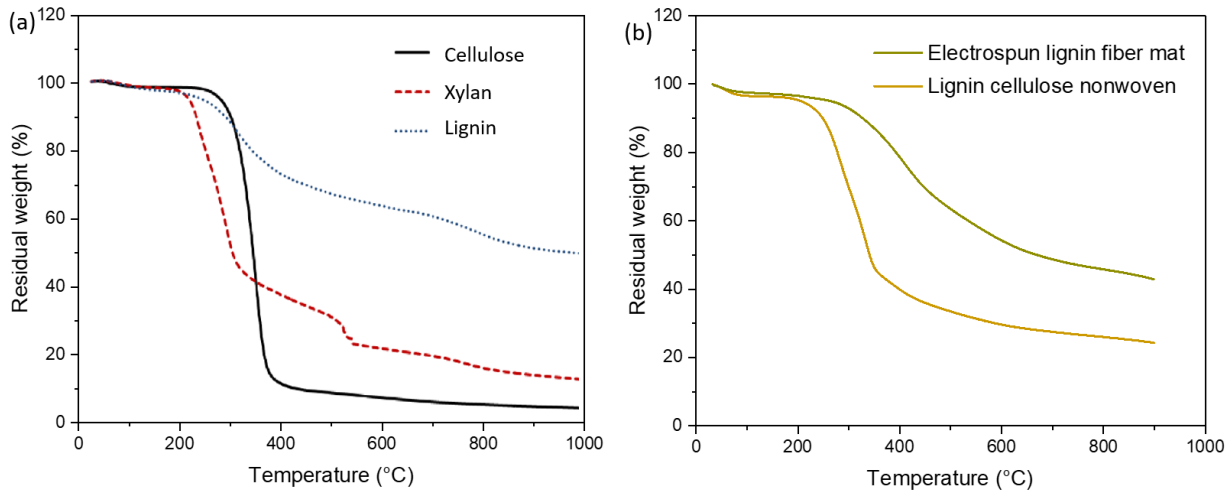

Figure 18. a) Weight loss profile from TGA of the major wood components [1] and b) lignin fiber and lignin cellulose composite nonwovens in a nitrogen atmosphere at a heating rate of 50 °C/ min

At lower temperatures reaching about waters boiling point 105 °C, moisture i.e., water that is chemically unbound evolves and then (-OH) breaks at higher temperatures up to 600 °C. At higher temperatures ranging from 190 to 800 °C: CO gas is produced by the thermal decomposition of carbonyl and carboxyl groups and CO_2 is produced by ether cleavage and carboxyl group decarboxylation reactions [71]. Between these temperature ranges starting about 500 °C until 1000 °C, also hydrogen gas evolves due to breakage and depolymerization of aliphatic and aromatic hydrocarbon bonds [71]. Through these reactions, aromatic carbon structures in biomass evolved gradually from non-condensed to condensed (aryl) structures. The types of reactions and thus the activated carbon yield is therefore highly influenced on the source of biomass as they contain varying amounts of lignin and cellulose. The controlling of heating rates is as important for crosslinking the aryl structures optimally to our advantage. Above carbonization temperatures of 1000 °C, the tensile strength decreases due to defects and a reduced fiber diameter [72]. Nevertheless, the inability to preserve the ordered carbon structure at higher temperatures leads to formation of functional porous morphologies with wide pore size distribution [73]. This can be used to benefit controlled pores by carefully optimizing the carbonization profile. The choice of secondary polymer is also critical for tailoring the carbon's porous structure with desirable pore size ranges [74]. In the ELCF spun without any fossil-based secondary polymer had a wide range of pore distribution with predominantly meso and mocropores (Figure 19 a).

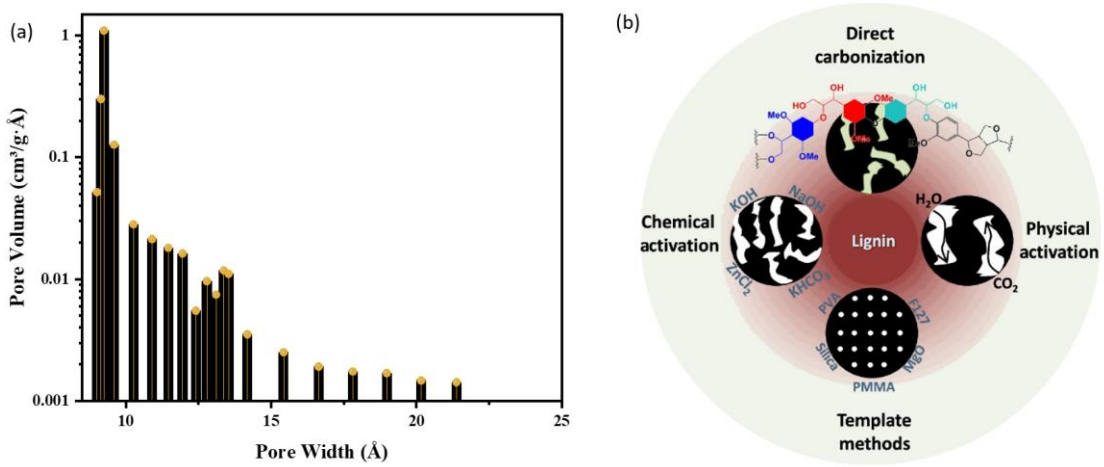

Figure 19. a) Pore size distribution in ELCF sample, b) Different pore engineering strategies for lignin-derived porous carbons [75].

More advanced pore engineering can be carried out by other routes such as templating and chemical activation involving various chemicals as shown in Figure 19 b.

Activation

Activated carbon is a highly adsorptive medium, that allows easy adsorption of organic molecules in its range of hierarchical or more ordered pores. To increase any organic raw materials adsorption capability, it is activated using physical or chemical treatments.

Physical or thermal activation produces activated carbon in two steps: the first is carbonization, which is the pyrolysis of carbonaceous materials at high temperatures in an inert atmosphere to remove most non-carbon atoms; the second is extended thermal activation in the presence of an oxidizing gas such as steam, carbon dioxide, or both. CO_2 activation causes etching of the carbon matrix surface developing abundant pores [75]. Chemical activation entails impregnating raw materials with dehydrating agents such as H_3PO_4 [76], KOH [77], NaOH [78], or $ZnCl_2$. Activation influencing the pyrolytic breakdown, delays char formation and results in a highly porous carbon-enriched solid.

Graphitization

Graphitization is the process of heating amorphous carbon over an extended length of time to restructure the atomic structure and obtain the ordered crystalline structure desirable to boost conductivity. In a fiber morphology graphitization aligns and orients the atoms along its axis. The process is undergone at much higher temperature ranges than activation to control atomic structuring as shown in the table below.

Less than 1300ºC	The amorphous carbon atom configuration has not changed significantly. Minimal structural alterations begin to occur.
1300ºC – 2000ºC	The crystal structure begins to form. This denotes atomic movement and rearranging. The interlaying spacing of atoms begins to reorganize and reduce to resemble that of graphite.
2000ºC – 3000ºC	To simulate graphite, crystal formation accelerates, and interlaying space reduces.

In the presence of oxidizing gases, atom rearranging in amorphous carbon is accelerated. This permits bonds to be broken in more disordered parts of the amorphous carbon. This comprises parts of the amorphous

structure where carbon to carbon bonds can be interconnected between stacked planes or other interwoven sections. Infact, over temperatures of 1600 °C, improved mechanical properties was observed due to the formation of nanocrystalline graphite [72], [79].

4.3. Surface enhancement of electrode

The performance of any EDLC materials typically shows high power densities. They can however drop considerably when there is poor accessibility for ions due to tortuous microporosity or non-graphitic carbon wall structures that creates ionic resistance. Surface modification of porous carbon materials is a valuable prerequisite to consider for effective adsorption and desorption of electrolyte ions both on the electrodes surface and in its bulk quickly without any accessibility issues. Although redox processes in pseudocapacitive materials are fast enough, the above conditions apply to utilize the surface confined reactions more effectively. The electrode/electrolyte interface could be altered also to increase cell voltage by designing passive layers on the carbon surface, which would move the electrolyte reduction and/or oxidation processes to greater over-voltages [80]. A solid electrolyte interphase (SEI) naturally occurs on the carbon surface of carbon anodes during the early cycles of a charge-discharge sequence. The SEI layer, which is created during the first cycle, blocks electrolyte ion intercalation into the carbon layers below while preventing further electrolyte reduction [80]. Designing, customized characteristics of the carbon surface (hydrophobic or hydrophilic groups, for example) might result in a significant over-voltage to expand the electrolyte's electrochemical stability window. Those techniques focused on modifying the carbon/electrolyte interface are obviously tempting in terms of performance improvements, but they are quite difficult. The surface modification must not modify or impede ion access to the porous carbon structure in the electrolyte. To facilitate ion transport from the electrolyte into the carbon pores, the modified carbon surface must be ionically conductive yet electrically insulating to reduce solvent oxidation and/or reduction at the carbon surface. The effective development of an artificial SEI-like layer on the surface of porous carbon would significantly improve EDLC performance.

Simple procedures like doping can help tailor the fundamental properties and improve the electrode’s compatibility to an electrolyte. The most used heteroatoms to dope into carbon frameworks are oxygen-functionalized nitrogen, boron, sulfur, phosphorus, fluorine, silicon, and chlorine [81]. The doping introduces defects acting as redox centers amplifying inherent pseudocapacitive contributions. In this way, doping also contributes to store more energy compared to a standard supercapacitor.

Nitrogen doping and oxygen functionalizing are two of the most common ways to modify a predominantly hydrophobic surface profile to hydrophilic. This does not change the nature of the material itself but only changes the polarity of the surface charge. The surface modification enhances the feature of electrode wettability to electrolytes. Wettability is an important criteria as insufficient electrode wetting of electrolytes leads to inconsistent reactions due to unsteady formation of the EDL interface. Nitrogen is incorporated into the carbon framework either by postprocessing with nitrogen rich components (ammonia, urea) or starting with a nitrogen rich precursor (like polyaniline, polypyrrole). Similarly, oxygen is introduced in a carbon matrix by simple non-degradational procedures like plasma treatment as in Paper [I].

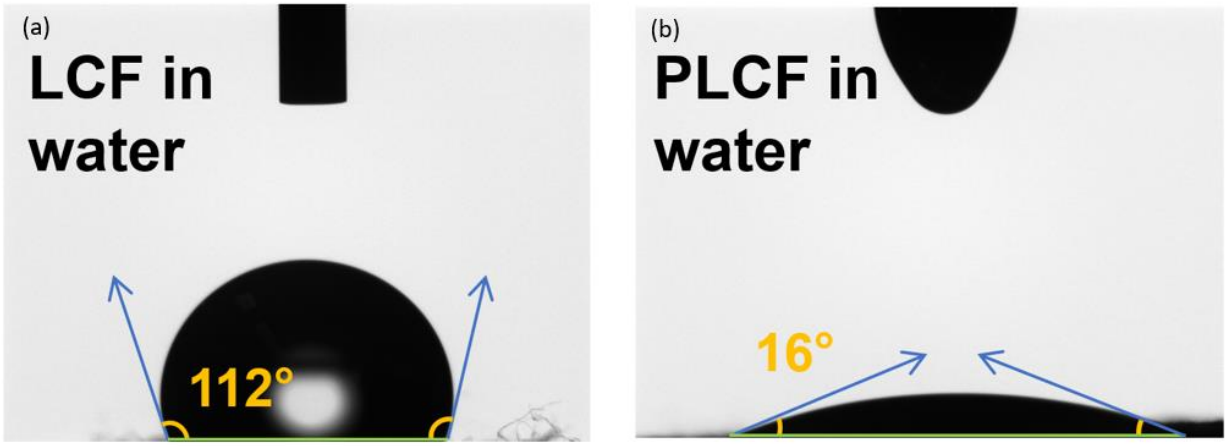

Figure 20. Wettability test to indicating a) hydrophobic nature of LCF mat samples before and b) hydrophilic nature after undergoing plasma treatment for 60s with 25W power.

Treating a carbon surface with plasma even for a shorter duration has been observed effective to eliminate hydrophobicity (Figure 20). This eventually allows access to internal surface area that otherwise goes unutilized.

4.3.1. Effect of O-functional groups on electrochemical behavior

The characteristics of an electrode's charge storage are significantly influenced by the electrolyte used. Only selective functional groups are redox-active in a particular type of electrolyte. For instance, only functional groups that evolve CO (hydroxyl, carbonyl, and lactone groups) contribute positively whilst CO_2 evolving groups (carbonyl, anhydride, and lactone groups) do not. Therefore, choosing the right electrolyte that stimulates the right groups is desirable.

Advantages

As aforementioned, some oxygen functional groups are more advantageous than others. The useful contributions may include

1. Oxygen configurations C-OH and C=O promoting hydrophilic of surfaces
2. Pseudocapacitive contribution of the introduced functional groups which depends on the electrolyte type. In fact, the electrochemical profile differs for the same electrode with varying electrolytes (Figure 21).

The quinone and carbonyl type oxygen produce pseudocapacitance in H_2SO_4 electrolyte involving the proton induced redox reaction (Equation 22) peaks in the CV curves [82].

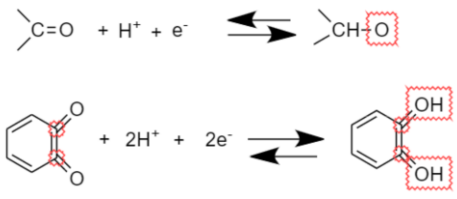

(Equation 22)

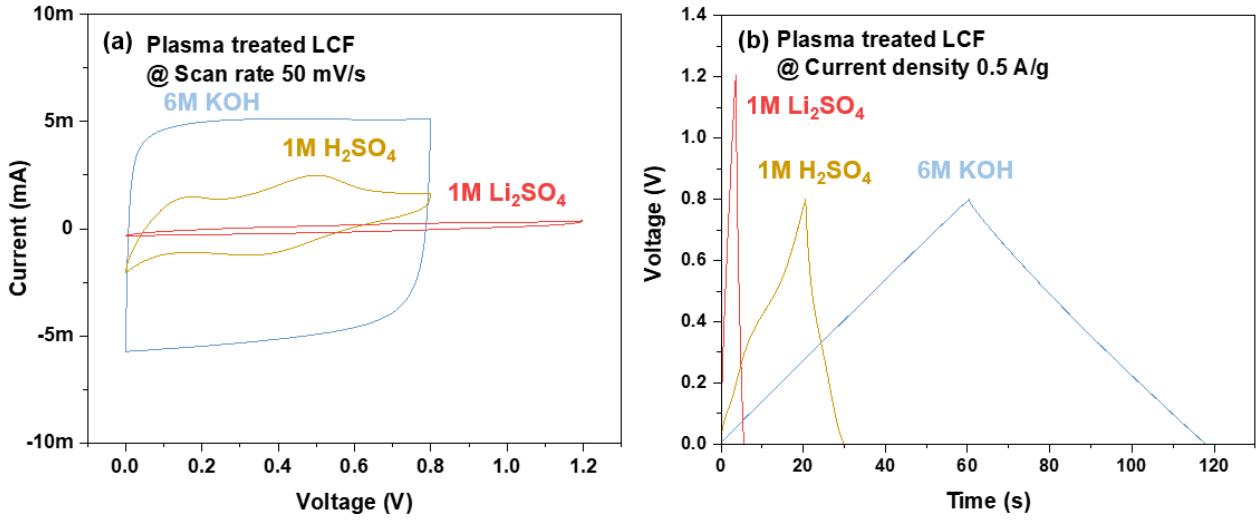

Figure 21. Electrochemical (a) CV and (b) GCD response curves of oxygen functional group introduced LCF in different aqueous electrolytes- KOH, Li_2SO_4, and H_2SO_4 electrolytes.

As from the X-ray photon spectra data on the oxygen configurations, the contributions here are from carbonyl and quinone groups. But on the other hand, it is mostly the carboxyl and hydroxyl groups that act as favorable sites for the KOH electrolyte to react (Equation 23).

(Equation 23)

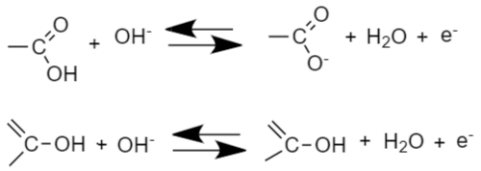

Though oxygen functionalization raises concerns of electrolyte decomposition, the PLCF electrodes performed well without hydrogen decomposition even at an increased voltage of 1 V

Disadvantages

Too high amounts of oxygen functional groups are not beneficial. They tend to have a detrimental effect on any electrode's performance in ways as

1. Aggravates already existing issue of self-discharge behavior with supercapacitors.
2. Increases internal resistivity by affecting their electronic conductivity.

When the disadvantages mentioned in points 1 and 2 prevail, the efficiency of tailored high surface area pores becomes compromised.

Metal oxide decoration

The conductivity of CNTs and the redox property of metal oxides can be exploited together as hybrid supercapacitors. Thus, a combination of metal oxide electrodeposition on nanostructures were tested expecting improved conductivity and electrochemical performance. As expected, their result showed enhanced efficiencies with higher capacitive performance due to increased available surface area for reactions to take place [15,16]. While carbon being the most explored material, efforts have also been taken to synthesize transition metal oxides and sulphides specifically in one-dimensional geometry [83], [84].

4.3.2. Electrochemical enhancement of capacitive behavior

As compared to other improvement strategies, electrochemical procedures are considered much simplified and mild procedures in a regular electrochemical setup. They have the advantage to enhance the structure, composition, property, or even morphology of materials by tuning basic parameters such as magnitudes of applied current or voltage, types, and concentrations of salts in electrolytes, reaction durations, and solution temperatures.

The performance of any supercapacitor is determined not only by the electrode materials but also by the electrolyte. The conductivity and temperature coefficient of electrolytes are the most significant features, as they influence the ESR and specific capacitance of a supercapacitor. Other characteristics include a broad voltage window, good electrochemical stability, high ionic concentration, low solvated ionic radius, low volatility, low viscosity, low cost, low toxicity, and high purity availability. The electrochemical potential window of supercapacitors is determined by the thermodynamic stability of electrolytes. In general, a broad electrochemical potential window leads to high energy and power densities. The electrolyte concentration must be high enough to prevent electrolyte depletion (the electrolyte starvation effect) during supercapacitor charging [85], [86]. A supercapacitor's performance will suffer if the electrolyte content is insufficient in comparison to the electrode surface area. Normally, electrolyte values with higher molarity are adequate. Because of the high mobility of OH- anion in water solutions, KOH has a high ionic conductivity [87].

Like the electrolyte starvation effect, inadequate range of electrode pore sizes combined with any attractive electrolyte is pointless if not accessible. This issue becomes more critical with higher scanning rates (or current densities) as observed from Figure 22.

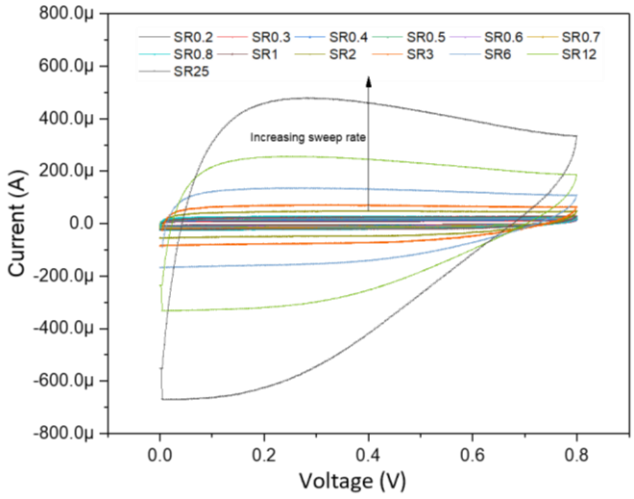

Figure 22. Pore starvation effect due to inaccessible pores in an electrode with wettability issues.

Ensuring proper interaction of electrode-electrolyte at the interface will resolve such issues enhancing mobility and hence charge storage efficiency particularly at high rates/currents. Over continuous cycling of charge-discharge the electrolyte ions intercalate and deintercalate repeatedly exposing available pores to more beneficial utilization as schematically represented in Figure 23. The influence becomes more effective on introducing beneficial heteroatoms like N and O in the carbon matrix.

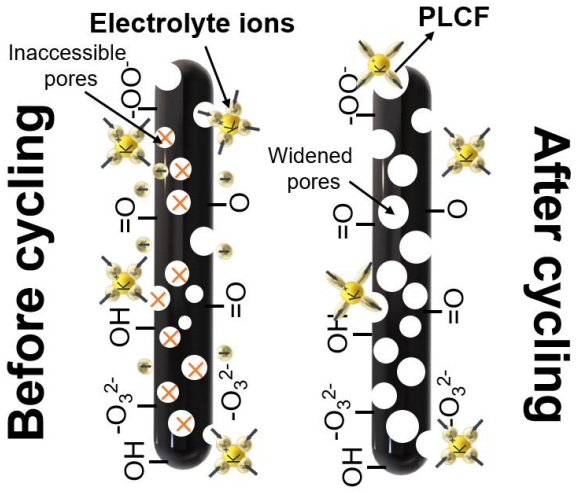

Figure 23. Schematic representation of the accessibility of solvated KOH electrolyte ions to unfit pores (red-crossed) after cycling over a series of continuous insertions and desertions in PLCF electrodes

During cycling, the ion diffusion paths are believed to be shortened, and at the same time given access to more EDL surface area from the opening of pores which are otherwise non-contributing. Too many or unfavorable functional groups can have a deteriorating effect due to increased ESR. An optimum amount of these active groups promotes good interface properties and capacitances, like the addition to pseudocapacitance discussed earlier. This has been identified to have a positive effect by increasing the capacitances of the samples after cycling (Figure 24).

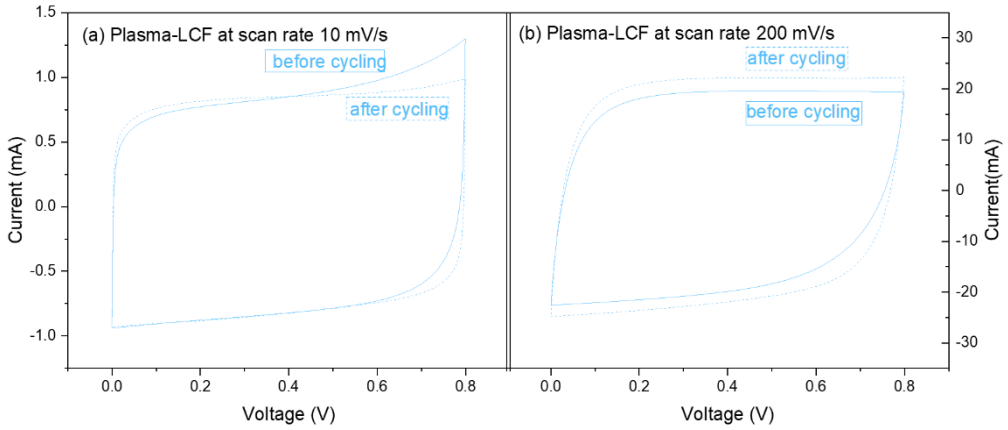

Figure 24. CV curves of PLCF at scan rate (a) 10 mV/s and (b) 200 mV/s

During electrochemical testing of an electrolytic cell, the electrode material undergoes a combination of processes like oxidation, reduction, ion intercalation and so. These oxidations and reductions especially limit the electrochemical stability window significantly for supercapacitors with aqueous electrolytes. This also limits their energy density.

EDL capacitance of carbon materials tends to significantly improve by electrochemical activation by extending the applied voltage [88]. Various strategies are used to increase the working voltage of aqueous electrolytes, including the use of redox-active additives, pH control of electrolytes, the use of water-in-salt electrolytes, and the identification of highly stable electrolyte salts [89]. Even operating a device with aqueous electrolyte near to electrolysis modifies the original state of the cathode and anode system

differently. This effect is identified to improve the capacitance of the device while testing at a voltage below the level for electrolysis. The effect was observed distinctly only for the electrodes functionalized with oxygen groups.

4.5. Electrode commercialization

4.5.1. Goal towards thicker electrodes

For any supercapacitor design, a thick electrode with high areal mass loading is preferred due to its benefits in increasing the supercapacitor device's energy density. Optimizing packing density of the electroactive electrode materials, lowers the excessive inactive material cost by avoiding or somehow utilizing them. During practical applications, a supercapacitor is made up of materials more than electrode materials such as a current collector, electrolyte, binders, additives, separator, and package. Commercial supercapacitors have an active electrode material coating of about 10 mg/cm^2 with 0.1- 0.2 µm thickness [90]. Current collectors containing the active material are an expensive component that comprises huge weight proportion in a device. They are available in form of graphite, aluminum, stainless steel, carbon foils and even foams made of nickel that allows easier percolation. Secondly it is the electrolyte that is an essential component that is needed in high dose for highly porous and thick electrodes.

Electrode materials with lower mass loading and electrode thickness store lower amount of energy per unit device weight due to fewer active sites. Increasing them seems to be a simple way to increase the capacitance and energy density of electrodes and/or devices. However, increased mass loading or electrode thickness has a detrimental effect on specific capacitance rate performance, cycling and structural stability of the electrode materials due to decreased accessible surface area (active sites), increased charge-transfer resistance [91], sluggish ion transport channels, and even electrolyte wettability issues (Figure 25) [90].

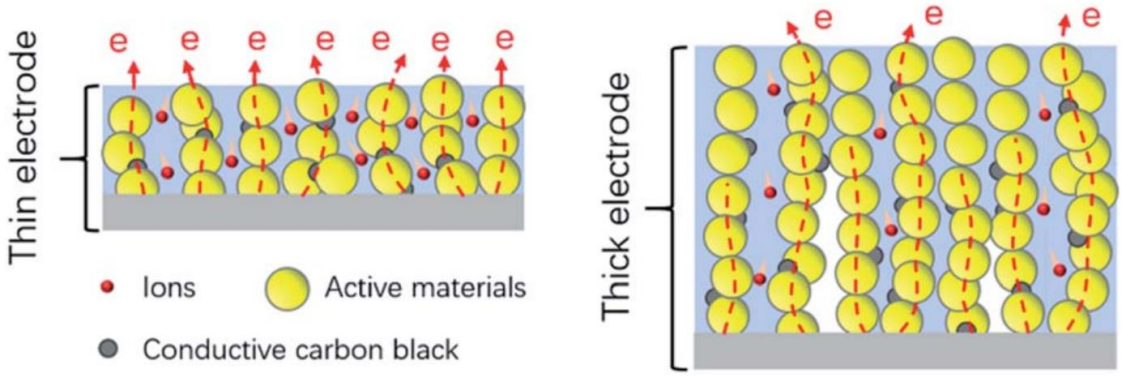

Figure 25. Electron and ion transport and electrolyte wetting in thin and thick electrodes are depicted schematically. The electron and ion transport channels are severely blocked and are inaccessible to the electrolyte in the thick electrode.

Highly porous materials lack such interconnectivity due to broken electrical conductivity networks. Addition of conductive carbon materials is a way to re-build conductivity pathways. Materials such as graphene quantum dots, graphene sheets (Figure 26), carbon fibers (Paper II) have been introduced into an activated carbon matrix and increase the capacitances and rate capability with improved charge transfer kinetics and efficient ion migration [92]. These conductive structures in electrodes also reduce the resistances arising from improper contact to the current collector due to poor binding and mechanical stability.

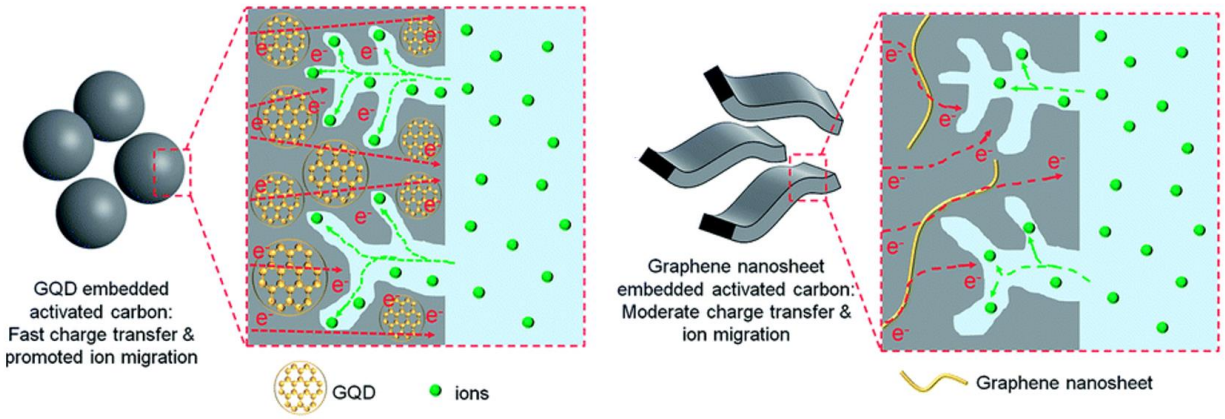

Figure 26. a) Graphene quantum dots and b) graphene nanosheets acting as electron transfer highways in activated carbon matrix by significantly promoting electron transport through the particles improving the utilization of the large surface area.

Fracturing of electrodes with high mass loading of active material is an issue. Employing robust electron conducting interconnected structures such as carbon nanofibers is a way to achieve mechanical strength, which is critical for long-term cycling and flexibility of the electrodes.

Although conductive materials like carbon black (CB) create electronic pathways in between particles, they are broken as their frequency of contact with these particles is reduced at several points in thicker electrodes. Introducing 2 wt% of longitudinal 1-D conductive carbon fibers alongside 3 wt% CB increases the surface contact creating multiple electron transport channels. The capacitances of AC improved from 85 F/g to 97 F/g under a mass loading of 5 mg/cm^2 (Paper II). With higher mass loadings the charge transfer resistance of the electrodes considerably reduces. In thicker electrodes, these fibers act as reinforcements that could keep larger masses of material together without falling apart. To some extent flexibility can also be induced on these electrodes on choosing stronger binders.

4.5.2. Overcoming self-discharge

Although much research in supercapacitors focuses on improving the energy and power densities, self-discharge is a concern where studies show that the voltage of commercial supercapacitors can decrease by 5 ~ 60% in only two weeks [93]. As a result, supercapacitors' use in long-term energy storage is severely limited. Supercapacitor self-discharge is a thermodynamically spontaneous voltage decay process that is monitored with discharging time after disconnecting from a power supply source. Ion concentration and potential field gradients at the electrode surfaces induce this unwanted feature in supercapacitors. It is mostly due to inhomogeneous charge redistribution, parasitic Faradaic reaction, and ohmic leakage. The desorption of charges from the electric double layer at the electrode surface causes charge redistribution, resulting in continual potential decay. The oxidation or reduction of redox active species or functional groups of electrodes or electrolytes is referred to as a parasitic Faradaic reaction. Ion diffusion has a significant impact on both charge redistribution and Faradaic processes. So far, research has mostly centered on changing electrode materials [94], electrolytes [95], [96], and, more recently, separators for self-discharge suppression [97], [98].

When charging carbon or metal oxide electrodes, charge distribution disparity develops because the collector charges faster and can achieve the required voltage faster than the inner surface. Extended charging lets the ions to distribute themselves more uniformly across the surface, reducing voltage decline during the rest time after charging [99]. Charge redistribution is classified into two types based on the rate-limiting process: diffusion-limited and resistance-limited. During the delay, charges diffuse on or near the surface of the electrode materials, whereas the latter is caused by a variety of resistance factors (e.g., pore accessibility resistance). Furthermore, the rate of self-discharge is affected by variables such as starting

voltage, temperature, charge time, and device operation history. In (Paper I) with the history of cycling PLCF, the self-discharge behavior of the device reduced noticeably giving the idea of possible time for ions to distribute across the available surface area which was previously obstructed by the introduced functional groups.

Typically, functional groups are known to aggravate the behavior of self-discharge causing unwanted side-reaction during supercapacitor rest time. They are classified as activation-controlled and diffusion-controlled responses. The presence of relatively large concentrations of impurities in the electrode or electrolyte causes the activation-controlled process where a potential-dependent redox reactions occur on the EDL. Self-discharge reduces over repeated cycling as the impurities get consumed during the initial cycles. When the supercapacitor is overcharged beyond the electrolyte decomposition potential limit, the activation-controlled reaction is activated.

Infact, the self-discharge varies with differences in pH based on the active redox reactions that occur with the surface functional groups. Therefore, their self-discharge in different aqueous electrolytes, be it basic, acidic or neutral is going to have a different rate and needs to be tested every time a new electrode is introduced.

‘

Conclusion

The performance of SC outperforms conventional energy storage systems like batteries and fuel cells in terms of long lifespan, good reversibility, high power density, shelf life, efficiency, operating temperatures, environmental friendliness, safety, and cost effectiveness.

Failing to optimize or access electrode surfaces largely inhibits the materials ability to perform at its best in a SC device. This thesis gives insight on the ways to overcome these challenges by effectively implementing strategies to efficiently reduce internal resistances caused by electrode-electrolyte interface and increased electrode mass loading. They have been quantified as potential possibilities for improving the SC's energy and performance. Additionally, the creation of carbon materials derived from affordable precursors has recently piqued the interest of the research community. The experimental work in the thesis reports a device's electrochemical performances by overcoming electrode surface wettability issues (Paper I) and by accessing deeper electrode layers in electrodes with high mass loading (Paper II) The electrochemical outcome of the ELCF is improved by addressing the wettability issues on performing a simple and short surface plasma treatment. On introducing desirable oxygen functional groups on the electrode surface, the capacitance was significantly improved. A higher power density was retained in PELCF without compromising the device's rate capability and cycling stability. Depending on the reactive species of the functional groups to electrolytes of different pH, their charge storage behavior was noticed to be varied. The importance of wettability by exposing more active surface area in electrodes is quantified by deconvoluting the capacitance contributions depending on both surface and diffusion-limited processes. Furthermore, the possibility to enhance the electrochemical performance via applying a voltage of 1.2 V and 10 000 cycles is described.

To approach energy storage capabilities as high as batteries, efforts have been taken to make thick SC electrodes. Such electrodes with high areal mass loading maximize the potential surface area of the electroactive cathode and anode materials while lowering the manufacturing cost by reducing the number of inactive material layers. The added-on surface area from more material becomes pointless if remains inaccessible for the electrolyte for charge storage or reaction. Herein, a new attempt to introduce hair like lignin-derived carbon fiber (LCF) inclusions were successfully attempted. Also, the fabricated electrodes were using the environmentally friendly binder microfibrillated cellulose (MFC), which showed stability even under high mass loadings with decent amount of flexibility. The increased capacitance in LCF incorporating electrodes was attributed to improved conductivity. The LCFs act as an intermediate layer among AC particles and serve as conductive pathways, facilitating exposure of more active surfaces to the electrolyte.

Future work

Besides improving electrolyte wettability, the plasma treatment introduced oxygen reaction sites, which are expected to be anchoring sites for depositing pseudocapacitive or other conductive materials. Therefore, in order to further enhance the performance of ELCFs utilizing them as carbon support for MOs will be a desirable step.

Further on, One of our ongoing projects with hopeful aims of electrode application concerns the extraction of lignin from hardwood black liquor is to fabricate low cost bio-based carbon fibers (CF) combined with cellulose. The nonlinear molecular structure of pure lignin, combined with its low flexibility, makes spinning difficult. However, attaining a larger carbon yield by carbonization from exclusively pure cellulose-based CFs is challenging as lignin is more carbon rich. Apart from its better thermal stability owing to the numerous aromatics, carbon-carbon bonds, and ether groups in its structure, lignin is favorable to carbonize at higher temperatures than cellulose. Research into the synthesis of nanomaterials from cellulose and/or lignin separately is plentiful, but the study of combined cellulose-lignin materials is yet not. Similarly, investigations and development of lignin-cellulose materials in different forms like carbon fiber, activated carbon, carbon nanotubes, and porous carbon structures are potentially yet to be pursued. Exploring them might be beneficial in order to build greener and more efficient electrodes. Furthermore, these macroscopic hair-like inclusions by themselves are capable of being used as electrode material by utilizing their morphology in advanced device configurations like spin yarn supercapacitors for flexible and wearable electronics.

References

[1] P. Sreevani, "Wood as a renewable source of energy and future fuel," presented at the international conference on Renewable Energy Research and Education (RERE-2018), Andhra Pradesh, India, 2018, p. 040007. doi: 10.1063/1.5047972.

[2] H. I. Becker, "Low voltage electrolytic capacitor," 423,042, 1957

[3] B.E. Conway, *Electrochemical Supercapacitors*. New York, U.S.: Kluwer Academic, 1999.

[4] S. Trasatti and G. Buzzanca, "Ruthenium dioxide: A new interesting electrode material. Solid state structure and electrochemical behaviour," *J. Electroanal. Chem. Interfacial Electrochem.*, vol. 29, no. 2, pp. A1–A5, Feb. 1971, doi: 10.1016/S0022-0728(71)80111-0.

[5] G. Zubi, R. Dufo-López, M. Cavalho, and G. Pasaoglu, "The lithium-ion battery: State of the art and future perspectives," *Renew. Sustain. Energy Rev.*, vol. 89, pp. 292–308, 2018.

[6] N. Nitta, F. Wu, J. T. Lee, and G. Yushin, "Li-ion battery materials: present and future," *Mater. Today*, vol. 18, no. 5, pp. 252–264, 2015.

[7] E. Gratz, Q. Sa, D. Apelian, and Y. Wang, "A closed loop process for recycling spent lithium ion batteries," *J. Power Sources*, vol. 262, pp. 255–262, Sep. 2014, doi: 10.1016/j.jpowsour.2014.03.126.

[8] T. R. Jow, S. A. Delp, J. L. Allen, J.-P. Jones, and M. C. Smart, "Factors Limiting Li+ Charge Transfer Kinetics in Li-Ion Batteries," *J. Electrochem. Soc.*, vol. 165, no. 2, pp. A361–A367, 2018, doi: 10.1149/2.1221802jes.

[9] J. S. Edge *et al.*, "Lithium ion battery degradation: what you need to know," *Phys. Chem. Chem. Phys.*, vol. 23, no. 14, pp. 8200–8221, 2021, doi: 10.1039/D1CP00359C.

[10] J. Partridge and D. I. Abouelamaimen, "The Role of Supercapacitors in Regenerative Braking Systems," *Energies*, vol. 12, no. 14, p. 2683, Jul. 2019, doi: 10.3390/en12142683.

[11] W. Jing, C. Hung Lai, S. H. W. Wong, and M. L. D. Wong, "Battery-supercapacitor hybrid energy storage system in standalone DC microgrids: areview," *IET Renew. Power Gener.*, vol. 11, no. 4, pp. 461–469, Mar. 2017, doi: 10.1049/iet-rpg.2016.0500.

[12] Y. Wang, Y. Song, and Y. Xia, "Electrochemical capacitors: mechanism, materials, systems, characterization and applications," *Chem. Soc. Rev.*, vol. 45, no. 21, pp. 5925–5950, 2016, doi: 10.1039/C5CS00580A.

[13] D. H. P. Kang, M. Chen, and O. A. Ogunseitan, "Potential Environmental and Human Health Impacts of Rechargeable Lithium Batteries in Electronic Waste," *Environ. Sci. Technol.*, vol. 47, no. 10, pp. 5495–5503, May 2013, doi: 10.1021/es400614y.

[14] W. Jing, C. H. Lai, W. S. H. Wong, and M. L. D. Wong, "A comprehensive study of battery-supercapacitor hybrid energy storage system for standalone PV power system in rural electrification," *Appl. Energy*, vol. 224, pp. 340–356, Aug. 2018, doi: 10.1016/j.apenergy.2018.04.106.

[15] B. L. Ellis and L. F. Nazar, "Sodium and sodium-ion energy storage batteries," *Curr. Opin. Solid State Mater. Sci.*, vol. 16, no. 4, pp. 168–177, Aug. 2012, doi: 10.1016/j.cossms.2012.04.002.

[16] H. Lu and X. S. Zhao, "Biomass-derived carbon electrode materials for supercapacitors," *Sustain. Energy Fuels*, vol. 1, no. 6, pp. 1265–1281, 2017, doi: 10.1039/C7SE00099E.

[17] C. Chen and L. Hu, "Nanocellulose toward Advanced Energy Storage Devices: Structure and Electrochemistry," *Acc. Chem. Res.*, vol. 51, no. 12, pp. 3154–3165, Dec. 2018, doi: 10.1021/acs.accounts.8b00391.

[18] S. Mehta, S. Jha, and H. Liang, "Lignocellulose materials for supercapacitor and battery electrodes: A review," *Renew. Sustain. Energy Rev.*, vol. 134, p. 110345, Dec. 2020, doi: 10.1016/j.rser.2020.110345.

[19] D. R. Lobato-Peralta *et al.*, "A review on trends in lignin extraction and valorization of lignocellulosic biomass for energy applications," *J. Clean. Prod.*, vol. 293, p. 126123, Apr. 2021, doi: 10.1016/j.jclepro.2021.126123.

[20] "SAFETY DATA SHEET -Lithium-ion and Lithium-ion Polymer Batteries (Li-ion Batteries)." Motorola Solutions. [Online]. Available: https://www.motorolasolutions.com/content/dam/msi/docs/about-us/cr/lithium-ion-and-lithium-ion-polymer-batteries-li-ion-batteries-sds-us-english.pdf

[21] D. Bresser, D. Buchholz, A. Moretti, A. Varzi, and S. Passerini, "Alternative binders for sustainable electrochemical energy storage – the transition to aqueous electrode processing and bio-derived polymers," *Energy Environ. Sci.*, vol. 11, no. 11, pp. 3096–3127, 2018, doi: 10.1039/C8EE00640G.
[22] S. Shahzad *et al.*, "Ionic Liquids as Environmentally Benign Electrolytes for High-Performance Supercapacitors," *Glob. Chall.*, vol. 3, no. 1, p. 1800023, Jan. 2019, doi: 10.1002/gch2.201800023.
[23] "https://honeywellaidc.force.com/supportppr/s/article/Do-Capacitors-reside-under-the-dangerous-good-regulations-DGR."
[24] L. A.-W. Ellingsen, G. Majeau-Bettez, B. Singh, A. K. Srivastava, L. O. Valøen, and A. H. Strømman, "Life cycle assessment of a lithium-ion battery vehicle pack," *J. Ind. Ecol.*, vol. 18, no. 1, pp. 113–124, 2014.
[25] D. A. Notter *et al.*, *Contribution of Li-ion batteries to the environmental impact of electric vehicles*. ACS Publications, 2010.
[26] J. F. Peters, M. Baumann, B. Zimmermann, J. Braun, and M. Weil, "The environmental impact of Li-Ion batteries and the role of key parameters–A review," *Renew. Sustain. Energy Rev.*, vol. 67, pp. 491–506, 2017.
[27] M.Wang, Q.Tan, Q.Huang, L.Liu, J.Chiang, and J.Li, "Converting spent lithium cobalt oxide battery cathode materials into high-value products via a mechanochemical extraction and thermal reduction route," *J. Hazard. Mater.*, vol. 413, p. 125222, 2021.
[28] "how many cycles can you get out of a lithium-ion battery?" [Online]. Available: https://au.renogy.com/blog/everything-you-need-to-know-about-lithium-battery-charging cycles/#:~:text=A%20lithium%2Dion%20battery%20can,voltage%20near%20the%20danger%20point.
[29] P. Kreczanik, P. Venet, A. Hijazi, and G. Clerc, "Study of Supercapacitor Aging and Lifetime Estimation According to Voltage, Temperature, and RMS Current," *IEEE Trans. Ind. Electron.*, vol. 61, no. 9, pp. 4895–4902, Sep. 2014, doi: 10.1109/TIE.2013.2293695.
[30] D. B. Murray and J. G. Hayes, "Cycle Testing of Supercapacitors for Long-Life Robust Applications," *IEEE Trans. Power Electron.*, vol. 30, no. 5, pp. 2505–2516, May 2015, doi: 10.1109/TPEL.2014.2373368.
[31] K. Liu, Y. Liu, D. Lin, A. Pei, and Y. Cui, "Materials for lithium-ion battery safety," *Sci. Adv.*, vol. 4, no. 6, p. eaas9820, Jun. 2018, doi: 10.1126/sciadv.aas9820.
[32] D. Di Francesco *et al.*, "Debottlenecking a Pulp Mill by Producing Biofuels from Black Liquor in Three Steps," *ChemSusChem*, vol. 14, no. 11, pp. 2414–2425, Jun. 2021, doi: 10.1002/cssc.202100496.
[33] "Stora Enso and Northvolt partner to develop wood-based batteries," *Stora Enso and Northvolt partner to develop wood-based batteries*, Jul. 22, 2022. https://northvolt.com/articles/stora-enso-and-northvolt/
[34] "Lignin Market Size, Share & Trends Analysis Report By Product (Ligno-Sulphonates, Kraft, Organosolv), By Application (Macromolecule, Aromatic), By Region, And Segment Forecasts, 2020 - 2027." Feb. 2020. [Online]. Available: https://www.grandviewresearch.com/industry-analysis/ligninmarket#:~:text=The%20global%20lignin%20market%20size,revenue%2C%20from%202020%20to%202027.&text=In%20addition%2C%20the%20well%2Destablished,likely%20to%20support%20the%20market.
[35] M. Kienberger, S. Maitz, T. Pichler, and P. Demmelmayer, "Systematic Review on Isolation Processes for Technical Lignin," *Processes*, vol. 9, no. 5, p. 804, May 2021, doi: 10.3390/pr9050804.
[36] J. Becker and C. Wittmann, "A field of dreams: Lignin valorization into chemicals, materials, fuels, and health-care products," *Biotechnol. Adv.*, vol. 37, no. 6, 2019, doi: 10.1016/j.biotechadv.2019.02.016.
[37] I. De Bari, A. Giuliano, A. Koutinas, and H. Lange, "Sustainable lignin valorization." Webinar on Sustainable Lignin Valorisation, 2021.
[38] M. Yu. Balakshin *et al.*, "New Opportunities in the Valorization of Technical Lignins," *ChemSusChem*, vol. 14, no. 4, pp. 1016–1036, Feb. 2021, doi: 10.1002/cssc.202002553.

[39] E. Ahmad and K. K. Pant, "Lignin Conversion: A Key to the Concept of Lignocellulosic Biomass-Based Integrated Biorefinery," in *Waste Biorefinery*, Elsevier, 2018, pp. 409–444. doi: 10.1016/B978-0-444-63992-9.00014-8.
[40] J.-C. Bonhivers and Paul. R. Stuart, "Applications of Process Integration Methodologies in the Pulp and Paper Industry," in *Handbook of Process Integration (PI)*, Elsevier, 2013, pp. 765–798. doi: 10.1533/9780857097255.5.765.
[41] "Report on other components and polymers present in the Black Liquors." EUCAlyptus LIgnin VAlorisation for Advanced Materials and Carbon Fibres. [Online]. Available: https://ec.europa.eu/research/participants/documents/downloadPublic?documentIds=080166e5d082a2ad&appId=PPGMS#:~:text=After%20the%20recovery%20of%20the,40%25%20inorganics%20(i.e.%20the%20residual
[42] M. Hubbe, R. Alén, M. Paleologou, M. Kannangara, and J. Kihlman, "Lignin recovery from spent alkaline pulping liquors using acidification, membrane separation, and related processing steps: A review," *BioResources*, vol. 14, no. 1, pp. 2300–2351, Feb. 2019, doi: 10.15376/biores.14.1.2300-2351.
[43] *US DOE. 2005. Genomics:GTL Roadmap, DOE/SC-0090, U.S. Department of Energy Office of Science. (p. 204)*. [Online]. Available: https://public.ornl.gov/site/gallery/detail.cfm?id=181
[44] H. Seddiqi *et al.*, "Cellulose and its derivatives: towards biomedical applications," *Cellulose*, vol. 28, no. 4, pp. 1893–1931, Mar. 2021, doi: 10.1007/s10570-020-03674-w.
[45] L. Weinstein and R. Dash, "Supercapacitor carbons," *Mater. Today*, vol. 16, no. 10, pp. 356–357, Oct. 2013, doi: 10.1016/j.mattod.2013.09.005.
[46] L. L. Zhang and X. S. Zhao, "Carbon-based materials as supercapacitor electrodes," *Chem. Soc. Rev.*, vol. 38, no. 9, Art. no. 9, 2009.
[47] L. Borchardt, M. Oschatz, and S. Kaskel, "Tailoring porosity in carbon materials for supercapacitor applications," *Mater Horiz*, vol. 1, no. 2, pp. 157–168, 2014, doi: 10.1039/C3MH00112A.
[48] S. Dutta, A. Bhaumik, and K. C.-W. Wu, "Hierarchically porous carbon derived from polymers and biomass: effect of interconnected pores on energy applications," *Energy Env. Sci*, vol. 7, no. 11, pp. 3574–3592, 2014, doi: 10.1039/C4EE01075B.
[49] C. Largeot, C. Portet, J. Chmiola, P.-L. Taberna, Y. Gogotsi, and P. Simon, "Relation between the Ion Size and Pore Size for an Electric Double-Layer Capacitor," *J. Am. Chem. Soc.*, vol. 130, no. 9, pp. 2730–2731, Mar. 2008, doi: 10.1021/ja7106178.
[50] D.-W. Wang, F. Li, M. Liu, G. Q. Lu, and H.-M. Cheng, "Mesopore-Aspect-Ratio Dependence of Ion Transport in Rodtype Ordered Mesoporous Carbon," *J. Phys. Chem. C*, vol. 112, no. 26, pp. 9950–9955, Jul. 2008, doi: 10.1021/jp800173z.
[51] J. Li *et al.*, "Enlarging energy density of supercapacitors using unequal graphene electrodes and ionic liquid electrolyte," *Electrochimica Acta*, vol. 258, pp. 1053–1058, Dec. 2017, doi: 10.1016/j.electacta.2017.11.157.
[52] W. Zuo, R. Li, C. Zhou, Y. Li, J. Xia, and J. Liu, "Battery-Supercapacitor Hybrid Devices: Recent Progress and Future Prospects," *Adv. Sci.*, vol. 4, no. 7, p. 1600539, Jul. 2017, doi: 10.1002/advs.201600539.
[53] L. Kouchachvili, W. Yaïci, and E. Entchev, "Hybrid battery/supercapacitor energy storage system for the electric vehicles," *J. Power Sources*, vol. 374, pp. 237–248, Jan. 2018, doi: 10.1016/j.jpowsour.2017.11.040.
[54] D. Karimi, H. Behi, J. Van Mierlo, and M. Berecibar, "A Comprehensive Review of Lithium-Ion Capacitor Technology: Theory, Development, Modeling, Thermal Management Systems, and Applications," *Molecules*, vol. 27, no. 10, p. 3119, May 2022, doi: 10.3390/molecules27103119.
[55] T. -C. Liu, W. G. Pell, B. E. Conway, and S. L. Roberson, "Behavior of Molybdenum Nitrides as Materials for Electrochemical Capacitors: Comparison with Ruthenium Oxide," *J. Electrochem. Soc.*, vol. 145, no. 6, pp. 1882–1888, Jun. 1998, doi: 10.1149/1.1838571.

[56] J. Wang, J. Polleux, J. Lim, and B. Dunn, "Pseudocapacitive Contributions to Electrochemical Energy Storage in TiO_2 (Anatase) Nanoparticles," *J. Phys. Chem. C*, vol. 111, no. 40, pp. 14925–14931, Oct. 2007, doi: 10.1021/jp074464w.
[57] S. Ardizzone, G. Fregonara, and S. Trasatti, "'Inner' and 'outer' active surface of RuO2 electrodes," *Electrochimica Acta*, vol. 35, no. 1, pp. 263–267, Jan. 1990, doi: 10.1016/0013-4686(90)85068-X.
[58] A. J. Gibson and S. W. Donne, "A step potential electrochemical spectroscopy (SPECS) investigation of anodically electrodeposited thin films of manganese dioxide," *J. Power Sources*, vol. 359, pp. 520–528, Aug. 2017, doi: 10.1016/j.jpowsour.2017.05.082.
[59] H. Shao, Z. Lin, K. Xu, P.-L. Taberna, and P. Simon, "Electrochemical study of pseudocapacitive behavior of Ti3C2Tx MXene material in aqueous electrolytes," *Energy Storage Mater.*, vol. 18, pp. 456–461, Mar. 2019, doi: 10.1016/j.ensm.2018.12.017.
[60] J. Sun *et al.*, "Ultralight carbon aerogel with tubular structures and N-containing sandwich-like wall from kapok fibers for supercapacitor electrode materials," *J. Power Sources*, vol. 438, p. 227030, Oct. 2019, doi: 10.1016/j.jpowsour.2019.227030.
[61] L. Li *et al.*, "Flexible double-cross-linked cellulose-based hydrogel and aerogel membrane for supercapacitor separator," *J. Mater. Chem. A*, vol. 6, no. 47, pp. 24468–24478, 2018, doi: 10.1039/C8TA07751G.
[62] Z. Wang, P. Tammela, J. Huo, P. Zhang, M. Strømme, and L. Nyholm, "Solution-processed poly(3,4-ethylenedioxythiophene) nanocomposite paper electrodes for high-capacitance flexible supercapacitors," *J. Mater. Chem. A*, vol. 4, no. 5, pp. 1714–1722, 2016, doi: 10.1039/C5TA10122K.
[63] D. Zhao *et al.*, "High Performance, Flexible, Solid-State Supercapacitors Based on a Renewable and Biodegradable Mesoporous Cellulose Membrane," *Adv. Energy Mater.*, vol. 7, no. 18, p. 1700739, Sep. 2017, doi: 10.1002/aenm.201700739.
[64] C. Zhao and W. Zheng, "A Review for Aqueous Electrochemical Supercapacitors," *Front. Energy Res.*, vol. 3, May 2015, doi: 10.3389/fenrg.2015.00023.
[65] O. Hosseinaei and D. A. Baker, "High Glass Transition Lignins and Lignin Derivatives for the Manufacture of Carbon and Graphite Fibers"
[66] T. Pang, G. Wang, H. Sun, W. Sui, and C. Si, "Lignin fractionation: Effective strategy to reduce molecule weight dependent heterogeneity for upgraded lignin valorization," *Ind. Crops Prod.*, vol. 165, p. 113442, Jul. 2021, doi: 10.1016/j.indcrop.2021.113442.
[67] K. Nasouri, A. Haji, A. Mousavi Shoushtari, and A. Kaflu, "A Novel Study of Electrospun Nanofibers Morphology as a Function of Polymer Solution Properties," presented at the proceedings of the international conference nanomaterials: applications and properties.
[68] V. Poursorkhabi, M. A. Abdelwahab, M. Misra, H. Khalil, B. Gharabaghi, and A. K. Mohanty, "Processing, Carbonization, and Characterization of Lignin Based Electrospun Carbon Fibers: A Review," *Front. Energy Res.*, vol. 8, no. 208, 2020, doi: https://doi.org/10.3389/fenrg.2020.00208.
[69] I. Norberg, Y. Nordström, R. Drougge, G. Gellerstedt, and E. Sjöholm, "A new method for stabilizing softwood kraft lignin fibers for carbon fiber production," *J. Appl. Polym. Sci.*, vol. 128, no. 6, pp. 3824–3830, Jun. 2013, doi: 10.1002/app.38588.
[70] A. Bengtsson, J. Bengtsson, M. Sedin, and E. Sjöholm, "Carbon Fibers from Lignin-Cellulose Precursors: Effect of Stabilization Conditions," *ACS Sustain. Chem. Eng.*, vol. 7, no. 9, pp. 8440–8448, May 2019, doi: 10.1021/acssuschemeng.9b00108.
[71] Q. Yan, J. Li, J. Zhang, and Z. Cai, "Thermal Decomposition of Kraft Lignin under Gas Atmospheres of Argon, Hydrogen, and Carbon Dioxide," *Polymers*, vol. 10, no. 7, p. 729, Jul. 2018, doi: 10.3390/polym10070729.
[72] A. Bengtsson, P. Hecht, J. Sommertune, M. Ek, M. Sedin, and E. Sjöholm, "Carbon Fibers from Lignin–Cellulose Precursors: Effect of Carbonization Conditions," *ACS Sustain. Chem. Eng.*, vol. 8, no. 17, pp. 6826–6833, May 2020, doi: 10.1021/acssuschemeng.0c01734.
[73] S. Wang, Y. Li, H. Xiang, Z. Zhou, T. Chang, and M. Zhu, "Low cost carbon fibers from bio-renewable Lignin/Poly(lactic acid) (PLA) blends," *Compos. Sci. Technol.*, vol. 119, pp. 20–25, Nov. 2015, doi: 10.1016/j.compscitech.2015.09.021.

[74] S. Wang *et al.*, "Lignin-based carbon fibers: Formation, modification and potential applications," *Green Energy Environ.*, vol. 7, no. 4, pp. 578–605, Aug. 2022, doi: 10.1016/j.gee.2021.04.006.
[75] W. Zhang *et al.*, "Lignin derived carbon materials: current status and future trends," *Carbon Res.*, vol. 1, no. 1, p. 14, Dec. 2022, doi: 10.1007/s44246-022-00009-1.
[76] F. J. García-Mateos *et al.*, "Activation of electrospun lignin-based carbon fibers and their performance as self-standing supercapacitor electrodes," *Sep. Purif. Technol.*, vol. 241, p. 116724, Jun. 2020, doi: 10.1016/j.seppur.2020.116724.
[77] M. Song, L. Yu, B. Song, F. Meng, and X. Tang, "Alkali promoted the adsorption of toluene by adjusting the surface properties of lignin-derived carbon fibers," *Environ. Sci. Pollut. Res.*, vol. 26, no. 22, pp. 22284–22294, Aug. 2019, doi: 10.1007/s11356-019-05456-9.
[78] S. Hu and Y.-L. Hsieh, "Ultrafine microporous and mesoporous activated carbon fibers from alkali lignin," *J. Mater. Chem. A*, vol. 1, no. 37, p. 11279, 2013, doi: 10.1039/c3ta12538f.
[79] W.-J. Youe, S.-M. Lee, S.-S. Lee, S.-H. Lee, and Y. S. Kim, "Characterization of carbon nanofiber mats produced from electrospun lignin-g-polyacrylonitrile copolymer," *Int. J. Biol. Macromol.*, vol. 82, pp. 497–504, Jan. 2016, doi: 10.1016/j.ijbiomac.2015.10.022.
[80] Y. Zhu and O. Fontaine, "Most Modern Supercapacitor Designs Advanced Electrolyte and Interface," in *Supercapacitors for the Next Generation*, D. Tashima and A. Kumar Samantara, Eds. IntechOpen, 2022. doi: 10.5772/intechopen.98352.
[81] X. Feng *et al.*, "Untangling the respective effects of heteroatom-doped carbon materials in batteries, supercapacitors and the ORR to design high performance materials," *Energy Environ. Sci.*, vol. 14, no. 4, pp. 2036–2089, 2021, doi: 10.1039/D1EE00166C.
[82] S. Ghosh, S. Barg, S. M. Jeong, and K. Ostrikov, "Heteroatom-Doped and Oxygen-Functionalized Nanocarbons for High-Performance Supercapacitors," *Adv Energy Mater*, vol. 10, no. 32, Art. no. 32, 2020.
[83] G. Zhang, X. Xiao, B. Li, P. Gu, H. Xue, and H. Pang, "Transition metal oxides with one-dimensional/one-dimensional-analogue nanostructures for advanced supercapacitors," *J. Mater. Chem. A*, vol. 5, no. 18, pp. 8155–8186, 2017, doi: 10.1039/C7TA02454A.
[84] J. Rehman *et al.*, "Engineering of Transition Metal Sulfide Nanostructures as Efficient Electrodes for High-Performance Supercapacitors," *ACS Appl. Energy Mater.*, vol. 5, no. 6, pp. 6481–6498, Jun. 2022, doi: 10.1021/acsaem.1c03937.
[85] W. G. Pell, B. E. Conway, and N. Marincic, "Analysis of non-uniform charge/discharge and rate effects in porous carbon capacitors containing sub-optimal electrolyte concentrations," *J. Electroanal. Chem.*, vol. 491, no. 1–2, pp. 9–21, Sep. 2000, doi: 10.1016/S0022-0728(00)00207-2.
[86] C. Prehal, C. Koczwara, H. Amenitsch, V. Presser, and O. Paris, "Salt concentration and charging velocity determine ion charge storage mechanism in nanoporous supercapacitors," *Nat. Commun.*, vol. 9, no. 1, p. 4145, Dec. 2018, doi: 10.1038/s41467-018-06612-4.
[87] B. Pal, S. Yang, S. Ramesh, V. Thangadurai, and R. Jose, "Electrolyte selection for supercapacitive devices: a critical review," *Nanoscale Adv.*, vol. 1, no. 10, pp. 3807–3835, 2019, doi: 10.1039/C9NA00374F.
[88] T.-Y. Yi, C.-W. Dai, J.-A. Wang, C.-C. M. Ma, and C.-C. Hu, "Electrochemical activation and capacitance enhancement of expanded mesocarbon microbeads for high-voltage, symmetric supercapacitors," *Electrochimica Acta*, vol. 359, p. 136941, Nov. 2020, doi: 10.1016/j.electacta.2020.136941.
[89] F. Wan, J. Zhu, S. Huang, and Z. Niu, "High-Voltage Electrolytes for Aqueous Energy Storage Devices," *Batter. Supercaps*, vol. 3, no. 4, pp. 323–330, Apr. 2020, doi: 10.1002/batt.201900229.
[90] Y. Dong, J. Zhu, Q. Li, S. Zhang, H. Song, and D. Jia, "Carbon materials for high mass-loading supercapacitors: filling the gap between new materials and practical applications," *J. Mater. Chem. A*, vol. 8, no. 42, pp. 21930–21946, 2020, doi: 10.1039/D0TA08265A.
[91] C. Wan, L. Yuan, and H. Shen, "Effects of Electrode Mass-loading on the Electrochemical Properties of Porous MnO2 for Electrochemical Supercapacitor,"

HttpswwwresearchgatenetjournalInternational-J.--Electrochem.-Sci.-1452-3981, vol. 9, no. 7, pp. 4024–4038, 2014.
[92] Y. Qing *et al.*, "Boosting the supercapacitor performance of activated carbon by constructing overall conductive networks using graphene quantum dots," *J. Mater. Chem. A*, vol. 7, no. 11, pp. 6021–6027, 2019, doi: 10.1039/C8TA11620B.
[93] R. Yuan, Y. Dong, R. Hou, S. Zhang, and H. Song, "Review—Influencing Factors and Suppressing Strategies of the Self-Discharge for Carbon Electrode Materials in Supercapacitors," *J. Electrochem. Soc.*, vol. 169, no. 3, p. 030504, Mar. 2022, doi: 10.1149/1945-7111/ac56a1.
[94] Y.-Z. Wang, X.-Y. Shan, D.-W. Wang, H.-M. Cheng, and F. Li, "Mitigating self-discharge of carbon-based electrochemical capacitors by modifying their electric-double layer to maximize energy efficiency," *J. Energy Chem.*, vol. 38, pp. 214–218, Nov. 2019, doi: 10.1016/j.jechem.2019.04.004.
[95] L. Chen, H. Bai, Z. Huang, and L. Li, "Mechanism investigation and suppression of self-discharge in active electrolyte enhanced supercapacitors," *Energy Env. Sci*, vol. 7, no. 5, pp. 1750–1759, 2014, doi: 10.1039/C4EE00002A.
[96] M. Haque *et al.*, "Self-discharge and leakage current mitigation of neutral aqueous-based supercapacitor by means of liquid crystal additive," *J. Power Sources*, vol. 453, p. 227897, Mar. 2020, doi: 10.1016/j.jpowsour.2020.227897.
[97] K. Wang *et al.*, "Ion-Exchange Separators Suppressing Self-Discharge in Polymeric Supercapacitors," *ACS Energy Lett.*, vol. 5, no. 10, pp. 3276–3284, Oct. 2020, doi: 10.1021/acsenergylett.0c01783.
[98] H. Peng, L. Xiao, K. Sun, G. Ma, G. Wei, and Z. Lei, "Preparation of a cheap and environmentally friendly separator by coaxial electrospinning toward suppressing self-discharge of supercapacitors," *J. Power Sources*, vol. 435, p. 226800, Sep. 2019, doi: 10.1016/j.jpowsour.2019.226800.
[99] M. Kaus, J. Kowal, and D. U. Sauer, "Modelling the effects of charge redistribution during self-discharge of supercapacitors," *Electrochimica Acta*, vol. 55, no. 25, pp. 7516–7523, Oct. 2010, doi: 10.1016/j.electacta.2010.01.002.

Effect of plasma treatment on the electrochemical performance of lignin carbon fibers for supercapacitor applications

Azega.R.K[a,e,*], Mazharul Haque[a], Qi Li[c], Omid Hosseinaei[d], Hans Theliander [b,e], Peter Enoksson[a,f], Per Lundgren[a]

[a] *Department of Microtechnology and Nanoscience, Chalmers University of Technology, Göteborg, Sweden*

[b] *Department of Chemistry and Chemical Engineering, Chalmers University of Technology, Göteborg, Sweden*

[c] *Smoltek Hydrogen AB, Kaserntorget 7, 411 18 Göteborg, Sweden*

[d] *RISE Research Institutes of Sweden, Drottning Kristinas väg 61, 114 28 Stockholm, Sweden*

[e] *Wallenberg Wood Science Center, Sweden*

[f] *Enoaviatech AB, 112 26 Stockholm, Sweden*

*Corresponding author.

E-mail address: azega@chalmers.se

Highlights

- Demonstrates carbon fibers from wood-based lignin as supercapacitor electrodes.
- Low-power plasma treatment with short exposure beneficially modifies fiber surface.
- Introduced surface functional groups improves aqueous wettability.
- Carbonyl and hydroxyl functional groups enhance the capacitive performance.
- Reduced diffusion limitation and enhanced pore surface utilization results in better rate performance and cycle stability.

Abstract

The interaction of the electrode's surface with the electrolyte crucially determines a supercapacitor's capacitance, charging rate, stability, and voltage constraints. Introducing basic functional groups containing oxygen such as COO^-, C-OH, C-O, and C=O on carbon surfaces in a controlled manner is known to be favorable for electrolyte-electrode interfacial interactions that ultimately improve the overall capacitive performance. However, quite often the surface functional groups negatively affect the electrochemical performance such as slow kinetics, increased resistance, and parasitic faradaic reactions. Therefore, in this work, we have carried out a comprehensive material and electrochemical investigation on electrospun lignin carbon fibers (LCF) and oxygen plasma-treated lignin carbon fibers (PLCF) to explore the potential of supercapacitor electrodes and investigate the influence of the oxygen functional groups on the capacitive performance. Different aqueous electrolytes, particularly KOH, have been utilized for the electrochemical characterization of the devices containing both types of electrodes. The investigated electrodes demonstrate highly capacitive signatures. However, plasma treatment improves the wettability of the electrodes, facilitates increased ion accessibility to the active surface area, and consequently demonstrates superior capacitance (120 vs 95 F/g, at 0.5 A/g), good rate capability (68% and 60% from scan rate 10 mV/s to 1000 mV/s), high energy and power density (11 Wh/kg and 0.8 kW/kg vs 8 Wh/kg and 0.8 kW/kg, respectively at 0.5 A/g current density) compared to the electrodes without any plasma

treatment. Moreover, the long-term stability and self-discharge characteristics of the device are not compromised, regardless of the presence of the surface functional groups, which could occur due to parasitic faradaic reactions or increased resistance from the surface functional groups. The underlying complex interaction between the functional groups and electrolyte ions has been further studied with X-ray photoelectron spectroscopy (XPS) at different states of health of the devices, which highlights the importance of the types and the extents of the surface functional groups and their interactions at the electrode/electrolyte interface.

Keywords: supercapacitor, lignin, carbon fiber, wettability, surface functional groups

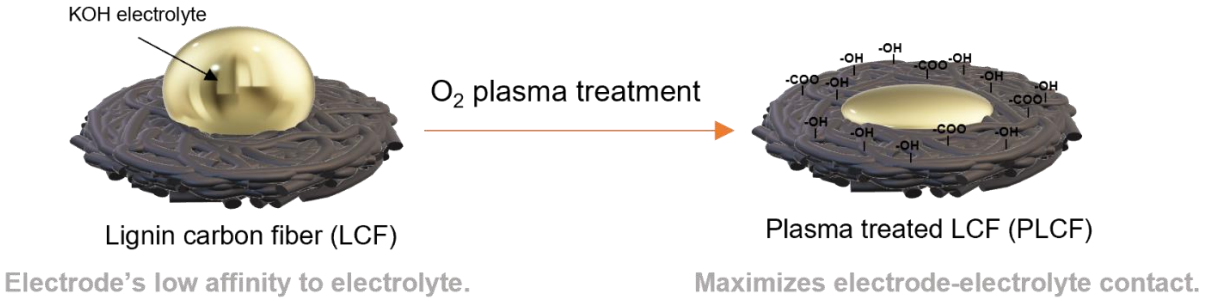

Graphical abstract: Schematic representation of advantageous surface functional groups via oxygen plasma treatment and the resulting increased affinity (i.e. wettability) of lignin carbon fiber electrodes to KOH electrolyte.

1. Introduction

Carbon fibers' exceptional tensile strength, low weight, high chemical resistance, and temperature tolerances attract much attention to them for a variety of specialized applications. Amongst the carbon fibers now in use, PAN or pitch-derived ones with excellent fiber formation ability combines great mechanical strength with good electrical conductivity and electrochemical characteristics [1]. They are viable as electrodes for high-performing supercapacitors, which provide efficient rechargeable energy storage with more power per unit of space than batteries of equivalent size today. However, producing these carbon fibers demands fossil-based precursors, hazardous chemicals, and unsustainable energy use, making them expensively unfriendly to the environment [2], [3]. This pushes the need for new, inexpensive, accessible, and ecologically acceptable sources, like biomasses. Lignin is one of the biomasses that is rich in carbon, with only aromatic biopolymers from abundant and renewable solid resources such as wood. Aromatic carbon is particularly interesting as it offers a range of available hydrocarbons with varying molecular structures for the production of highly graphitic and porous materials [4]. Besides, lignin is an excellent choice for electrode materials due to its intrinsic presence of a plethora of redox-active functional groups, great biocompatibility, biodegradability, high thermal stability, and low toxicity [5], [6]. Owing to these attractive features, lignin-derived materials have been utilized as active material or framework substrates in different types of electrochemical storage devices like lithium-ion batteries, sodium-ion batteries, fuel cells [7], supercapacitors, and hybrid devices.

Typically, lignin is combined with fossil-based co-polymers and harmful chemicals for pre/during/post-processing steps to produce mechanically stronger fibers with good on-device flexibility, and better operational stabilities [8]–[12]. However, non-fossil-based plasticizers or solvent fractionation eliminating low molecular weight fractions is developed for more eco-friendly materials [13]–[15]. In addition, lignin fibers can be synthesized with very efficient techniques such as electrospinning [16] which is particularly a suitable method for producing electrode materials with tailored structures [17]. Upon carbonization, carbon nanofibers (CNF)

from lignin precursors possess advantageous properties as an electrode material such as high specific surface area, mechanical flexibility, moderate electrical conductivity, and numerous beneficial surface functional groups [18]. Moreover, due to its freestanding nature with micro- and nano-sized fibers, electrospun lignin carbon fibers (LCF) do not require any binder materials that result in higher content of active surface for energy storage. They could also potentially function as both current collector and active material that minimize contact resistance (from binders, additives, and current collectors) and prevents performance deterioration [19].

In general, charge storage in a typical supercapacitor comprises electrical double-layer capacitance (EDLC) through electrostatic and pseudocapacitance through surface-confined redox reaction owing to high carbon surface area and different surface functional groups. Functional groups containing oxygen configuration, such as hydroxyl (-OH), carbonyl (C=O), and quinone (1,4-benzoquinone) groups are redox-active (varying dependent on the choice of electrolyte ions) that positively contribute to the pseudocapacitance [20]. Some of these surface functional groups also improve the interfacial properties to a large extent by increasing the electrode wettability. Unfortunately, high-temperature treatments during the carbonization diminish many attractive features of the lignin fibers. For example, the tensile strength and moduli of electrospun LCF decrease significantly after temperature treatments due to the breaking of aliphatic chains that are randomly arranged between the aromatic units [21]. In addition, the reduction of beneficial functional groups from the carbon surface makes the electrodes extremely hydrophobic which creates a disadvantageous effect on the electrode/electrolyte interface, specifically with aqueous electrolytes, making the intrinsic high ionic conductivity of aqueous electrolyte redundant. Therefore, an optimized surface treatment of the electrode materials for a specific electrolyte is essential to enhance the overall capacitive performance of the supercapacitors [12], [22], [23].

In this regard, heteroatom-doping, such as O, N, P, and B-doping to carbon frameworks can be utilized to re-introduce these essential functional groups that significantly enhance the hydrophilicity and also promote pseudocapacitive contributions in aqueous and organic electrolytes [24], [25]. However, common treatment methods like doping or activation [12] of carbon fibers are known to degrade or even collapse the fiber morphology [26], [27]. For example, CO_2 activation increased the meso- and micro pores of the oxygen functional group containing electrodes, but the device performance suffered from poor cyclic stability and reduced energy density [20]. Another study demonstrated that the addition of oxidizing salt such as $NaNO_3$ in the electrospinning solutions enhanced the (ultra-)microporosity of the carbonized electrodes with increased oxygen groups that resulted in high capacitance values in alkaline media. However, the oxidizing salt also created a very dense fiber network in the electrodes during carbonization. As a result, the capacitive performance degraded at higher rates, and the device suffered from low rate capability and low power density [28]. Therefore, a non-invasive treatment on the electrode or, the electrode surface is essential to keep the material composition intact. Oxygen plasma treatment is a non-invasive technique, which can synergistically introduce regulated oxygen functionalities to the carbon matrix. During the process, plasma exposure alters the kind and coverage of the surface functionalities by radical generation and adsorption. This way of oxygen functionalization by plasma as intended improves the electrode wettability through the formation of polar groups, enables the development of stronger chemical linkages in aqueous electrolytes (e.g. carboxylic acids generated by carbon oxidation) [29], and may increase defects without compromising the compositional integrity. The treatment duration and power required to produce the desired changes in the surface fiber chemistry ranges from a few seconds to a few minutes, which

makes plasma treatment a highly promising surface enhancement strategy with lesser processing steps during scalable industrial production [30].

Electrode functionalization with an optimum amount of functional groups is vital to take advantage of the positive attributes of the functional groups such as improved wettability, increased pseudocapacitive contribution and at the same time to avoid the detrimental effects such as accelerated self-discharge and low power performance due to increased resistance [31], [32]. Considering above mentioned requisites and concerns, in this study we have synthesized electrospun LCF without any fossil-based secondary polymers. The surface properties of the LCF have been modified with low-power oxygen plasma and hence assigned to plasma-treated lignin carbon fiber (PLCF). Comprehensive material characterization and electrochemical investigation have been carried out in combination with different aqueous electrolytes, particularly with potassium hydroxide (6M KOH), to explore the positive influence of the plasma treatment on the overall capacitive performance.

2. Experimental

2.1.Materials synthesis

Softwood lignin from the LignoBoost method was used as the starting precursor for the procedure [33]. In order to extract lignin of high molecular weight, an already established sequential solvent extraction technique was carried out by dissolving 1000 grams of the softwood lignin in 10 L of methanol followed by agitating for 4 h at room temperature [34]. Solids recovered from the last step after filtration was followed by treating 1 part of it with 10 times 70/30 volume methanol and methylene chloride for about 4 h. The filtered lignin from the extracted solution was concentrated using a rotary evaporator and dried in a vacuum oven for 12 h at 80 °C before proceeding to electrospinning.

2.1.1. Electrospinning and treatment of lignin fibers

A similar method as reported by Peuvot et al. was followed for the electrospinning of the polymer-free lignin fibers [35]. The extracted isolated lignin was dissolved in dimethylformamide at a concentration of 47 wt%. A cylindrical Becton Dickinson plastic syringe was filled with the dissolved lignin using a KdScientific pump which fed the solution to the needle at a rate of 0.5 mL/h. The electrospun lignin fibers were collected on an aluminum foil-wrapped collector rotating at 60 rpm. A continuous electric field of 17 kV was applied between the needle and the collector which was kept 17 cm apart. The as-spun fiber mats were vacuum-dried at 105 °C for 180 min before storing them in nitrogen desiccator cabinets to avoid moisture contamination.

2.1.2. Carbonization of lignin fibers

For utilizing the lignin fibers as electrodes for supercapacitors, carbonization and activation are essential to increase the mechanical strength, electrical conductivity, and surface area of the fibers [36]. We employ a two-step method with thermostabilization before carbonization (Fig.1).

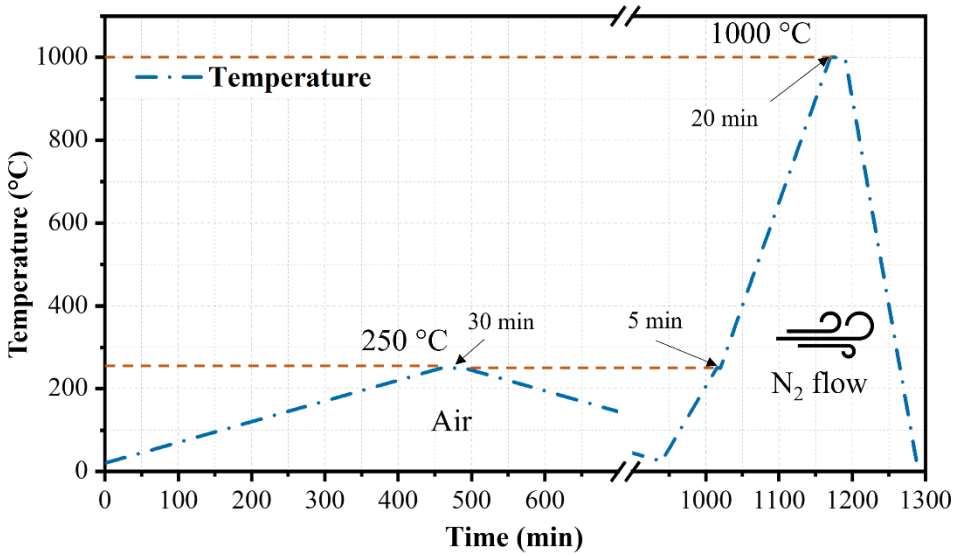

Fig.1. LCF carbonization profile; Stabilization using Nabertherm box furnace and carbonization using Thermolyne - Open Tube/1600 °C furnace.

The dried as-electrospun lignin fiber mats were thermally stabilized in a Nabertherm Box Furnace (Labotherm L15) by heating to 250 °C with a rate of 0.5 °C/min. They were allowed to stand at that temperature for about 30 min before cooling down to room temperature. The thermostabilized lignin fibers were then transferred for carbonization to a high-temperature Thermolyne - Tube furnace. The temperature was increased from ambient to 600 °C at a rate of 3 °C/min with supplied nitrogen gas flow in the reaction tube (approximately 1.5 L/min). The fibers were allowed to stay at that temperature for 5 min to stabilize again before ramping the temperature by 5 °C/min until the carbonization temperature of 1000 °C was reached. The fiber mats at this point are allowed to dwell at the carbonization temperature for 20 min and are then allowed to cool down to room temperature at 20 °C/min. Afterward, the carbonized lignin fiber mats were vacuum-dried again for 3 h at 105 °C and stored in nitrogen desiccator cabinets to avoid contaminations from moisture.

2.1.3. Plasma-treatment of LCF

Oxygen plasma treatment was performed to modify the surface of the LCF. The Plasmatherm Batchtop, an RF plasma system, was used to treat vacuum-dried LCF with plasma. The exposure periods were limited to 30 s on each side of the fiber mat with a low power of 25 W, and the gas utilized was oxygen. Short-time exposure and low power were chosen because prolonged exposures have been reported to result in detrimental effects on fibers' mechanical and electrical properties [37], [38].

2.1.4. Supercapacitor cell assembly

Both the LCF and PLCF electrodes were used to prepare the symmetric supercapacitor devices. Electrodes with identical masses (ranging between 1.7 to 2.2 mg), diameters of 10 mm, and a commercially available glass fiber membrane (Whatman® GF) separator with a thickness of 200 µm and a diameter of 12 mm were used to prepare one unit device. Different aqueous electrolytes, such as 6M KOH, 1M H_2SO_4, and 1M Li_2SO_4 with a volume of approximately 100 µL were used for different devices to investigate the compatibility of the as-prepared electrodes with the electrolytes. The supercapacitor devices have been assembled in CR2025 coin cells. All the devices were kept idle for at least 24 h before any electrochemical measurements for the complete penetration of the electrolyte into the electrodes. Electrode

materials have been retrieved after all the electrochemical measurements with the help of a disassembly machine for the post-investigation of the electrode materials.

3. Characterizations

3.1.Material characterization

Surface morphology **-** *SEM LEO Ultra 55* was used to analyze the fiber morphology of the electrospun LCF and PLCF. The secondary electron detector was used to analyze the fiber surface in high vacuum mode while the microscope was operating at 5 kV accelerating voltage. A working distance of 6.4 mm was maintained for all samples.

Functional group analysis- X-ray photoelectron spectroscopy (XPS) was used to further investigate the surface composition and chemical states of the components of interest. The PHI 5000 VersaProbe III Scanning XPS MicroprobeTM was used, which was equipped with a monochromatic AlK X-ray source with a photon energy of 1486.6 eV and a beam size of 100 µm. During the experiments, dual charge correction with an electron neutralizer and an argon ion cannon was used to compensate for the limited conductivity in non-carbonized samples. The surface composition was determined using a survey scan with a scanning energy range of 0 eV to 1250 eV, a pass energy of 280 eV, and a step size of 1.0 eV. High-resolution regional scans with a pass energy of 26 eV and a step size of 0.1 eV were used to examine the chemical states of each element. The data from narrow scans were aligned with the adventitious carbon C1s peak at 284.8 eV before qualitative analysis. The system's energy scale, on the other hand, was calibrated using ISO 15472:2010, with the core levels of pure gold (Au $4f_{7/2}$), silver (Ag $3d_{5/2}$), and copper (Cu $2p_{3/2}$) set at 83.96 eV, 368.21 eV, and 932.62 eV, respectively. The MultiPakTM program was used to perform peak deconvolution. The fitted peaks were allocated to a specific energy peak location in the spectral envelope after the spectra were fitted above the Shirley background. The peak shape was fitted using a Gaussian-Lorentzian function, and the full width at half maximum (FWHM) of the peak width was less than 2.0 eV in all the fitted curves. The area ratios of the fitted peaks in the spectral envelope were used to calculate the contribution of each chemical state in a single element.

3.2.Electrochemical characterization

Electrochemical analysis- All the electrochemical measurements were conducted using a *Gamry Reference 3000AE* Galvanostat/Potentiostat workstation. Electrochemical measurements such as cyclic voltammetry (CV), and galvanostatic charge-discharge (GCD) were carried out in a wide range of scan rates (10 to 1000 mV/s) and current densities (0.5 to 15 A/g). Electrochemical impedance spectroscopy (EIS) was carried out at different states of health of the devices. The spectrum was recorded at the frequency range of 100 kHz to 10 mHz at 0 V with an alternating current (ac) perturbation of 10 mV at open circuit potential. Additionally, the stability of the devices was investigated with cyclic charge-discharge (CCD) at a current density of 2 A/g for 10000 cycles. Self-discharge characteristics of the devices were carried out by charging the devices at the rated voltage with a constant current of 0.2 A/g and immediately followed by monitoring the open circuit potential for 60 min. All the tests were carried out at room temperature (25 ˚C).

The specific capacitance, $C_{s,CV}$ (F/g) is calculated according to the following equation:

$$C_{\mathrm{s,CV}} = 4 \times 1000 \times \frac{\int_0^{2\cdot\Delta V/\nu_s} |i| dV}{2 \cdot \mathrm{m} \cdot \Delta \mathrm{V}} \qquad \text{Equation (1)}$$

where *I(A)* is the current response, *m* (g) is the mass of the cell's electrode, ΔV (mV) is the working voltage window, and ν (mV/s) is the scan rate. The factor of 4 modifies the device capacitance (normalized to the mass of two electrodes) to the capacitance of a single electrode.

The specific capacitance, $C_{sp,GCD}$ (F/g) from GCD curves is determined as follows.

$$C_{s,GCD} = 4 \times \frac{I_d \cdot t_d}{m \cdot V_d} \quad \text{Equation (2)}$$

where I_d is the discharge current, t_d is the discharge duration (s), and V_d (mV) is the discharge voltage excluding the internal resistance (IR) drop.

The power density and energy density of the devices are calculated from GCD measurements according to the following equations.

$$C_d = \frac{C_{sp,GCD}}{4} \quad \text{Equation (3)}$$

$$E = \frac{1}{2} \times \frac{C_d \cdot {V_d}^2}{3.6} \quad \text{Equation (4)}$$

$$P_{avg} = 3600 \times \frac{E}{t_d} \quad \text{Equation (5)}$$

where C_d is the device capacitance from the GCD measurements. E (Wh/kg) is the energy density and P_{avg} (W/kg) is the average power density of the device. The numbers 3.6 and 3600 are unit conversion factors.

4. Results and discussion

4.1. Surface morphology

Fig. 2 shows the scanning electron microscope (SEM) image of the LCF and PLCF. Fig. 2 (a) demonstrates the cross-section of the LCF.

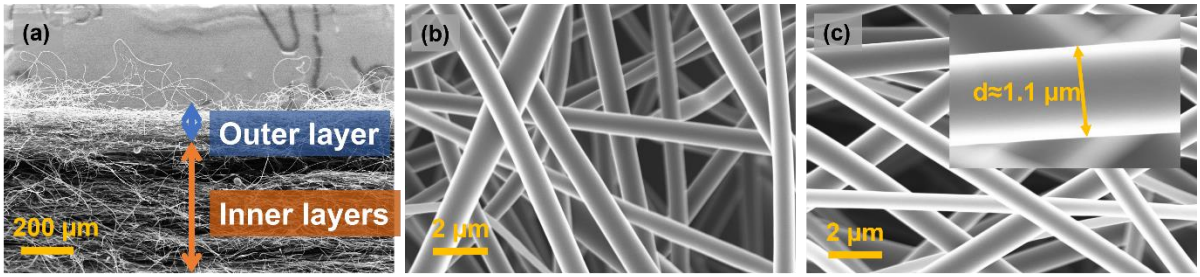

Fig.2. SEM images (a) cross-section of electrospun LCF, (b) as-carbonized LCF, and (c) PLCF.

It can be seen that LCF electrode is comprised of randomly oriented fibers both in the inner and outer layers. Fig. 2 (b) and (c) shows the top view of the electrodes of LCF and PLCF, respectively. The diameters of the fibers are around 1.1 µm. Most importantly, there is no significant difference in the appearance between the fibers of LCF and PLCF, which demonstrates that the plasma treatment did not visibly damage the morphology of the fibers. In order to investigate the compatibility of these electrodes with the aqueous solution, contact angle measurements have been carried out. As can be seen from Fig. S1, the contact angle is around 112º for LCF and only 16º for PLCF which confirms the inherent hydrophobic nature of LCF. Plasma treatment with a duration of just 30 seconds significantly improves the wettability/hydrophilicity by modification of the fiber surface's chemical state as can be noticed from the contact angle measurements (Fig. S1). Fig. S2 shows the SEM images of both LCF and PLCF electrodes soaked in KOH electrolyte after the devices have gone through all the electrochemical measurements. It can be seen that the KOH electrolyte is well distributed all along the fibers of PLCF, while in the case of LCF only limited to the walls of the electrodes. Since there are no visible morphological surface alterations such as increased roughness, or defects noticed in the PLCF (Fig. 2a) compared to LCF (Fig. 2b), we infer that the better

compatibility of PLCF with the electrolyte is primarily due to the modifications of the surface's chemical state.

4.2.Surface functional groups

Quantitative surface elemental analysis has been conducted with XPS. Fig. 3 demonstrates the XPS survey spectra of both the LCF and PLCF.

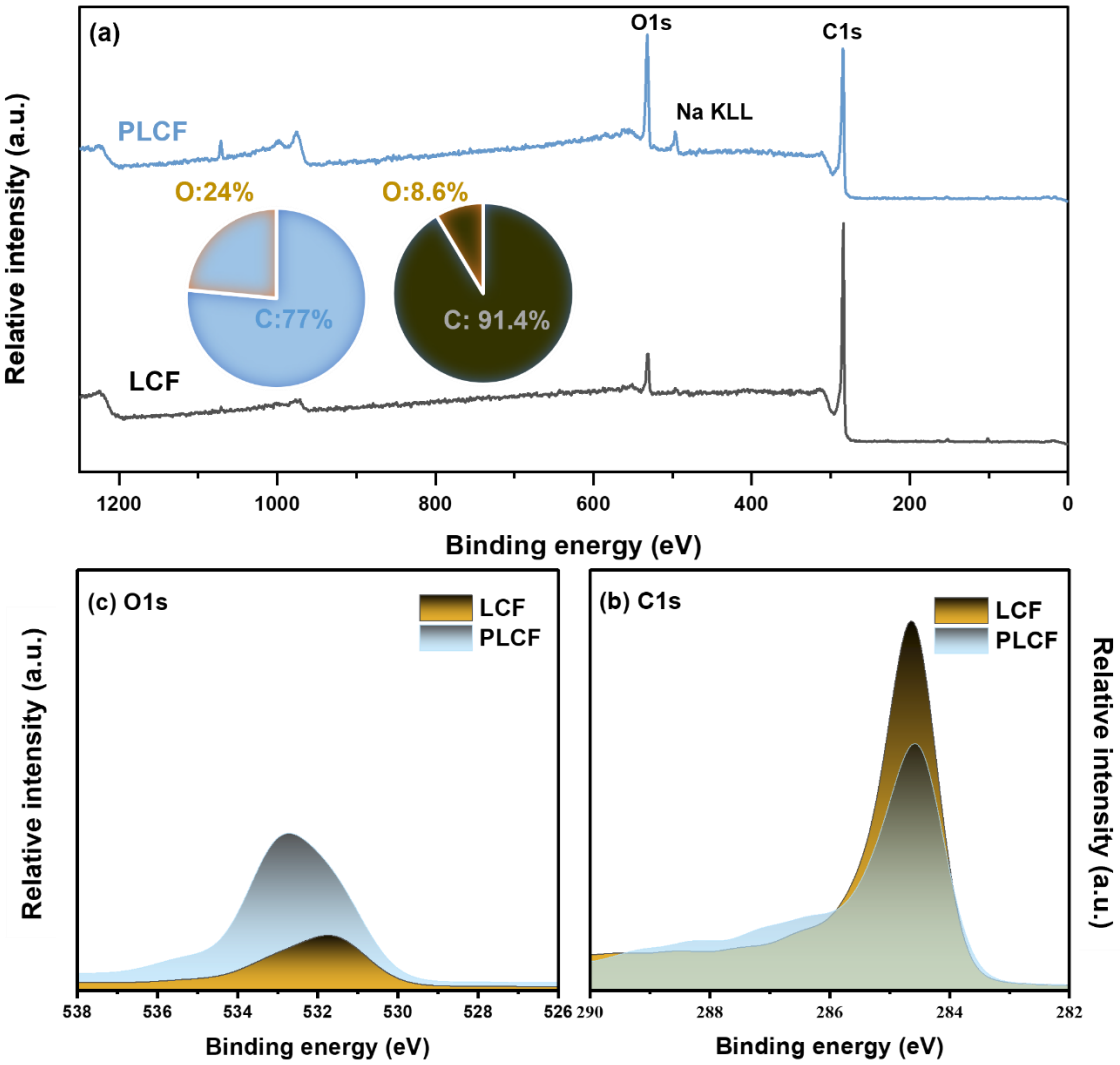

Fig.3. XPS results showing (a) wide scan spectrum, (b) the C-spectrum, and (c) the O-spectrum of LCF and PLCF

Fig 3a shows that the predominant elemental composition is carbon and oxygen in both electrodes. As can be seen, from the narrow scan for the C1s electron orbital in Fig. 3 (a), the primary signal at 285 eV is ascribed to the existence of sp3 hybridized C bonds. The samples detected with small traces of sodium could originate from the remnant residues from the LignoBoost processing chemicals [39]. Most importantly, plasma treatment induced an increased oxygen weight percentage in PLCF compared to LCF, and the increased oxygen content is not just on the surface, but it reaches a depth of several hundred microns in the fiber layers of the PLCF as displayed in Fig. S3.

The amount of oxygen in the LCF surface is significantly reduced following deoxygenation during the high-temperature carbonization. Fig. 3 (b) shows that after exposure to plasma for even a short time, the C-spectrum in the PLCF shifted to the direction of a much higher binding energy, indicating that some C-groups in the PLCF changed from a low-energy to a high-energy state. On the other hand, Fig. 3 (c) shows a completely different shift of the O-spectrum, where the O-spectrum moved in the direction of the low binding energy. These findings confirm that when fiber surfaces are treated with plasma in an oxygen atmosphere, the chemical composition of the fiber surface changes considerably [37]. It should be noted that the effect of plasma treatment on the fiber surface is still highly influenced by a variety of other parameters (such as power intensity and gas atmosphere) which would be very interesting to investigate and requires a separate study.

The C1s and O1s spectra for LCF and PLCF are deconvoluted to identify specific functional groups and peak area ratios. As shown in Fig. 4 (a) and (b), the deconvolution of the C1s reveals numerous peaks with different binding energies. The chemical environment of sp3 carbon (C–C) such as CH_2 groups is reflected by a peak centered at 285 eV (range between 284.6 and 285.2 eV). Furthermore, the C–OH indicating hydroxyl groups peak centers at 285.5 eV (range between 286.1 and 286.7 eV), C–O at 286.5 indicative of alcohol or ether groups, the C=O peak indicating carbonyl groups are located at 287.5 eV (range between 288.5 and 289.5 eV), and the O–C=O peak for carboxyl and esters groups is centered at 289 eV. Likewise, 531.5 eV (C=O), 532.6 eV (C–O), and 534 eV (C–OH) are the corresponding O1s peaks (Fig. 4 (b)).

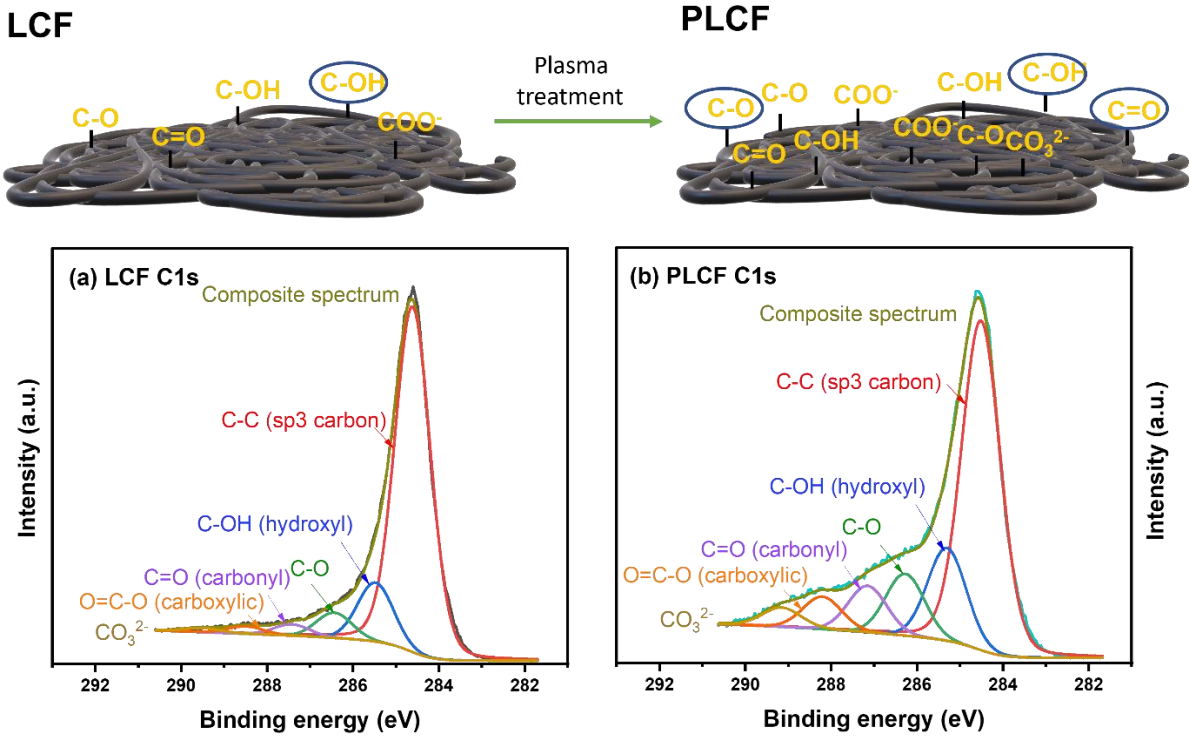

Fig. 4. The C-spectrum peaks before and after plasma treatment: (a) LCF and (b) PLCF. The experimentally acquired spectra (dashed line), peak fits for distinct chemical states of C-atoms including sp3 C (red curve), C−O feature (green curve), C=O feature (purple curve), O=C−O feature (yellow curve), carbonates (fluoro-blue line), and the cumulative fit (black line). Top: Schematic representation of the introduced oxygen functional groups on the carbon fiber.

It can be seen from Fig. 4 (a) and (b) that the density of carboxylic acids (O=C−O) on the fiber slightly increased (3%) on the surface of PLCF. The prevalence of C–O and C=O groups

increases substantially in PLCF, almost doubling and quadrupling, respectively. Similarly, the O1s spectra validate the C1s data with C–O groups increasing from 29% in LCF to 55% in PLCF. Traces of some carbonates could be originated from insoluble residual carbohydrates as impurities from the kraft lignin [20].

4.3. Capacitive properties of LCF and PLCF electrodes

Fig. 5 demonstrates the results of the electrochemical measurements of the devices containing both LCF and PLCF-containing electrodes in a 6M KOH electrolyte. Fig. 5a displays the CV plots of the devices with a scan rate of 20 mV/s in the voltage range of 0-0.8V.

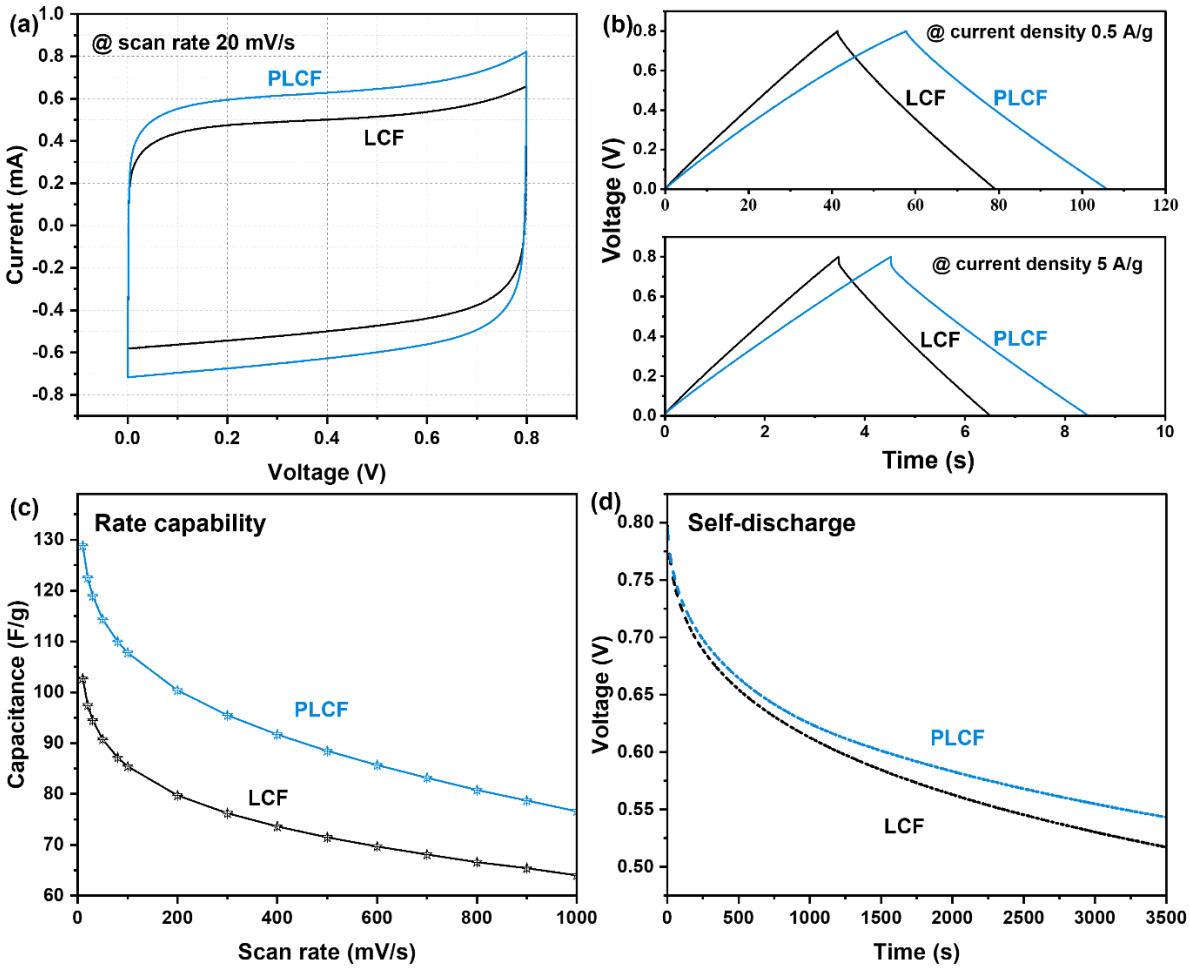

Fig.5. Electrochemical performance of the LCF and PLCF containing devices (a) CV curves at a scan rate of 20 mV/s, (b) GCD curves at a current density of 0.5 and 5 A/g, (c) self-discharge for 1 h, (d) rate capability (10 to 1000 mV/s).

Both devices exhibit a nearly rectangular shape indicating an ideal EDLC behavior. The width of the CV shape is considerably larger for the PLCF-containing device suggesting an improved capacitive property compared to the LCF-containing device. Consequently, the specific capacitance is calculated to be 26% higher for the device with PLCF than the device with LCF.

The GCD plot is shown in Fig. 5b, where a linear and symmetrical charge and discharge curve at both the low (0.5 A/g) and high current (5 A/g) within the rated voltage of 0.8 V for both the devices indicates a similar ideal capacitive signature as noticed in the CV plots. It can also be seen that the internal resistance (IR) drop is large at the high current (LCF: 4.3 mV and PLCF:

5.2 mV) for both devices while it is quite negligible at the low current (LCF: 1.2 mV and PLCF: 0.6 mV). The change of IR drop with increasing current density is expected due to the direct proportionality of the IR drop with the current density. The device containing PLCF electrodes shows a marginally higher IR drop compared to the device containing LCF electrodes, particularly at the high current density of 5 A/g. This could be due to the presence of excess oxygen functional groups on the surface of the PLCF, which tends to increase the IR drop, as has been reported in the previous study [32]. However, the marginal difference in the IR drop does not negatively affect the capacitive properties of the PLCF-containing device. For instance, the specific capacitance is calculated to be 99 F/g for PLCF and 76 F/g for LCF at 5 A/g. At the low current density of 0.5 A/g, the specific capacitance is even higher, 120 F/g for PLCF- and 95 F/g for LCF-containing devices which is comparable with the previous reports [20], [40], [41].

At a very high current or scan rate, only the outer surface of the electrodes contributes to the charge storage whereas, at a low current or scan rate both the outer and the inner layer contribute to the overall charge storage as the electrolyte ions have enough time to penetrate to the inner layers of the electrodes. Therefore, it is quite common to observe high capacitance at low current densities or low scan rates as can also be noticed in the devices under the current study. However, operating devices at extremely low currents can initiate unavoidable parasitic reactions that are more prone in the presence of certain surface functional groups such as carboxyl and C-O [42]. These parasitic reactions are often responsible for a high self-discharge rate which is detrimental to the overall capacitive performance. Therefore, capacitive measurements in a wide range of currents or scan rates are very critical to understand the true performance of the devices. The capacitive properties at the lowest current give a hint about the self-discharge behavior and the highest current can indicate the rate limitation. In this regard, Fig 5c shows the self-discharge profile of both devices. As can be seen, voltages retained are at 54% for LCF and at 47% for PLCF after 1 h in open circuit conditions without any voltage holding after the devices have been charged to the rated voltage of 0.8 V at a constant current density of 0.2 A/g (LCF:0.52 mA and PLCF:0.32 mA currents). The higher voltage retention of the PLCF-containing device indicates that the introduced surface functional groups do not contribute to any parasitic reactions.

Fig 5d shows the rate capability (capacitance retention from 10 mV/s to 1000 mV/s) of both devices. It can be seen that both the devices retain a quite decent rate capability (LCF: 60% and PLCF: 68%). The higher rate capability of the PLCF-containing devices compared to the LCF-containing device is interesting as generally, the surface functional groups such as C–O and –OH [43] tend to increase the resistance of the electrodes which reduces the rate performance as observed in the previous studies [28]. The improved rate performance of the PLCF electrodes containing device validates that the short period of plasma treatment did not have any detrimental impact on the electrodes, moreover it improves the kinetics in the interface.

Generally, different oxygen functional groups present on the surface evolve as CO_2 or CO that directly impact the capacitive performance. CO_2 mainly originates from the carboxyl, anhydrate, and lactone groups. It has been shown that the carboxylic groups can improve the wettability of the electrodes and be in favor of the capacitance improvement. However, another study highlights the downside of the carboxylic groups which is detrimental to the capacitive performance as it can lead to non-capacitive diffusion-controlled faradaic reactions. The strongly polar double-bonded oxygen atom in carboxyl tends to lose a lone-pair electron and thus forms a positively polarized group, which then reacts with the hydroxide (OH^-) in the electrolyte solution and causes non-capacitive reactions [44]. On the other hand, CO evolves

from the phenolic hydroxyl, carbonyl, and quinone groups. Several investigations on a variety of carbon materials showed that the CO-type oxygen functional groups contribute positively to the improvement of capacitance. Phenolic groups also improve hydrophilicity due to their weaker polarity compared to the carboxylic group as it enhances the surface capacitance without any parasitic catalytic effect [45], [46]. As can be seen from Table 1, after plasma treatment there is only a slight increase in the carboxyl group on the PLCF. On the other hand, the increase in the beneficial phenolic groups particularly the carbonyl group is quite significant. In addition, the hydrophobic C-C bond [47] reduces quite significantly after the plasma treatment both on the surface and the inner layer of the PLCF.

Table 1. Distribution of functional groups in LCF, PLCF, and inner layers of PLCF at C1s chemical state.

Binding energy	285.0 eV	286.5 eV	287.5 eV	289.0 eV	285.5 eV	289.5 eV
Chemical state	C-C (sp3 carbon)	C-O	C=O (carbonyl)	COO^- (carboxyl)	C-OH (hydroxyl)	CO_3^{2-}
LCF	77%	5%	2%	2%	13%	1%
PLCF	58%	10%	8%	5%	16%	3%
Inner layer PLCF	56%	9%	10%	6%	14%	5%

Regarding charge storage, different mechanisms concurrently occur in the electrode/electrolyte interface and generally comprise capacitive and diffusion-controlled charge storage mechanisms. In the presence of surface functional groups, the capacitive charge storage can have a contribution from both EDLC and pseudocapacitance originating from fast reversible surface-confined redox reactions. Ideally, the electrochemical signature of these charge storage mechanisms is similar such as rectangular CV and symmetrical GCD. Depending on the types of electrodes, pseudocapacitance could also originate from the intercalation, doping in conductive polymers, and underpotential depositions, which typically involve the bulk of the electrodes and consequently display a peak in the CV and non-linearity in the GCD [48]. As this is not the case in the devices under this study, we can certainly consider that the pseudocapacitance in the capacitive charge storage could only originate from the surface-confined redox reaction of the introduced functional groups. Due to the very fast kinetics of surface-confined pseudocapacitance, it is quite complex to separate it from the EDLC. The diffusion-controlled charge storage mechanism could also originate either from the bulk-redox reaction that results in a peak in the CV, or kinetic limitation in the interface (no peak in the CV). Again, as there is no visible peak in the CV of the devices under study, the diffusion limitation is most likely to originate from the kinetic limitation at the interface. Due to the different kinetics of diffusion-controlled charge storage and capacitive charge storage, it is possible to distinguish and quantify their contribution through the CV scan rate dependence on the voltammetric current according to the following equation [49]:

$$i(V) = k_1 v + k_2 v^{\frac{1}{2}} \quad \text{Equation (6)}$$

$$i(V)\Big/_{v^{\frac{1}{2}}} = k_1 v^{\frac{1}{2}} + k_2 \quad \text{Equation (7)}$$

where, $i(V)$ is the current response at a specific voltage, $k_1 v$, and $k_2 v^{1/2}$ correspond to the current contributions from the surface capacitive effects and the diffusion-controlled process, respectively. Consequently, the capacitive and diffusion-controlled charge storage mechanisms

can be obtained from the slope (k_1) and Y-intercept (k_2) of the plot of $i(V)/v^{1/2}$ versus $v^{1/2}$ at a specific voltage.

Fig. 6 demonstrates the CV curves of both the devices containing LCF and PLCF electrodes at scan rates of 10 and 500 mV/s at a voltage range of 0 - 0.8 V. The total current is obtained experimentally, and the capacitive currents (the shadowed regions) are determined by using equation 6. The detailed plot to extract the k_1 and k_2 values can be seen in Fig. S5.

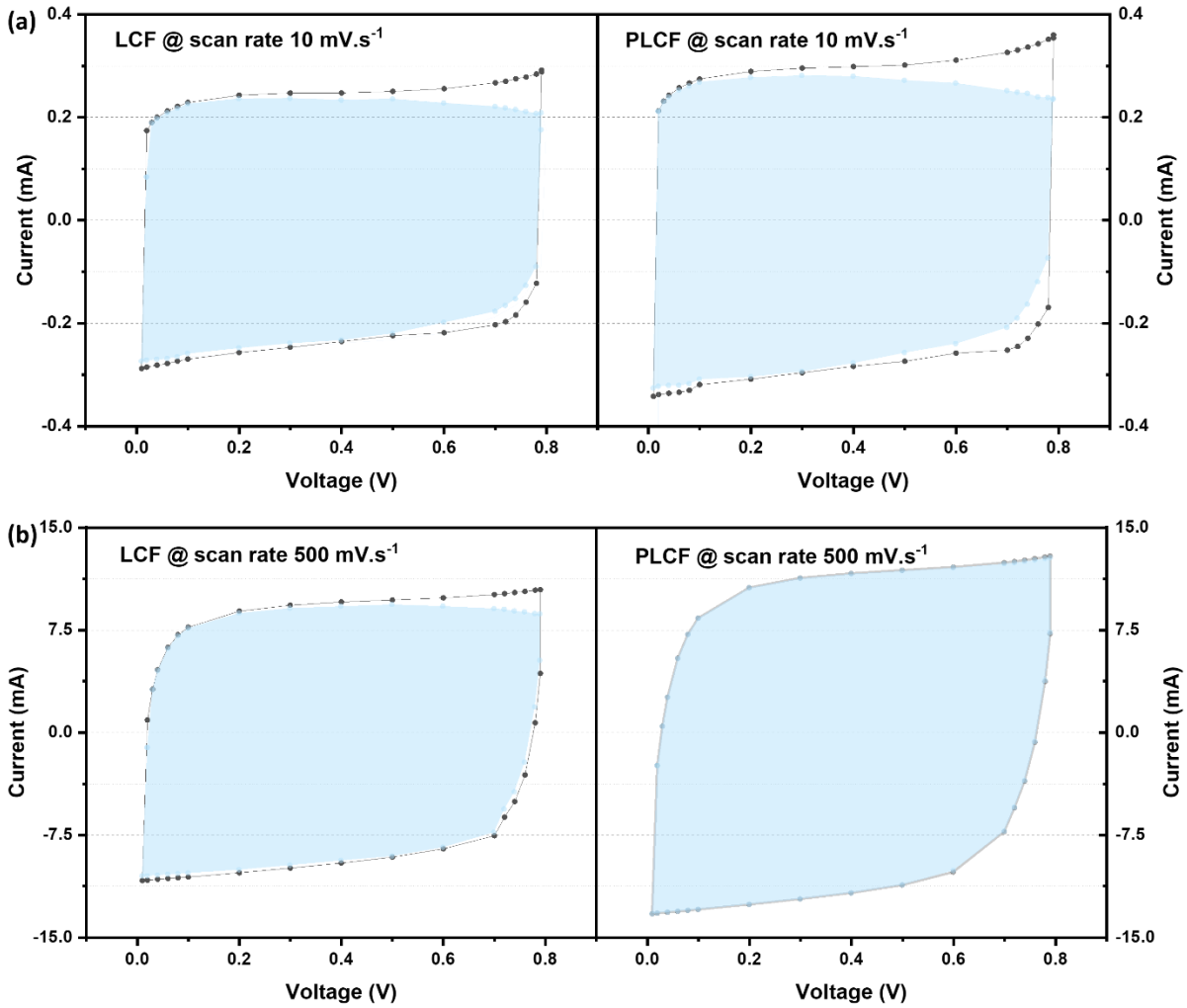

Fig.6. Capacitive currents (regions shaded in blue) of LCF and PLCF-containing devices at scan rates of (a) 10 and (b) 500 mV/s.

The calculation quantitively confirms the dominance of the surface capacitive contribution. Both the LCF and PLCF-containing devices hold around 93% of capacitive current at the low scan rate of 10 mV/s, see Fig. 6a. These high and similar percentages of the capacitive current in both devices suggest that the observed difference in the specific capacitance between the devices should be from the extent of pseudocapacitance originating from the surface functional groups. Additionally, the capacitance improvement could also be due to the enhanced wettability of the electrodes. The impact of the wettability on the capacitive performance is more prominent at a high scan rate compared to a low scan rate as the kinetics is slow at the low scan rate which could compensate for the wettability issue to some extent. Accordingly, it can be seen from Fig. 6 b that at the higher scan rate of 500 mV/s, the capacitive contribution increases to 96% for LCF- and 100% for the PLCF-containing device. A negligible

contribution from the diffusion-limited process in the PLCF-containing device compared to the LCF-containing device suggests that the kinetic limitation is reduced with the plasma treatment to a large extent and the inner layers of the electrodes participate in the capacitive charge storage. Owing to the improved wettability and pseudocapacitive contributions of the surface functional groups, the device containing PLCF demonstrates a significant improvement in energy and power density compared to the LCF-containing device. For instance, the PLCF-containing device exhibits an energy density and power density of 11 Wh/kg and 0.8 kW/kg, while LCF exhibits 8 Wh/kg and 0.8 kW/kg at a low current density of 0.5 A/g. At a higher current density of 10 A/g, both PLCF and LCF exhibits a high-power density of 16 kW/kg with an energy density of 8 Wh/kg and 6 Wh/kg, respectively.

At this point, it is worth mentioning the contribution of the electrolyte ions to the overall capacitive performance of the PLCF electrodes, particularly the compatibility and reactivity of certain surface functional groups with the electrolyte ions. For instance, it has been shown that mainly the carbonyl and hydroxyl groups are favorable for pseudocapacitance in a basic medium [23], such as a 6M KOH electrolyte. In order to verify the compatibility of the PLCF electrodes with the other types of aqueous mediums such as acidic and neutral, a brief electrochemical investigation has been carried out with 1M H_2SO_4, and 1M Li_2SO_4 as can be seen in Fig. S4. The capacitive properties of the acidic and neutral medium are not as impressive as the basic medium. A detailed investigation is necessary to fully understand the complex interactions at the interface with the acidic and neutral medium and therefore requires a separate study.

4.4.Device stability and cycling effect on capacitive performance

To verify the long-term stability of the electrodes, a new set of devices have been assembled with fresh electrodes and repetitive GCD experiments are carried out with a current density of 2 A/g within the voltage range of 0 - 0.8V for 10000 cycles. Fig. 7 shows the capacitance retention and coulombic efficiency of the devices containing both electrodes. The inset shows the GCD curve at different cycles.

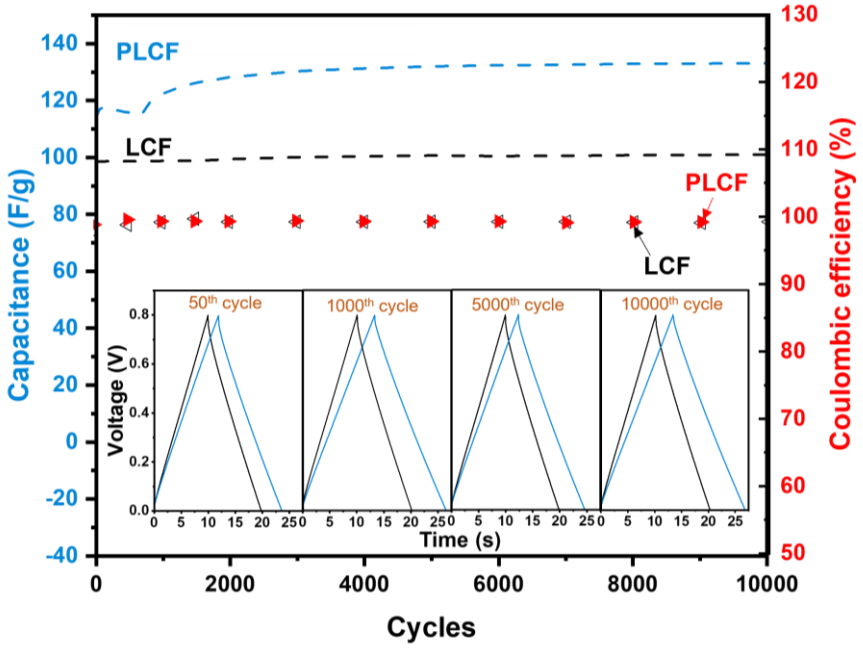

Fig.7. Cyclic stability and coulombic efficiency of the devices containing LCF and PLCF: capacitance (left axis) and coulombic efficiency (right axis) over 10 000 cycles. Inset: charge-discharge cycles in different intervals.

As can be seen, the linear and symmetric GCD curves of both devices are intact throughout the cycling period with a high coulombic efficiency of 99 %. Most importantly, the capacitive performance is not degraded over the test period. The observed phenomenon of no deterioration in the cyclic stability of the device further confirms an efficient and compatible electrode/electrolyte interface and shows that the selection of plasma power and duration is suitable. Introducing an adequate amount of stable functional groups is critical or else it can cause capacitance degradation with cycling, as reported in a previous study [40].

The LCF-containing device exhibits a stable capacitance during cycling with a marginal increase of 4%. As mentioned before, due to additional pseudocapacitance and improved wettability, the PLCF-containing device exhibits a higher capacitance of 115 F/g compared to the LCF-containing device of 99 F/g. An interesting behavior can be observed in the PLCF-containing device where the specific capacitance decreases in the initial 800 cycles and then monotonically increases up to 10 % at the end of cycling. The evolution of the capacitance in this manner could be related to multiple underlying competing mechanisms during charge/discharge that reach equilibrium over cycling and stabilizes the capacitance. It has been shown that some of the surface functional groups such as acidic carboxyl are unstable and during the initial charge/discharge cycle they go through conversion and result in a decrease in the oxygen content [50]. Therefore, the capacitance decrease in the initial 800 cycles could be related to the reduced pseudocapacitive contribution due to the transformation and elimination of these unstable surface functional groups [29]. Afterward, the capacitance gradually increases with cycling.

In order to verify the evolution of the capacitive signature, Fig. 8 shows the CV plot of both the devices before and after 10000 cycles with a scan rate of 10 mV/s in the voltage range of 0 - 0.8 V.

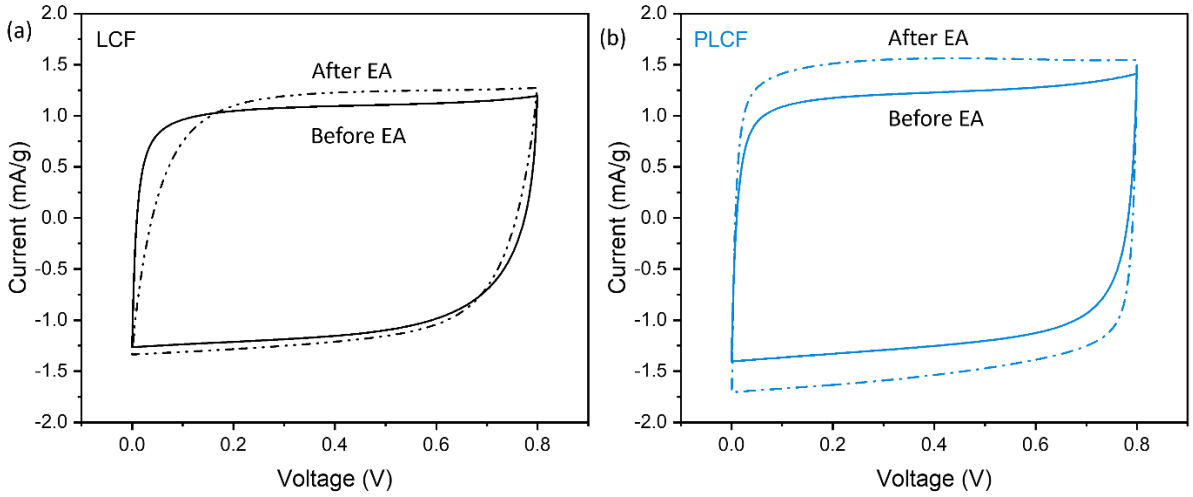

Fig.8. CV curves comparing the capacitive current contributions of (a) LCF- and (b) PLCF- containing devices before and after undergoing 10000 cycles.

It can be seen that the capacitive performance of both devices has been improved as indicated by the wider CV of the devices after cycling. Consequently, the increase of the specific capacitance of the cycled PLCF-containing device is calculated to be 16%, and cycled LCF-

containing device is to be 10% higher than the non-cycled devices. The improvement is noticed for higher scan rates as well, suggesting the rate performance is also improved after cycling.

The improved capacitive performance of both the devices after cycling could be related to the increased surface area that is easily accessible to the electrolyte ions as noticed in a previous study, where XPS analysis suggests that additional accumulated oxygen, CO_2, and soluble carbonates on the surface could also enhance the surface area as a result of the electrode surface etching [51]. It could also be attributed to the repeated insertions and desertions of K^+ ions in the electrode that opens up more pores as shown schematically in Fig. S6, which expands the active surface area [29] that was inaccessible for the ion penetration to the micro-sized pores in the initial cycles. However, the extent of the capacitive improvement is quite large for the PLCF-containing device as the strongly attached surface functional groups provide hydrophilicity and electronegativity to the electrodes which gets further improved with repetitive cycling and facilitates enhanced pore surface utilization. It is worth mentioning that, in order to accelerate the process of enhanced pore surface utilization an attempt of electrochemical activation is carried out where a new set of devices are exposed to an extended voltage of 1.2 V for 30 cycles at a scan rate of 20 mV/s. Subsequently, the capacitive performance is compared back at 0.8 V (Fig. S7) with the same scan rate. As can be seen, the capacitive currents degrade by 1.5% in LCF-containing devices and improve by up to 21% in PLCF-containing devices compared to the capacitive currents before cycling at the extended voltage. Although the theoretical decomposition voltage of water is 1.23 V, in practice it could shift below or above this value depending on the nature of the electrodes and electrolytes. Due to the presence of the surface functional groups in the PLCF, the electrode potential may have shifted away from the electrolyte decomposition voltage during the extended voltage operation as seen in the previous study [52], while the LCF-containing device suffered from the extended voltage operation.

Typically, during the cycling test, the device is exposed to the nominal voltage for a very short period. Therefore, it requires a considerable amount of cycling to obtain the impact which might be time-consuming. By electrochemical activation with an extended voltage, the process could be accelerated, but care must be taken to make sure the prevention of complete electrolyte decomposition. Regardless, the impact of cycling and electrochemical activation seems to have a positive influence on the overall performance of the PLCF-containing devices, particularly with improvement in both the capacitive and diffusion-limited charge storage mechanisms. The evolution of this improvement could be further verified with the impedance profile of the device at different states of health.

Fig. 9 shows the Nyquist plots from the EIS measurement.

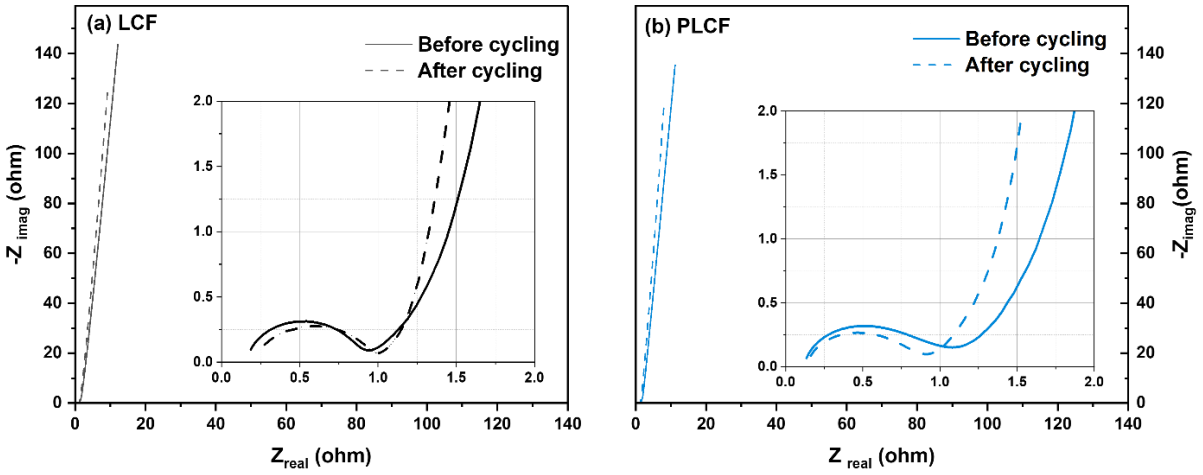

Fig.9. Nyquist plots of (a) LCF, and (b) PLCF-containing devices before and after 10,000 cycles.

EIS provides insight into the electrolyte transport properties in the two different electrodes. In a Nyquist plot, the first intersection point in the higher frequency domain represents equivalent series resistance (ESR) that predominantly originates from the bulk electrolyte and is quite often reported as the electrolyte resistance. Commercial supercapacitors report their ESR value at 1 kHz. The second intersection point of the semi-circle in the mid-frequency region is related to the interfacial resistance (R_{int}), considering the charge storage mechanism is primarily capacitive. R_{int} depends on the type of bulk electrolyte and gives a valuable understanding of the nature of the electrolyte/electrode interface. The transition from the mid-frequency region to the lowest-frequency region provides a qualitative measure of electrolyte diffusion to the electrodes.

It can be seen that the electrolyte resistance values are quite similar for both the devices before and after cycling, ranging from 0.19 to 0.27 Ω. This indicates that the electrolyte properties are not compromised during the cycling process. The ESR values extracted at 1kHz are 0.90, and 1.0 Ω for the LCF and PLCF-containing device before cycling, while the values change to 0.95, and 0.84 Ω, respectively, after cycling. A very small increase of the R_{int} can be seen in the LCF-containing device, while a noticeable decrease of R_{int} can be seen in the PLCF-containing device suggesting a gradual improvement of the kinetics in the interface. A significant change in the diffusion resistance can be noticed in both devices, where the diffusion resistance decreases by 2.8 and 6.2 Ω in the LCF-and PLCF-containing devices after cycling. At the lowest frequency, the devices behave in a purely capacitive way where the phase angles approach close to 90˚. Both the devices exhibit phase angle ranging from 84˚ to 86˚ before and after cycling (Fig S8), which is nearly as ideal capacitors. The observed change of the impedance characteristics, particularly ESR, $R_{int,}$ and the diffusion resistance is in agreement with the previous electrochemical measurements and reflects the positive contribution of the surface functional groups introduced by the plasma treatment.

5. Conclusion

We have demonstrated that electrospun LCF is a promising electrode material for supercapacitors. The intrinsic hydrophobicity of the LCF material can be overcome by decorating the electrode surface with different oxygen functional groups with a non-invasive technique, such as oxygen plasma treatment. The low-power and short-duration plasma treatment significantly improve the wettability/hydrophilicity by modifying the fiber surface's chemical state without compromising the compositional integrity of the electrodes. Therefore, the device containing the PLCF electrodes demonstrates 26% higher capacitance than the LCF

devices at scan rate 20 mV/s in an alkaline medium (6M KOH). The observed performance is due to the improved kinetics of the electrodes where, in addition to the pseudocapacitive contribution from the surface functional groups, the inner layers of the PLCF electrodes significantly contribute to the capacitive charge storage mechanisms with the negligible diffusion-limited process. XPS analysis confirms an increased amount of CO-type oxygen functional groups, such as phenolic, hydroxyl, and carbonyl are present in the PLCF electrodes, which favorably contributes to the capacitive performance improvement. Due to a less amount of carboxyl group on the surface, the device demonstrates a slower voltage decay in the self-discharge profile. The observed high cyclic stability and coulombic efficiency of the PLCF device over 10000 cycles indicate that the introduced surface functional groups do not have any detrimental impact on the electrodes. Rather, the capacitive performance enhancement after cycling validates a compatible electrode/electrolyte interface, where the pore surface utilization enhances over a repeated cycling period.

Although the charge storage of plasma-treated carbon fibers has been extensively investigated in this work, a more detailed inquiry into the plasma treatment conditions and gases remains. The underlying mechanisms of the role of oxygen functional groups for the boosted capacitive performance with cycling in alkaline media need further elucidation. In addition, the electrochemical performance of supercapacitors could be improved to a great extent by incorporating pseudocapacitive metal oxides on the LCF and PLCF that serves as a physical scaffold for the composite material. These are interesting venues for future work.

Acknowledgments

Authors acknowledge the *Wallenberg Wood Science Centre's (WWSC)* project 4.1.4 financially supported by the *Knut and Alice Wallenberg Foundation* of Sweden and the support of the European Research Council (ERC) under the European *Union's Horizon 2020 Program EU Horizon 2020 project GreEnergy* for this work. The authors acknowledge the technical assistance of Dr. Eric Tam at the Chalmers XPS facility.

References:

[1] Y. Liu and S. Kumar, "Recent Progress in Fabrication, Structure, and Properties of Carbon Fibers," *Polym. Rev.*, vol. 52, no. 3, pp. 234–258, Jul. 2012, doi: 10.1080/15583724.2012.705410.

[2] T. Peijs, R. Kirschbaum, and P. J. Lemstra, "Chapter 5: A critical review of carbon fiber and related products from an industrial perspective," *Adv. Ind. Eng. Polym. Res.*, vol. 5, no. 2, pp. 90–106, Apr. 2022, doi: 10.1016/j.aiepr.2022.03.008.

[3] J. Avossa, G. Herwig, C. Toncelli, F. Itel, and R. M. Rossi, "Electrospinning based on benign solvents: current definitions, implications and strategies," *Green Chem.*, vol. 24, no. 6, pp. 2347–2375, 2022, doi: 10.1039/D1GC04252A.

[4] Y. Yuan and G. Zhu, "Porous Aromatic Frameworks as a Platform for Multifunctional Applications," *ACS Cent. Sci.*, vol. 5, no. 3, pp. 409–418, Mar. 2019, doi: 10.1021/acscentsci.9b00047.

[5] H. Liu *et al.*, "Lignin-based electrodes for energy storage application," *Ind. Crops Prod.*, vol. 165, no. 113425, 2021.

[6] H. Wang *et al.*, "Lignin-based materials for electrochemical energy storage devices," *Nano Mater. Sci.*, p. S2589965122000022, Feb. 2022, doi: 10.1016/j.nanoms.2022.01.002.

[7] C. Lai, P. Kolla, Y. Zhao, H. Fong, and A. L.Smirnova, "Lignin-derived electrospun carbon nanofiber mats with supercritically deposited Ag nanoparticles for oxygen reduction reaction in alkaline fuel cells," vol. 130, pp. 431–438, 2014, doi: https://doi.org/10.1016/j.electacta.2014.03.006.

[8] X. Xu, J. Zhou, L. Jiang, G. Lubineau, S. A. Payne, and D. Gutschmidt, "Lignin-based carbon fibers: Carbon nanotube decoration and superior thermal stability," *Carbon*, vol. 80, pp. 91–102, Dec. 2014, doi: 10.1016/j.carbon.2014.08.042.
[9] H. Wu *et al.*, "Electrospun flexible lignin/polyacrylonitrile-based carbon nanofiber and its application in electrode materials for supercapacitors," *Text. Res. J.*, vol. 92, no. 3–4, pp. 456–466, Feb. 2022, doi: 10.1177/00405175211037191.
[10] S. Wang *et al.*, "Lignin-based carbon fibers: Formation, modification and potential applications," *Green Energy Environ.*, vol. 7, no. 4, pp. 578–605, Aug. 2022, doi: 10.1016/j.gee.2021.04.006.
[11] C. Lai *et al.*, "Free-standing and mechanically flexible mats consisting of electrospun carbon nanofibers made from a natural product of alkali lignin as binder-free electrodes for high-performance supercapacitors," *J. Power Sources*, vol. 247, pp. 134–141, Feb. 2014, doi: 10.1016/j.jpowsour.2013.08.082.
[12] S. Hu, S. Zhang, N. Pan, and Y.-L. Hsieh, "High energy density supercapacitors from lignin derived submicron activated carbon fibers in aqueous electrolytes," *J. Power Sources*, vol. 270, pp. 106–112, Dec. 2014, doi: 10.1016/j.jpowsour.2014.07.063.
[13] V. Passoni, C. Scarica, M. Levi, S. Turri, and G. Griffini, "Fractionation of Industrial Softwood Kraft Lignin: Solvent Selection as a Tool for Tailored Material Properties," *ACS Sustain. Chem. Eng.*, vol. 4, no. 4, pp. 2232–2242, Apr. 2016, doi: 10.1021/acssuschemeng.5b01722.
[14] I. Khan, B. Hararak, and G. F. Fernando, "Improved Procedure for Electro-Spinning and Carbonisation of Neat Solvent-Fractionated Softwood Kraft Lignin," In Review, preprint, Feb. 2021. doi: 10.21203/rs.3.rs-195377/v1.
[15] H. Jia *et al.*, "Electrospun Kraft Lignin/Cellulose Acetate-Derived Nanocarbon Network as an Anode for High-Performance Sodium-Ion Batteries," *ACS Appl. Mater. Interfaces*, vol. 10, no. 51, pp. 44368–44375, Dec. 2018, doi: 10.1021/acsami.8b13033.
[16] M. Kumar, M. Hietala, and K. Oksman, "Lignin-Based Electrospun Carbon Nanofibers," *Front. Mater.*, vol. 6, no. 62, 2019, doi: https://doi.org/10.3389/fmats.2019.00062.
[17] G. Sun, L. Sun, H. Xie, and J. Liu, "Electrospinning of Nanofibers for Energy Applications," *Nanomaterials*, vol. 6, no. 7, p. 129, Jul. 2016, doi: 10.3390/nano6070129.
[18] J. P. Jyothibasu, R.-H. Wang, Y.-C. Tien, C.-C. Kuo, and R.-H. Lee, "Lignin-Derived Quinone Redox Moieties for Bio-Based Supercapacitors," *Polymers*, vol. 14, no. 15, p. 3106, Jul. 2022, doi: 10.3390/polym14153106.
[19] H. Young Jung, J. Seok Lee, H. Taek Han, J. Jung, and K. Eom, "Lignin-Based Materials for Sustainable Rechargeable Batteries," *Polymers*, vol. 14, no. 673, 2022, doi: https://doi.org/10.3390/polym14040673.
[20] P. Schlee *et al.*, "From Waste to Wealth: From Kraft Lignin to Free-standing Supercapacitors," *Carbon*, vol. 145, pp. 470–480, 2019.
[21] A. A. Adam *et al.*, "State of the Art and New Directions on Electrospun Lignin/Cellulose Nanofibers for Supercapacitor Application: A Systematic Literature Review," *Polymers*, vol. 12, no. 12, p. 2884, Dec. 2020, doi: 10.3390/polym12122884.
[22] R. A. Perera Jayawickramage and J. P. Ferraris, "High performance supercapacitors using lignin based electrospun carbon nanofiber electrodes in ionic liquid electrolytes," *Nanotechnology*, vol. 30, no. 15, p. 155402, Apr. 2019, doi: 10.1088/1361-6528/aafe95.
[23] S. Ghosh, S. Barg, S. M. Jeong, and K. Ostrikov, "Heteroatom-Doped and Oxygen-Functionalized Nanocarbons for High-Performance Supercapacitors," *Adv Energy Mater*, vol. 10, no. 32, Art. no. 32, 2020.
[24] T. Liu, K. Wang, Y. Chen, S. Zhao, and Y. Han, "Dominant role of wettability in improving the specific capacitance," *Green Energy Environ.*, vol. 4, no. 2, pp. 171–179, Apr. 2019, doi: 10.1016/j.gee.2019.01.010.
[25] B. Szubzda, A. Szmaja, and A. Halama, "Influence of structure and wettability of supercapacitor electrodes carbon materials on their electrochemical properties in water and organic solutions," *Electrochimica Acta*, vol. 86, pp. 255–259, Dec. 2012, doi: 10.1016/j.electacta.2012.08.060.
[26] Y. Li and M. Zhang, "Mechanical properties of activated carbon fibers," in *Activated Carbon Fiber and Textiles*, Elsevier, 2017, pp. 167–180. doi: 10.1016/B978-0-08-100660-3.00006-7.

[27] M. Zhu *et al.*, "Electrospun Lignin-Based Carbon Nanofibers as Supercapacitor Electrodes," *ACS Sustain. Chem. Eng.*, vol. 8, no. 34, pp. 12831–12841, Aug. 2020, doi: 10.1021/acssuschemeng.0c03062.
[28] P. Schlee *et al.*, "Free-standing supercapacitors from Kraft lignin nanofibers with remarkable volumetric energy density," *Chem. Sci.*, vol. 10, pp. 2980–2988, 2019.
[29] Y. He *et al.*, "Capacitive mechanism of oxygen functional groups on carbon surface in supercapacitors," *Electrochimica Acta*, vol. 282, pp. 618–625, Aug. 2018, doi: 10.1016/j.electacta.2018.06.103.
[30] Y. Can Gorur, "Surface Treatment of Softwood Lignin Based Carbon Fibers for Enhanced Interfacial Adhesion." Luleå University of Technology, Department of Engineering Sciences and Mathematics, 2017.
[31] Z. Ding, V. Trouillet, and S. Dsoke, "Are Functional Groups Beneficial or Harmful on the Electrochemical Performance of Activated Carbon Electrodes?," *J. Electrochem. Soc.*, vol. 166, no. 6, pp. A1004–A1014, 2019, doi: 10.1149/2.0451906jes.
[32] K. Okajima, K. Ohta, and M. Sudoh, "Capacitance behavior of activated carbon fibers with oxygen-plasma treatment," *Electrochimica Acta*, vol. 50, no. 11, pp. 2227–2231, Apr. 2005, doi: 10.1016/j.electacta.2004.10.005.
[33] W. Zhu, G. Westman, and H. Theliander, "Investigation and Characterization of Lignin Precipitation in the LignoBoost Process," *J. Wood Chem. Technol.*, vol. 34, no. 2, pp. 77–97, Apr. 2014, doi: 10.1080/02773813.2013.838267.
[34] O. Hosseinaei and D. A. Baker, "High Glass Transition Lignins and Lignin Derivatives for the Manufacture of Carbon and Graphite Fibers"
[35] K. Peuvot, O. Hosseinaei, P. Tomani, D. Zenkert, and G. Lindbergh, "Lignin Based Electrospun Carbon Fiber Anode for Sodium Ion Batteries," *J. Electrochem. Soc.*, vol. 166, no. 10, pp. A1984–A1990, 2019.
[36] F. Souto, V. Calado, and N. Pereira, "Lignin-based carbon fiber: a current overview," *Mater. Res. Express*, vol. 5, no. 7, p. 072001, Jul. 2018, doi: 10.1088/2053-1591/aaba00.
[37] N. Dilsiz, "Plasma surface modification of carbon fibers: a review," *J. Adhes. Sci. Technol.*, vol. 14, no. 7, pp. 975–987, Jan. 2000, doi: 10.1163/156856100743013.
[38] D. Tashima, M. Hirano, S. Kitazaki, T. Eguchi, and S. Kumagai, "Oxygen-Plasma Surface Treatment of an Electrode Sheet Using Carbon from Japanese Distilled Liquor Waste for Double-layer Capacitors," *Electrochem*, vol. 1, no. 3, pp. 322–328, Sep. 2020, doi: 10.3390/electrochem1030020.
[39] K. G. Latham, L. Matsakas, J. Figueira, U. Rova, P. Christakopoulos, and S. Jansson, "Examination of how variations in lignin properties from Kraft and organosolv extraction influence the physicochemical characteristics of hydrothermal carbon," *J. Anal. Appl. Pyrolysis*, vol. 155, p. 105095, May 2021, doi: 10.1016/j.jaap.2021.105095.
[40] M. W. Thielke *et al.*, "Full Lignin-Derived Electrospun Carbon Materials as Electrodes for Supercapacitors," *Front. Mater.*, vol. 9, p. 859872, May 2022, doi: 10.3389/fmats.2022.859872.
[41] N. Thongsai, K. Hrimchum, and D. Aussawasathien, "Carbon fiber mat from palm-kernel-shell lignin/polyacrylonitrile as intrinsic-doping electrode in supercapacitor," *Sustain. Mater. Technol.*, vol. 30, p. e00341, Dec. 2021, doi: 10.1016/j.susmat.2021.e00341.
[42] R. Yuan, Y. Dong, R. Hou, S. Zhang, and H. Song, "Review—Influencing Factors and Suppressing Strategies of the Self-Discharge for Carbon Electrode Materials in Supercapacitors," *J. Electrochem. Soc.*, vol. 169, no. 3, p. 030504, Mar. 2022, doi: 10.1149/1945-7111/ac56a1.
[43] Y. Peng *et al.*, "Oxygen-Containing Functional Groups Regulating the Carbon/Electrolyte Interfacial Properties Toward Enhanced K+ Storage," *Nano-Micro Lett.*, vol. 13, no. 1, p. 192, Dec. 2021, doi: 10.1007/s40820-021-00722-3.
[44] L. Li and F. Li, "The effect of carbonyl, carboxyl and hydroxyl groups on the capacitance of carbon nanotubes," *New Carbon Mater.*, vol. 26, no. 3, pp. 224–228, Jun. 2011, doi: 10.1016/S1872-5805(11)60078-4.
[45] H. Oda, A. Yamashita, S. Minoura, M. Okamoto, and T. Morimoto, "Modification of the oxygen-containing functional group on activated carbon fiber in electrodes of an electric double-

layer capacitor," *J. Power Sources*, vol. 158, no. 2, pp. 1510–1516, Aug. 2006, doi: 10.1016/j.jpowsour.2005.10.061.
[46] Y.-R. Nian and H. Teng, "Influence of surface oxides on the impedance behavior of carbon-based electrochemical capacitors," *J. Electroanal. Chem.*, vol. 540, pp. 119–127, Jan. 2003, doi: 10.1016/S0022-0728(02)01299-8.
[47] Q. Li *et al.*, "Explanation of anomalous rate capability enhancement by manganese oxide incorporation in carbon nanofiber electrodes for electrochemical capacitors," *Electrochimica Acta*, vol. 340, p. 135921, Apr. 2020, doi: 10.1016/j.electacta.2020.135921.
[48] A. Noori, M. F. El-Kady, M. S. Rahmanifar, R. B. Kaner, and M. F. Mousavi, "Towards establishing standard performance metrics for batteries, supercapacitors and beyond," *Chem. Soc. Rev.*, vol. 48, no. 5, pp. 1272–1341, 2019, doi: 10.1039/C8CS00581H.
[49] M. Forghani and S. W. Donne, "Method Comparison for Deconvoluting Capacitive and Pseudo-Capacitive Contributions to Electrochemical Capacitor Electrode Behavior," *J. Electrochem. Soc.*, vol. 165, no. 3, pp. A664–A673, 2018, doi: 10.1149/2.0931803jes.
[50] X. Li *et al.*, "Effect of the oxygen functional groups of activated carbon on its electrochemical performance for supercapacitors," *New Carbon Mater.*, vol. 35, no. 3, pp. 232–243, Jun. 2020, doi: 10.1016/S1872-5805(20)60487-5.
[51] B. W. Allen and C. A. Piantadosi, "Electrochemical activation of electrodes for amperometric detection of nitric oxide," *Nitric Oxide*, vol. 8, no. 4, pp. 243–252, Jun. 2003, doi: 10.1016/S1089-8603(03)00029-6.
[52] E. Raymundo-Piñero, F. Leroux, and F. Béguin, "A High-Performance Carbon for Supercapacitors Obtained by Carbonization of a Seaweed Biopolymer," *Adv. Mater.*, vol. 18, no. 14, pp. 1877–1882, Jul. 2006, doi: 10.1002/adma.200501905.

Supplementary information

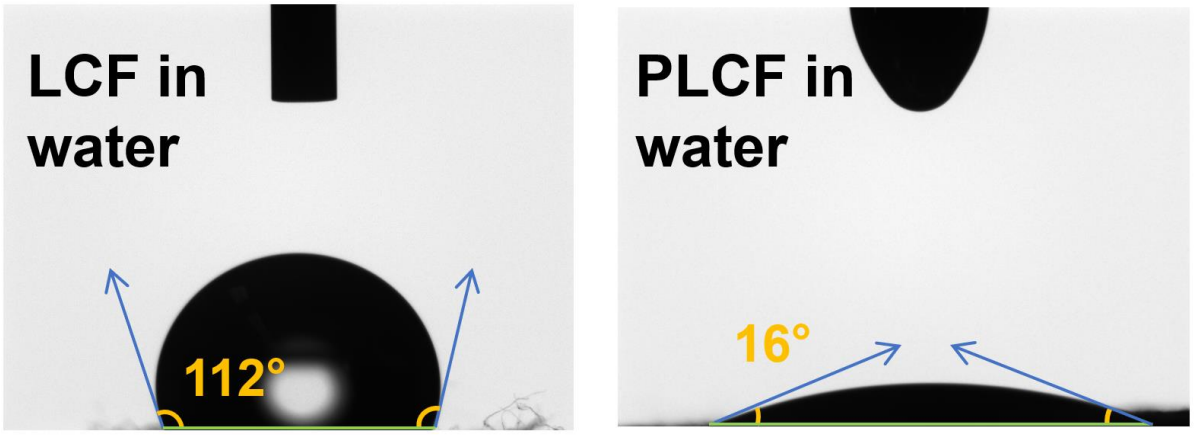

Fig.S1. Images obtained from contact angle measurements of LCF versus PLCF mat surfaces reveal that the latter after plasma treatment has a stronger affinity for a water droplet than the former.

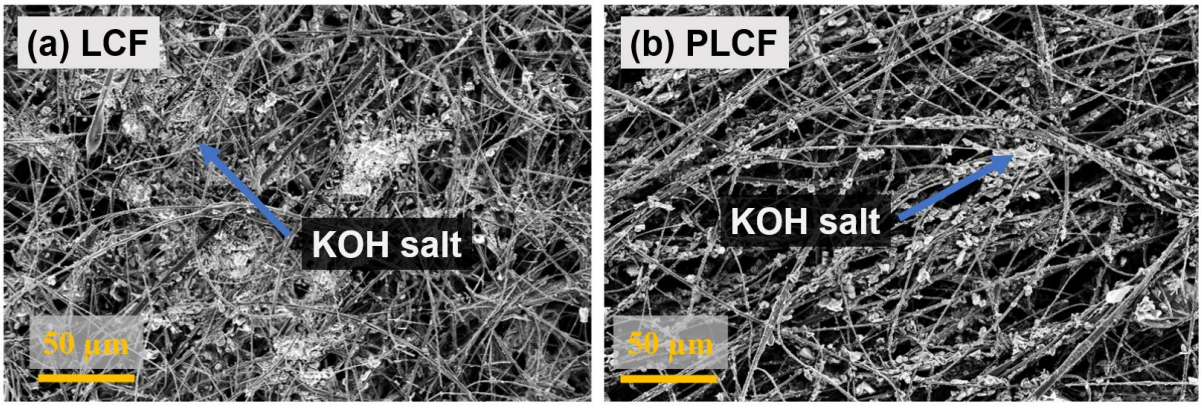

Fig.S2. Images of dried KOH electrolyte salts deposited on the surfaces of recovered (a) LCF and (b) PLCF electrodes after cell disassembly. It gives information about the heavily restricted accessibility of electrolyte ions limited to the outer layers of the fiber mat in LCF vs the ability for electrolyte ions to penetrate easily through the interlayers in the PLCF with improved wettability by plasma treatment.

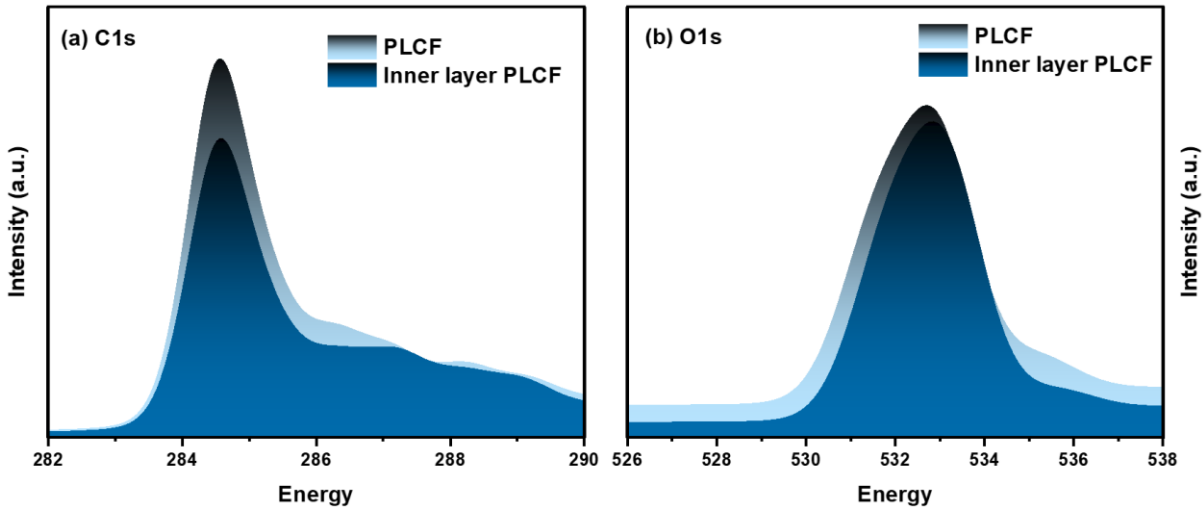

Fig.S3. The C-spectrum (a) And O-spectrum (b) of the outer and deeper layers of PLCF.

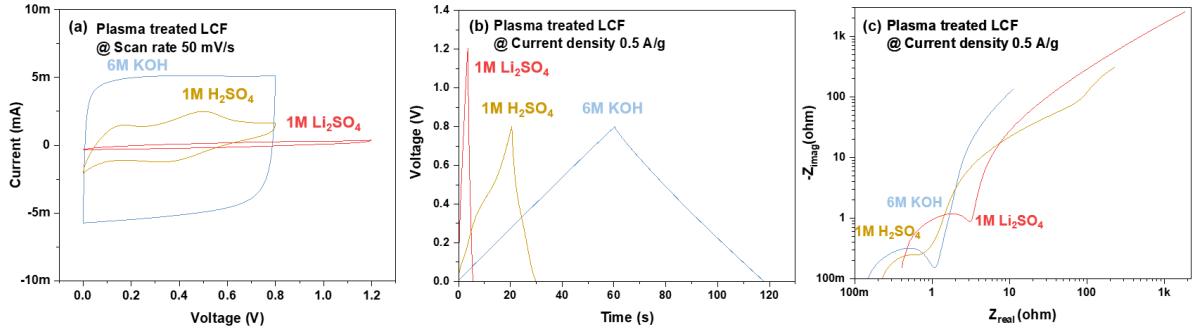

Fig. S4. Comparison of (a) CV curves (b) GCD curves,(c) EIS, and (d) B0.04 s and 0.0.ode plot of PLCF in different aqueous electrolytes- KOH, Li_2SO_4, and H_2SO_4 electrolytes

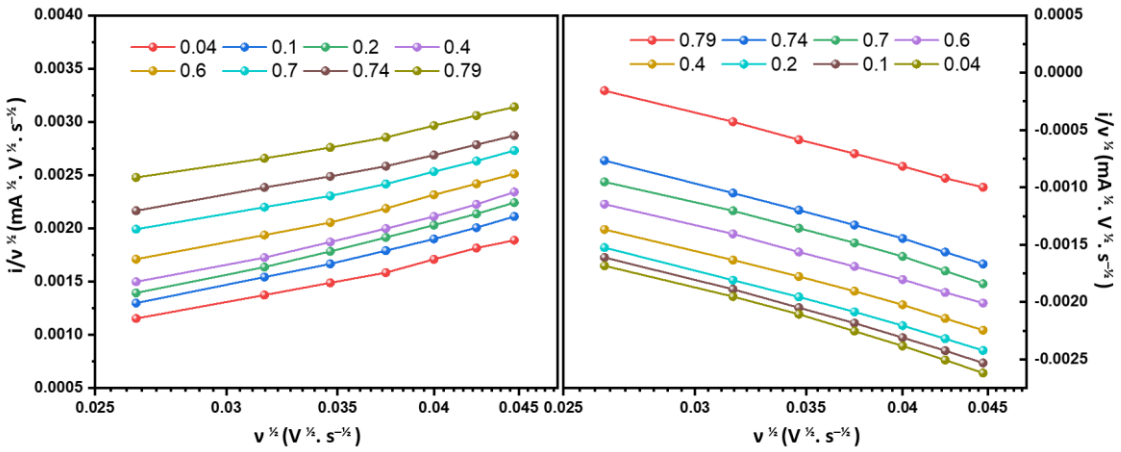

Fig. S5. (a) Linear fitting of the anodic and cathodic CV scan rates at different voltage points.

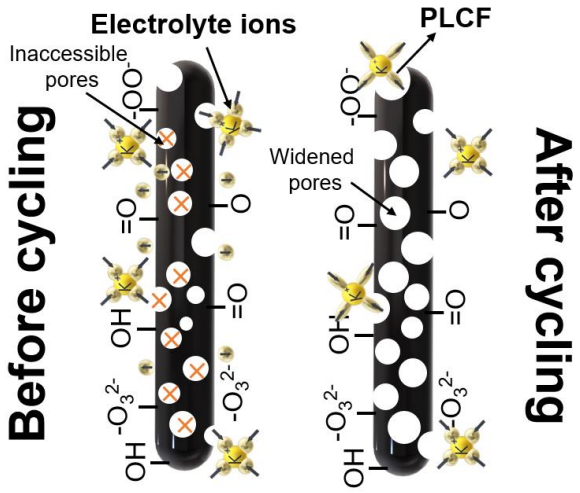

Fig.S6. Schematic representation of the accessibility of solvated KOH electrolyte ions to unfit pores (red-crossed) after cycling over a series of continuous insertions and desertions in PLCF electrodes

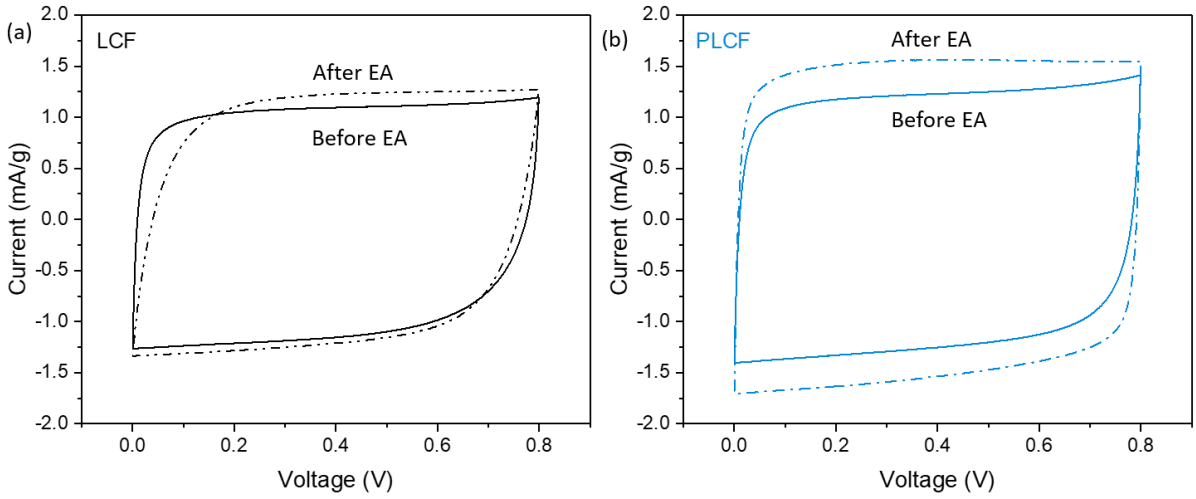

Fig. S7. GCD curves comparing the capacitive current contributions of LCF and PLCF (a) before and (b) after undergoing 20 cycles of electrochemical activation at 1.2V.

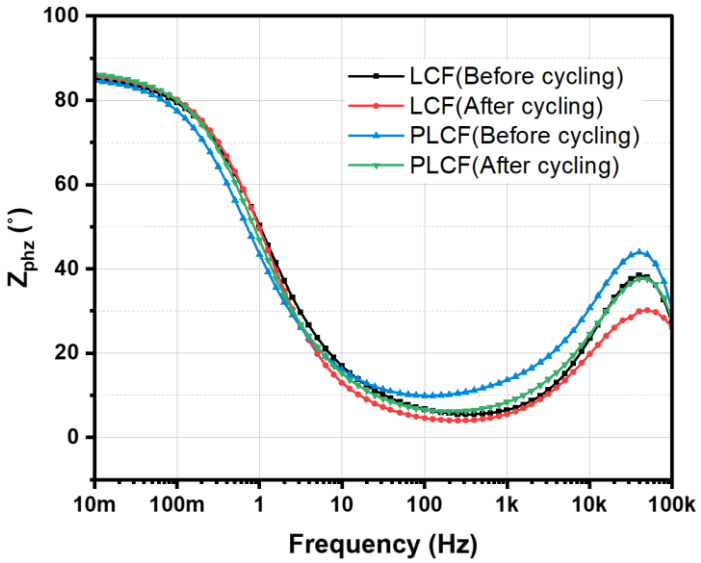

Fig.S8. Bode plot curves of both LCF and PLCF before and after undergoing cycling.

physica status solidi b
www.pss-b.com

Durable Activated Carbon Electrodes with a Green Binder

Azega R. K., Mohammad Mazharul Haque, Agin Vyas, Pui Lam Tam, Anderson D. Smith, Per Lundgren, and Peter Enoksson*

Herein, the fabrication and electrochemical performance of thick (180–280 µm) activated carbon (AC) electrodes with carbonized lignin-derived carbon fiber (LCF) inclusions are reported. Efforts are taken in fabricating robust free-standing electrodes from an environmentally friendly binder, microfibrillated cellulose (MFC), considering the biologically hazardous nature of other commonly used binders like polytetrafluoroethylene (PTFE), n-methyl-2-pyrrolidone (NMP), and polyvinylidene fluoride (PVDF). Generally, electrodes composed of MFC binder are prone to cracking upon drying, especially with higher mass loadings, which leads to nonflexibility and poor device stability. The LCF inclusions into the AC electrode with MFC binders not only increase flexibility but also contribute to better conductivity in the electrodes. The LCFs act as an intermediate layer among AC particles and serve as conductive pathways, facilitating exposure of more active surfaces to the electrolyte. A thick electrode with high mass loading of 10 mg cm^{-2} is achieved. The results show that by incorporating 2 wt% LCF to the AC material, the best device with 5 mg cm^{-2} delivers a specific capacitance of 97 F g^{-1}, while the specific capacitance of the reference AC device without LCF is 85 F g^{-1}.

1. Introduction

Activated carbon (AC) is the predominant commercial choice of electrode material for charge storage in supercapacitors today. AC has an advantageous high surface area, and its mature manufacturing technology makes it a convenient commercially available low-cost material. Generally, environmentally unsafe fluorinated polymers have been used as binders to fabricate supercapacitors and battery electrodes to bind the AC particles together alongside conductive agents like carbon black (CB).[1] As alternatives, carboxymethyl cellulose (CMC), starch, casein, and natural polymers have been some of the green binder material choices.[2,3] In the interest of moving toward ecofriendly electrodes, a trial to use a cellulose-based binder, microfibrillated cellulose (MFC), is undertaken. The good binding property of MFC facilitates an increased packing density of the material, which is highly beneficial for the synthesis of thick electrodes. Utilizing such thick electrodes is a viable strategy to increase the stored charge per packaged device, as they contain more material compared with thin electrodes. However, the capacitive contribution from the deeper parts of the thick electrodes is insignificant if they are limited by the through-plane conductivity or inaccessible to the electrolyte ions in the system, which is typically the case. Therefore, the involvement of highly packed or mass-loaded electrodes risks the rate capability and specific power performance of the device. To resolve such issues, the incorporation of engineered structured materials such as quantum dots,[4,5] carbon nanomaterials,[6–8] MXenes,[9] and microspheres[10] into the electrode materials is a promising solution as they serve as good conductive pathways aiding through-plane conductivity of the electrodes with improved dynamics. For example, Gryglewicz et al. demonstrated a composite material containing ACs grafted with carbon nanofibers (CNFs) deposited by a chemical vapor deposition (CVD) process through the decomposition of propane with a 5% Ni catalyst. The composite material with shorter carbon fibers showed better electrical double layer capacitor (EDLC) performances explained by the presence of herringbone CNFs enacting as electronic bridges between AC particles facilitating better diffusion of ions.[11] Carbon nanotubes' inclusions in AC matrix provisions as channels for charge transport, improving site accessibility.[12] Polyacrylonitrile precursor-based conductive carbon fibers function as current collectors for depositing AC particles for flexible supercapacitors.[13]

Azega R. K., M. M. Haque, A. Vyas, P. Lundgren, P. Enoksson
Micro-Nano Systems Group
Electronics Materials and Systems
Department of Microtechnology and Nanoscience
Chalmers University of Technology
412 58 Gothenburg, Sweden
E-mail: azega@chalmers.se

A. D. Smith
Department of Electrical Engineering
Chalmers University of Technology
Hörsalvägen 7, 41296 Gothenburg, Sweden

P. L. Tam
Department of Industrial and Materials Science
Chalmers University of Technology
Rännvägen 2A, 412 96 Gothenburg, Sweden

P. Enoksson
Enoaviatech AB
112 26 Stockholm, Sweden

P. Enoksson
Smoltek AB
Kaserntorget 7, 411 18 Gothenburg, DS, Sweden

The ORCID identification number(s) for the author(s) of this article can be found under https://doi.org/10.1002/pssb.202100311.

DOI: 10.1002/pssb.202100311

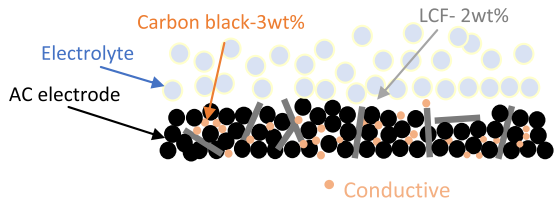

Figure 1. Schematic representation of the AC/LCF electrode depicting the fibers as reinforcements for the AC particles to be held together and its in-plane and through-plane conductive contribution in the AC matrix.

Likewise, lignin-based carbon fibers (LCFs) synthesized under optimized stabilization and carbonization conditions are well known for their higher graphitic nature contributing to higher electrical conductivity besides their function as a superior active material and current collector for the electrodes.[14] Apart from that, the fibers synthesized by the melt-spinning process have a high interfacial shear strength.[15]

Therefore, in this work, we have synthesized electrodes of different mass loadings by incorporating LCF in the commercially available AC material and characterized their initial electrochemical performance. The scope is to analyze the contributions of LCFs as a conductive agent (**Figure 1**) compared with the AC electrodes with only CB as the conductive agent.

2. Experimental Section

2.1. Materials

AC from the TCI chemicals supplier was used as the main component of electrode materials. The conductive agents, CB and LCF (carbonized at 1000 °C), were supplied by RISE in Sweden. MFC with 2.1% dry content was used as the electrode binder material.

2.2. Fabrication of AC/LCF Electrodes

The vacuum-dried samples of AC powder, 3 wt% CB, and 2 wt% LCF were mixed with 5 wt% MFC to prepare a suspension that was stirred overnight. The suspension with different mass loadings, 5, 7, and 10 mg cm^{-2}, was transferred to glass Petri dishes in the open air for a maximum of 2 days to prepare freestanding films. Afterward, the freestanding films were dried in the furnace for 4 h at 75 °C under vacuum to minimize the moisture. The reference electrodes without LCF were prepared in a similar procedure but with an increased CB amount of 5 wt%. Finally, the freestanding electrodes were punched out from the films with a circular disc cutter. The diameter of the individual electrodes was 8 mm.

Throughout this work, pure AC electrodes and LCFs that included AC electrodes were named AC-n and AC/LCF-n, respectively, where the n indicates the mass loadings, which were 5, 7, or 10 mg cm^{-2}. Their corresponding thicknesses were 180, 220, and 280 µm, respectively, with uncertainties lesser than ±5 µm.

2.3. Materials' Characterization

Scanning electron microscopy (SEM) LEO Ultra 55 was used to analyze the fiber morphology of the electrospun LCF. The secondary-electron detector was used to analyze the fiber surface in a high-vacuum mode of 3 kV, while the microscope operated at 1 kV accelerating voltage.

The conductivity measurements of LCFs were carried out with a Keithley 2400 conductivity analyzer. The resistivity, ρ, reciprocal of conductivity σ was calculated using the standard four-point probe formula

$$\sigma = \left[\frac{V}{I} \cdot \frac{w \cdot t}{s}\right]^{-1} \quad (1)$$

where V stands for the voltage difference, I for the current, w the fiber width, t for the fiber thickness, and s separation between the electrodes.

Surface composition and the chemical states of the elements of interests were studied by means of X-ray photoelectron spectroscopy (XPS). PHI 5000 VersaProbe III Scanning XPS Microprobe equipped with a monochromatic Al Kα X-ray source of photon energy 1486.6 eV was used, and the used beam size was set at 100 µm. For the insufficient sample conductivity, dual-charge compensation by an electron neutralizer and argon-ion gun was applied during the measurements. Surface composition was evaluated based on the survey scan with a wide scanning energy range between 0 and 1250 eV; the pass energy was at 280 eV and step size was at 1.0 eV. To analyze the chemical states of each element, high-resolution regional scans were conducted with the pass energy 26 eV and step size 0.1 eV. Prior to the qualitative analysis, the results from narrow scans were aligned with the adventitious carbon C 1s peak at 284.8 eV. The energy scale of the system, in contrast, was calibrated with reference to ISO 15 472:2010, in which the core levels of pure gold (Au $4f_{7/2}$), silver (Ag $3d_{5/2}$), and copper (Cu $2p_{3/2}$) were aligned at 83.96, 368.21, and 932.62 eV, respectively. Peak deconvolution was conducted using the MultiPak software. The spectra were first fit above the Shirley background, and the fit peaks were assigned at a specific energy peak position in the spectral envelope. Gaussian–Lorenztian function was used to fit the peak shape, and the full width at half maximum (FWHM) of the peak width was less than 2.0 eV in all the fitted curves. The contributions of each chemical state in a specific element were determined with reference to the area ratios of the fit peaks in the spectral envelope.

2.4. Electrochemical Measurements

The electrochemical performance was studied for a symmetrical supercapacitor device containing two similar electrodes assembled in a CR2025 coin cell, as shown in **Figure 2**. For their construction, the two identically mass-loaded electrodes were electrically isolated with a Whatman glass fiber membrane separator (10 mm in diameter). The assembled sandwich structure containing the aforementioned materials was soaked with 50 µL of 6 M KOH electrolyte before encapsulating the device.

Electrochemical measurements were carried out by cyclic voltammetry (CV), galvanostatic charge–discharge (GCD), cyclic charge–discharge (CCD), and electrochemical impedance spectroscopy (EIS) using a Gamry Reference 3000AE electrochemical workstation. The specific capacitance ($C_{s,CV}$ in F g^{-1}) was measured from CV data using Equation (2), as follows:

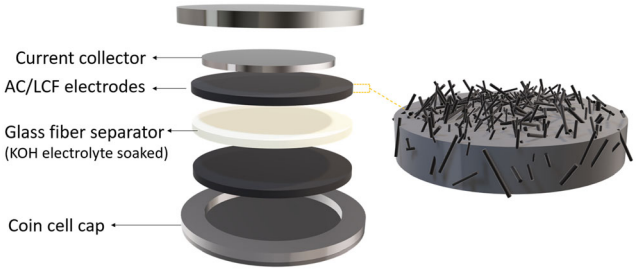

Figure 2. Schematic representation of the device construction with the prepared electrodes.[16]

$$C_{s,CV} = 4 \times 1000 \times \frac{\int_0^{2\cdot\Delta V/\nu_s} |i| dt}{2 \cdot m \cdot \Delta V} \quad (2)$$

where $I(A)$ is the current, ν is the scan rate, ΔV is the operating voltage window, and m is the mass of both the electrodes in the cell. The specific capacitances ($C_{s,GCD}$ in F g^{-1}) from GCD curves were calculated using Equation (3) as follows:[16]

$$C_{s,GCD} = 4 \times \frac{I_d \cdot t_d}{m \cdot V_d} \quad (3)$$

where I_d is the discharge current, t_d is the discharge time, and V_d is the voltage from the discharge curve excluding the internal resistance (IR) drop.

In addition, energy density (E in Wh kg^{-1}) and average power density (P_{avg} in W kg^{-1}) of the device are calculated from GCD curves, according to the following equations.[16]

$$C_d = \frac{C_{s,GCD}}{4} \quad (4)$$

$$E = \frac{1}{2} \times \frac{C_d \cdot {V_d}^2}{3.6} \quad (5)$$

$$P_{avg} = 3600 \times \frac{E}{t_d} \quad (6)$$

where the 3.6 and 3600 are unit time conversion factors. To calculate the specific device capacitance C_d, the $C_{s,GCD}$ values were divided by a factor of 4.

3. Results and Discussion

3.1. Material Characterization

The MFC-based electrodes are freestanding and not prone to breakage without stress. Under all mass loadings, the LCF alongside CB and MFC binder cooperated in holding the AC particles well, while the electrodes without LCFs were quite fragile during device assembly. **Figure 3**a shows the magnified SEM image of the AC electrode with large-sized AC particles ranging between 10 and 15 μm. The LCF fiber included in the AC matrix has a diameter of 13 μm and lengths ranging between 300 and 400 μm. The distribution of the fibers was observed to be uniform throughout the electrode even with the small LCF inclusion wt%. The low-magnification SEM image from a cracked middle cross section of AC/LCF-10 in Figure 3b shows the functionality of LCF as reinforcement in holding the AC particles together.

In addition, the LCF's measurements from the four-point probe show resistivity of 0.03 Ω cm, assuring their highly conductive nature that eventually facilitates good electronic conductivity to the AC particles in deeper layers, as demonstrated in Figure 1. Moreover, the observed unfilled voids around the AC electrode particle−LCF interface besides other voids additionally could aid in electrolyte impregnation as remarked for some commercial electrodes.[17] For further improvement of the electrode flexibility, the MFC binding could be complemented with strong elastomeric materials like styrene−butadiene−rubber (SBR).[18,19]

Figure 4a shows the survey-scan spectra from the XPS measurements of the AC and AC/LCF electrodes. Both samples show two distinct peaks. They correspond to carbon (C1s ≅ 284.8 eV) and oxygen (O1s ≅ 532.7 eV), respectively.

Results from XPS and XRD (see Figure S1, Supporting Information) show that LCF, as an additive, does not modify the surface composition of the AC electrode. However, in view of chemical state analyses, the contributions from carboxylic (COO^-), hydroxyl (−OH), and ketone (C═O) groups were altered. A slight increase in the carboxylic group and a significant increase in quinone/ketone groups are observed for the AC electrodes (Figure 4b). The presence of quinone/ketone groups usually contributes to an increased pseudocapacitance[20] that originates from the redox reaction by hydroquinone/quinone moieties in the system. The additional quinone groups for AC electrodes indicate the reduced availability of these redox functional groups by adding LCF inclusion to AC electrode. With corresponding conversion procedures, LCF−OH could be modified to form additional hydroquinones, which could potentially add to AC/LCF electrodes' pseudocapacitance.[21]

3.2. Electrochemical Performance

The CV curves of electrodes with mass loadings of 5 and 7 mg cm^{-2} at 20 mV s^{-1} scan rate, are shown in **Figure 5**a. The electrode's ability to store charge with 6 M KOH electrolyte was found effective in the electrochemical voltage window of 0−0.8 V. An EDLC-based reversible capacitive behavior is observed for both the electrodes as the CV curves exhibit a typical rectangular shape. The specific capacitance value for AC/LCF-5 is calculated to be 97 F g^{-1}, while for the AC-5, it is 85 F g^{-1}. However, with increasing mass loadings of 7 and 10 mg cm^{-2}, the capacitance values remain similar for both the AC and AC/LCF electrodes, especially at higher scan rates of 100 mV s^{-1} and above. The additional specific capacitance of the AC/LCF electrodes at lower scan rates suggests that the LCF promotes better ion penetration into the pores but only at a limited rate.

The GCD curves at a current density of 1 A g^{-1} are shown in Figure 5b. The curves are almost symmetrically triangular but have a small IR drop for all devices regardless of their electrodes. It is slightly larger for the electrodes with higher mass loading of 7 mg cm^{-2}, and it is higher by about 13 mV in AC electrodes compared with AC/LCF electrodes, indicating slightly lower IRs at 5 mg cm^{-2} mass loading. The AC electrodes with

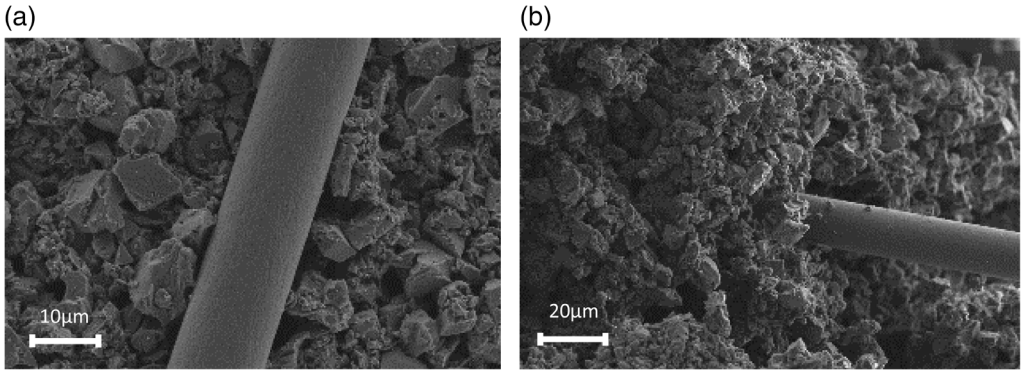

Figure 3. SEM images of a) AC/LCF electrodes fabricated with MFC as the binder and b) LCF reaching intermediary AC layers.

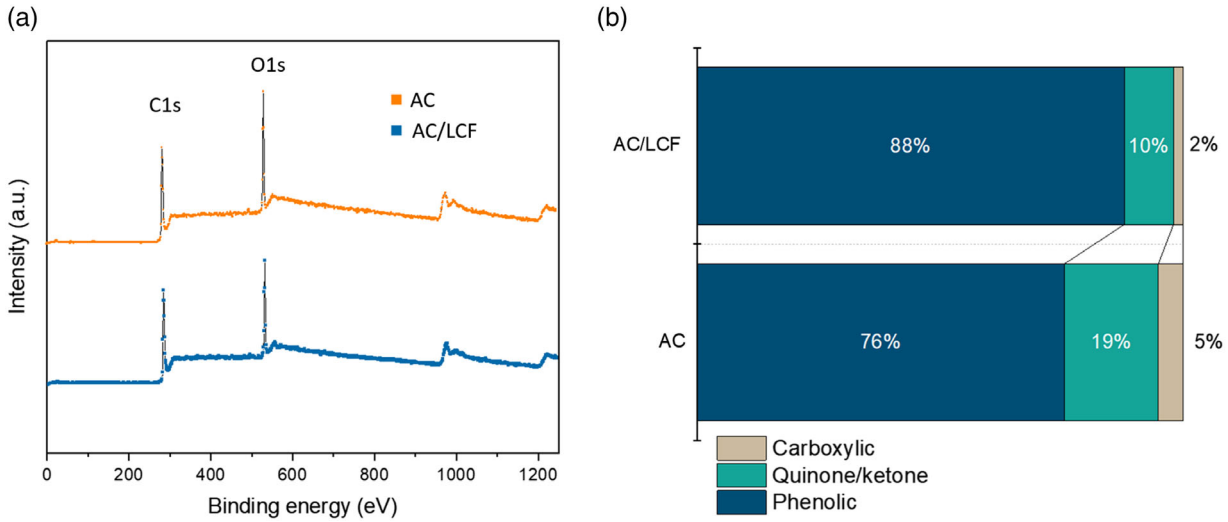

Figure 4. a) XPS broad-scan spectra of AC and AC/LCF samples. b) Distribution of predominant reactive and pseudocapacitive chemical states in the samples.

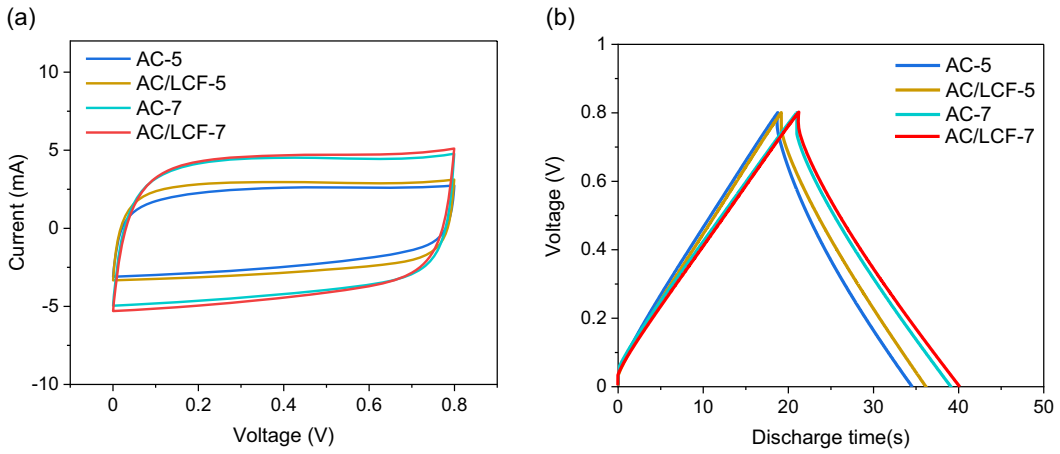

Figure 5. AC and AC/LCF electrode's (with mass loadings of 5 and 7 mg cm^{-2}) a) CV at 20 mV s^{-1} scan rate and b) GCD curve at 1 A g^{-1} current density.

CB-LCF and only CB as conductive agent delivered an energy density of 34 and 31 Wh kg^{-1}, respectively, at approximately the same power density of 71 kW kg^{-1}.

Figure 6 shows the EIS in the form of a Nyquist plot performed in the frequency range from 100 kHz to 10 mHz with an alternating current (ac) perturbation of 10 mV.

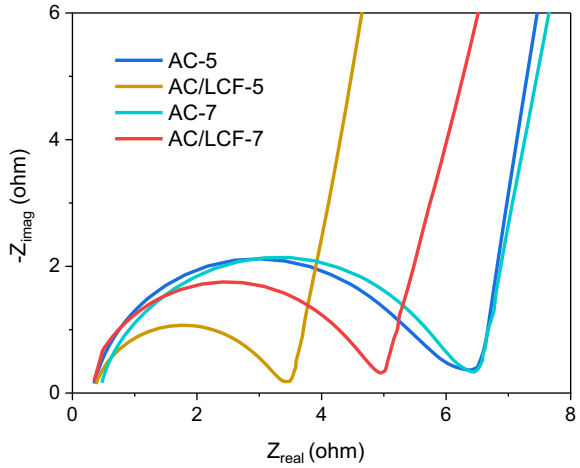

Figure 6. Nyquist plot for AC and AC/LCF electrodes at 5 and 7 mg cm^{-2} mass loadings (enlarged images of the high- and intermediate-frequency region).

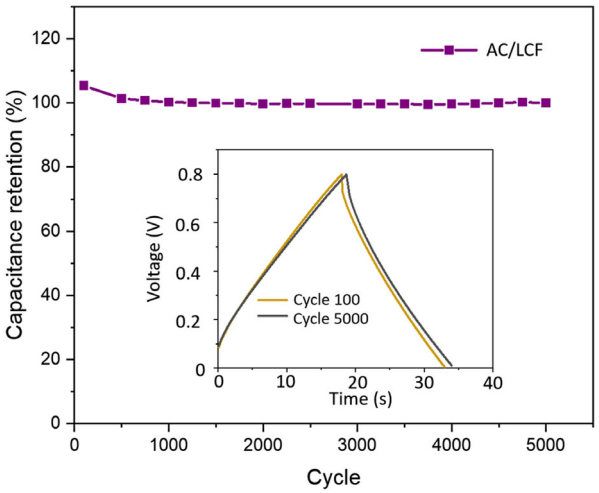

Figure 7. The specific capacitance of AC and AC/LCF electrodes at 5 mg cm^{-2} mass loading over 5000 cycles (inset: charge–discharge cycles of the same AC/LCF electrode during different cycling intervals).

The second intersection of the semicircle in the x-axis represents the charge transfer resistance or interfacial resistance that mostly originates from the electrode/electrolyte interface or electrode/current collector interface. However, as the first intersection representing electrolyte resistance is similar for all the devices, the resistances are confirmed to not originate from electrolyte wetting. As shown, the interfacial resistance is lower for the AC/LCF electrodes compared with pure ACs, which further confirms the contribution of LCF in the overall enhanced capacitance observed in CV and GCD measurements. However, with high mass loading of 10 mg cm^{-2}, the interfacial resistance increased for both electrodes, that is, the contributions from lesser LCF mass loadings for such thicker electrodes contributed to as much charge transfer resistance as AC electrodes devoid of added inclusion (Figure S2, Supporting Information). The increased charge transfer resistance is supposedly due to the limited space/volume available in the coin cell. The possibility to accommodate electrodes with only certain thickness affects the contact between electrode and stainless steel current collector. Cramping the cell with high pressure could create microfractures in thicker electrodes, decreasing the electrical conductivity contributions from LCF.

Additional modifications are necessary to truly utilize the useful features of LCF in the electrodes with a high mass loading. For instance, lowering the fiber diameter to a nanometer scale would potentially enhance the interaction between LCF and AC particles as a consequence of the larger available surface area.[11] As realized from the LCFs' SEM images, with a diameter of 13 μm, the interaction of all the AC particles around the LCF is very unlikely. Fiber diameters, lengths, and orientations are all interesting parameters to control and observe the impact for optimized electrode behavior, as are LCF surface modifications or functionalization. A net increase of the LCF content would, according to our XPS interpretation, increase the prevalence of surface functional groups in the electrode, which could be predicted to enhance the overall pseudocapacitive contribution.

A cycling stability test for 5000 cycles is shown in **Figure 7**. As seen, the AC/LCF electrodes show high capacitance retention of 98% with negligible performance deterioration after 1000 cycles. A very similar retention rate is observed for pure AC electrodes, and we thus see no reason to suspect a detrimental effect on the device's long-term stability from the LCF inclusions.

4. Conclusions and Future Work

A freestanding AC/LCF supercapacitor electrode is successfully fabricated using an MFC binder. The LCF serves both as a reinforcement agent in binding AC particles and as a conductive pathway in the AC matrix. The CV measurements indicate that the device containing AC/LCF-5 electrodes has a higher specific capacitance of 97 F g^{-1} compared with the device containing AC-5 electrodes with 85 F g^{-1}. EIS analysis confirms the less-resistive behavior of the AC/LCF electrodes up to 7 mg cm^{-2} mass loadings compared with pure AC electrodes. From the investigation with 2 wt% of LCF inclusions, the improved performances are distinctly superior for the electrodes with a mass loading of 5 mg cm^{-2}. For higher mass loadings (10 mg cm^{-2}), the performance is quite similar with and without LCF inclusions. With the further weight optimization and the reduction of the fiber dimensions along with control of their orientation in the AC matrix, the capacitive performance could be further improved in the thicker and highly mass-loaded electrodes. Thicker electrodes are essential for high-energy performances, and the faster charge transfer utilizing active material from all sites offers high power. Therefore, efficient compositing of highly conductive materials with AC can potentially contribute to the enhancement of the overall performances in existing commercially available supercapacitors. The understanding of synergy in compositing these materials requires more research.

Supporting Information

Supporting Information is available from the Wiley Online Library or from the author.

Acknowledgements

The authors acknowledge funding from Sweden's Wallenberg Wood Science Centre (WWSC) under Project 4.1.4.

Conflict of Interest

The authors declare no conflict of interest.

Data Availability Statement

The data that support the findings of this study are available from the corresponding author upon reasonable request.

Keywords

activated carbon, carbon fibers, cellulose, energy storage, lignin supercapacitors

Received: June 30, 2021
Revised: December 20, 2021
Published online:

[1] B. Dyatkin, V. Presser, M. Heon, M. R. Lukatskaya, M. Beidaghi, Y. Gogotsi, *Chem. Sustain. Energy Mater.* **2013**, *6*, 2269.
[2] D. Bresser, D. Buchholz, A. Moretti, A. Varzi, S. Passerini, *Energy Environ. Sci.* **2018**, *11*, 3096.
[3] P. Ruschhaupt, A. Varzi, S. Passerini, *Energy Mater.* **2020**, *13*, 763.
[4] W. Tian, J. Zhu, Y. Dong, J. Zhao, J. Li, N. Guo, H. Lin, S. Zhang, D. Jia, *Carbon* **2020**, *161*, 89.
[5] Y. Qing, Y. Qian, H. Lin, L. Wang, A. Liu, Y. Cao, R. Sheng, G. Yong, C. Fan, S. Zhang, D. Jia, Z. Fan, *J. Mater. Chem. A* **2019**, *7*, 6021.
[6] F. Cheng, X. Yang, S. Zhang, W. Lu, *J. Power Sources* **2020**, *450*, 227678.
[7] M. Mahmudul Huq, C.-T. Hsieh, C.-Y. Ho, *Diamond Relat. Mater.* **2016**, *62*, 58.
[8] C. Portet, P. L. Taberna, P. Simon, E. Flahaut, *J. Power Sources* **2005**, *139*, 371.
[9] A. Vahid Mohammadi, J. Moncada, H. Chen, E. Kayali, J. Orangi, C. A. Carrero, M. Beidaghi, *J. Mater. Chem. A* **2018**, *6*, 22123.
[10] A.-Y. Lo, C.-C. Chang, Y.-W. Lai, P.-R. Chen, B.-C. Xu, *ACS Omega* **2020**, *5*, 11522.
[11] G. Gryglewicz, A. Sliwak, F. Beguin, *ChemSusChem* **2013**, *6*, 1516.
[12] Y. Zhou, P. Jin, Y. Zhou, Y. Zhu, *Sci. Rep.* **2018**, *8*, 9005.
[13] S. Zhai, W. Jiang, L. Wei, H. E. Karahan, Y. Yuan, A. Keong Ng, Y. Chen, *Mater. Horizon* **2015**, *2*, 598.
[14] W. E. Tenhaeff, O. Rios, K. More, M. A. McGuire, *Adv. Funct. Mater.* **2014**, *24*, 86.
[15] N. Meek, D. Penumadu, O. Hosseinaei, D. Harper, S. Young, T. Rials, *Compos. Sci. Technol.* **2016**, *137*, 60.
[16] M. Haque, I. Abdurrokhman, A. Idström, Q. Li, A. Rajaras, A. Martinelli, L. Evenäs, P. Lundgren, P. Enoksson, *Electrochim. Acta* **2022**, *403*, 139640.
[17] V. Obreja, *Int. Rev. Electr. Eng.* **2010**, *5*, 272.
[18] R. Wang, L. Feng, W. Yang, Y. Zhang, Y. Zhang, W. Bai, B. Liu, W. Zhang, Y. Chuan, Z. Zheng, H. Guan, *Nanoscale Res. Lett.* **2017**, *12*, 575.
[19] A. Kvasha, I. Urdampilleta, I. Meatza, M. Bengoechea, J. A. Blázquez, L. Yate, O. Miguel, H.-J. Grande, *Electrochim. Acta* **2016**, *215*, 238.
[20] G. Milczarek, *Electroanalysis* **2007**, *19*, 1411.
[21] B. Zhou, J. Li, W. Liu, H. Jiang, S. Li, L. Tan, L. Dong, L. She, Z. Wei, *Energy Mater.* **2020**, *13*, 2628.

Supplementary information

S1. Material characterization

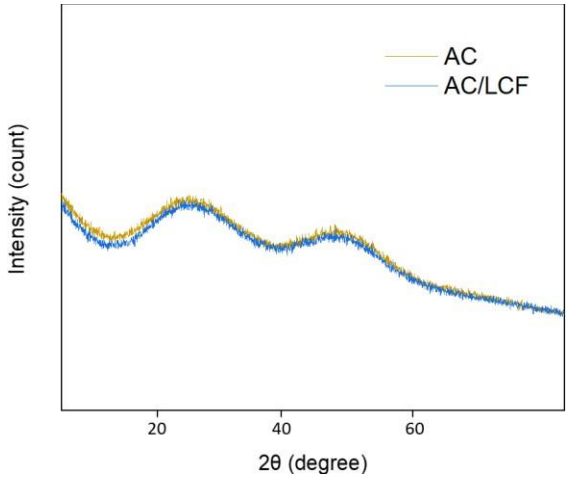

Figure S1. X-ray diffraction patterns of AC and AC/LCF with the typical diffraction peaks at 2θ= 22° and 44°.

S2. Electrochemical performance

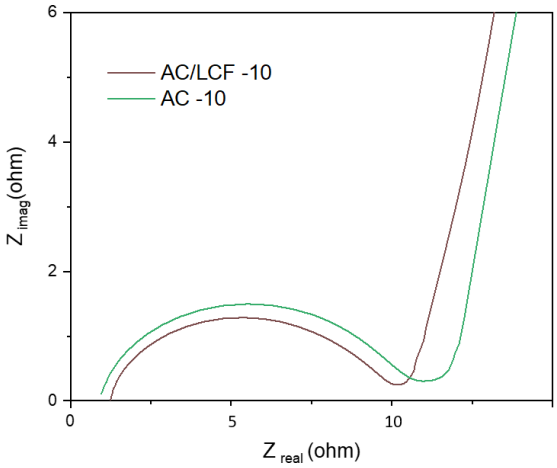

Figure S2. Nyquist plot for AC and AC/LCF electrodes at 10 mg/cm^2 mass loading (enlarged image of high and intermediate frequency region).